eman ta zabal zazu

Universidad del País Vasco

Euskal Herriko Unibertsitatea

Impact of the transient receptor potential vanilloid 1 deletion on the endocannabinoid system in the mouse dentate gyrus

Doctoral thesis

Jon Egaña Huguet BPharm, MSc

Leioa, 2020

Universidad del País Vasco Euskal Herriko Unibertsitatea

NAZIOARTEKO BIKAINTASUN CAMPUSA
CAMPUS DE EXCELENCIA INTERNACIONAL

A thesis submitted in fulfillment of the requirements for the degree of PhD IN NEUROSCIENCES

University of the Basque Country

The author was financially supported by a PhD contract from the University of the Basque Country (UPV/EHU)

This work was supported by The Basque Government (grant number IT1230-19), MINECO/FEDER, UE (grant number SAF2015-65034-R) and Red de Trastornos Adictivos, Instituto de Salud Carlos III (ISC-III) and European Regional Development Funds-European Union (ERDF-EU; grant RD16/0017/0012).

Supervisors:

PEDRO ROLANDO GRANDES MORENO, MD, PhD
IZASKUN ELEZGARAI GABANTXO, PhD

Department of Neurociences
Faculty of Medicine and Nursing

University of the Basque Country (EHU/UPV) Leioa, 2020

Laborategian igaro ditudan bost urte hauetan, pertsona asko ezagutu ditut eta hauengandik ikasteko aukera izan dut, DANORI eskerrak eman nahi dizkizuet, horregatik norbait ahaztuz gero, parkatuko didazue. Bide honetan zientzia egiteaz gain beste hainbat gauza ikasi ditut, duela bost urteko gaztea aldatu duzuela pentsatu nahiko nuke.

En primer lugar, me gustaría agradecer a mis directores, el Dr. Pedro Grandes Moreno y la Dra. Izaskun Elezgarai Gabantxo, la oportunidad que me dieron de realizar la tesis doctoral y la confianza que depositaron en mí al apostar por este proyecto.

Pedro, quisiera trasmitirte mi más sincero agradecimiento porque sin tu ayuda y confianza jamás hubiera llegado hasta aquí. Me has dirigido siempre con rigor, marcándome el camino a seguir y centrándome cuando me desviaba, entusiasmado por las preguntas que van surgiendo cada vez que ese obtiene un nuevo resultado. Muchas gracias por todo.

Izas, zer esan, eskerrik asko den-denagatik. Zure eguneroko prestutasuna edozertan lagunduteko, edozein duda argitzeko, gauzak diren moduen zintzotasunez esateko eta oker nauenien bide zuzenera bueltatzeko, hauek denak asko asko miresten ditut. Asko gozatu ditut izan ditugun eztabaida zientifikoak, nahiz eta gehienetan oker egon nire paja mentalak direla eta. Zure laguntza eta konfiantza barik ez nintzateke hemen egongo, bihotzez nire eskerrik beroenak.

Bi zuzendariez gain, Nagore, mila esker denagatik. Elektrofisiologian (asko izan delako!) zein beste arlotan laguntzeko beti prest egoteagatik, humore onagatik (beti irribarretsu) eta nahiz eta nire zuzendaria ez izan arren, eskaini didazun denbora guztiagatik, plazer bat izan da. Eskerrik asko.

Itziar B y Svein, me habéis acompañado desde el principio en este camino, prácticamente lo empezamos a la vez y lo acabaremos igual y para mí siempre ha sido una suerte contar con compañeros, amigos, así en la poyata. Aitor, aunque menos a menudo, no recuerdo mal momento junto a ti, eskerrik asko lagun, es que sin duda no se puede trabajar más que tú, es imposible. Vuestras ganas, maña e inteligencia son excepcionales y si seguís trabajando tal y como yo he visto, el límite lo pondréis vosotros.

Edgar, aunque tu incorporación al grupo haya sido más tardía, siento que tu llegada supuso aire fresco en mi perspectiva científica, en ser más crítico conmigo mismo. Tu ayuda para

afrontar la estancia en Burdeos, tus consejos de la vida, y en general por todo, muchas gracias compadre.

Ya que no puedo dedicaros un párrafo a cada uno de vosotros a los que quisiera agradeceros vuestra ayuda, sería otra tesis, permitirme que os agrupe. Como no, me gustaría dar las gracias por su ayuda para lo que fuera, a todos los compañeros que en algún momento han pasado por o que son permanentes en el grupo, como: Rafa (una firmilla?), Sonia (immuno vieja escuela), Almudena (que sería de los animales sin ti), Leire (cacho docente), Juan (beti prest behar denerako), Inma (imprescindible), Delbi (otra imprescindible), Elsa (gracias por preocuparte por nosotros, nuestra amatxu en el labo), Yolanda (trabajadora como ninguna), Ana, Sara (Referentes. mis madrileñas preferidas!!), Irantzu (jarraitzeko moduko eredua), Ianire (bizitzako eredu, betiereko borrokalaria), Naiara (pura fé), Itziar T (¡no dudes que acabaras!), Paula (motivación pura), Maria (brave, very, to achieve your goals in such conditions), Leire, Maitane, Amaia (mejor cambio generacional no se me ocurre, la vais a petar, animo neskak!). Todos habéis puesto vuestro granito de arena para que esta tesis pudiera llevarse a cabo, gracias de corazón. También agradecer a los compañeros del departamento como la gente del grupo dirigido por el Dr. Carlos Matute o el Dr. José Vicente Lafuente ya que en más de una ocasión he precisado de vuestra ayuda y hemos compartido risas en más de una comida, eskerrik asko Andrea, Alazne, Mari Paz, Ana, Álvaro, Alejandro, Ane, Anita, Carolina, Saioa, Juan Carlos, Manu, Asier, Naiara.

Me gustaría agradecer el trabajo que se ha realizado en colaboración con el grupo dirigido por el Dr. Joan Sálles Alvira. Gracias tanto a Joan y Gontzal por vuestra cercanía y disponibilidad, siempre es un placer ¡y por el trabajo realizado claro! En especial me gustaría agradecer el esfuerzo y el empeño al doctorando Mikel Saumell, ya que tu gran trabajo le ha aportado un valor añadido a mi tesis dándome argumentos con los que explicar los cambios que observaba y reforzando lo que ya veía con nuevas evidencias. Te has implicado tanto o más que yo con el proyecto, lo sé, eta hori bene benetan eskertzen dizut lagun.

I would like to thank all the people that I met in the stay in Bordeaux for doing it unforgettable. This experience taught me lot of things, not just scientific stuff, and gave me the opportunity to know another way of doing, basically, everything! Gio, thanks for giving me the opportunity to join your lab, I really appreciate it. F6, thanks for everything, you are awesone! Ula, Paulita, Imane, Carlos, Ignacio, Fran, Marjorie, Bastien, Geoffrey, Yamuna, Roman, Nuria, Christina,

Antonio, Jose, Luigi, Emma, Mari(Carmen), Christopher, Giangi, Zhe, Laurie, Arnau, Su, Astrich, Virginie, Mario, Dani, Ana and many others, you all deserve it, thanks a lot!

Azkenik, nire familia eta lagunei izandako pazientzia eta emandako laguntza guztia eskertu nahiko nieke, asko izan delako 5 urte hauetan zehar. Aita, Ama, Mikel, (Lur), la p*** NA, NRS, lagun danak, Andrea be, klaro, zeuek barik ez nintzatekeelako naizena izango eta ez nukeelako egiten dudana egingo, eta nahiz eta bide hau bere amaierara heldu hurrengoan ere nirekin batera egongo zariela badakidalako, beti ere nire eskerrik beroenak.

... Zure usain gozoa, lana,
amodioa, itsasoa,
nere baitan sartzen.
Atzo goizean entzun nuen
zure berbaren oihartzuna,
zure kantaren fereka,
bihotzean kilika
eta ohiartzunaren haunditasunean
murgilduz joan nintzen
jausika, hegaka...

B.L

INDEX

Index

Abbreviations

Abbreviations

- **AA:** Arachidonic acid
- **ABC**: Avidin-biotin complex
- **ABHD6:** α/β-hydrolase domain containing 6
- **AC:** Adenylyl cyclase
- **aCSF:** Artificial cerebrospinal fluid
- **AE:** Acquired epilepsy
- **AEA:** Arachidonoyl-ethanolamine or anandamide
- **AED:** Antiepileptic drug
- **AMG:** Amygdala
- **AMPA:** D-amino-3-hydroxy-5-methyl-4-isoxazole-propionic acid
- **ANOVA**: Analysis of variance
- **AP:** Anteroposterior
- **ATP:** Adenosine-triphosphate

- **BLA:** Basolateral amygdaloid nucleus
- **BM:** Barnes Maze
- **BNST:** Bed nucleus of the stria terminalis
- **BSA:** Bovine serum albumin

- **CA:** Cornu ammonis or Ammon´s horn
- **CA1:** Region 1 of Cornu ammonis
- **CA2:** Region 2 of Cornu ammonis
- **CA3:** Region 3 of Cornu ammonis
- **cAMP:** Cyclic adenosine monophosphate
- **Cb:** Cerebellar cortex
- **CB_1R:** Type I cannabinoid receptor
- **CB_1-eLTD:** CB_1 receptor-dependent excitatory long-term depression
- **CB_2R:** Type II cannabinoid receptor
- **CBD:** Cannabidiol
- **CBRs:** Cannabinoid receptors
- **CCK**: Cholecystokinin
- **Cg:** Cingulate cortex
- **CNS**: Central nervous system
- **CPu:** Caudate putamen
- **CPZ:** Capsazepine
- **CRE:** cAMP response element
- **CRIP1a:** Cannabinoid receptor associated protein 1a
- **Ctx:** Cortex

- **DAB:** Diaminobenzidine
- **DAG:** Diacylglycerol
- **DAGL:** Diacylglycerol lipase
- **DG:** Dentate gyrus
- **DGML:** Dentate gyrus molecular layer
- **DMSO:** Dimethyl sulfoxide
- **DRG:** Dorsal root ganglia
- **DRN:** Dorsal raphe nucleus
- **DSE**: Depolarization-induced suppression of excitation at glutamatergic synapses
- **DSI:** Depolarization-induced suppression of inhibition at GABAergic synapses
- **DV:** Dorsoventral

- **EC:** Entorhinal cortex
- **eCB:** Endocannabinoid
- **ECS:** Endocannabinoid system
- **eCB-LTD:** Endocannabinoid-mediated long-term depression
- **ECL:** Electrochemiluminescence
- **eLTD:** Long-term depression of excitation

Abbreviations

- **EM:** Electron microscopy
- **ER:** Endoplasmic reticulum
- **ERK**: Extracellular signal-regulated kinase
- **EtOH:** Ethyl alcohol or ethanol

- **FAAH**: Fatty acid amide hydrolase
- **fEPSP:** Field excitatory postsynaptic potential
- **FIJI:** Fiji is just IMAGE J

- **GABA:** Gamma-aminobutyric acid
- **$GABA_A$:** Type A gamma-aminobutyric acid
- **GFAP:** Glial fibrillary acidic protein
- **GCL:** Granule cell layer
- **GP:** Globus pallidus
- **GPCRs:** G-protein-coupled receptors
- **GPR55:** G protein-coupled receptor 55

- **HF:** Hippocampal formation
- **HRP:** horseradish peroxidase conjugated
- **HSP70:** Heat shock protein 70

-**ICH:** Immunohistocheministry
- **ICRS:** Ionotropic cannabinoid receptors
- **iLTD:** Long-term depression of inhibition
- **IML:** Inner molecular layer

- **KA:** Kainate or kainic acid
- **KO:** Knockout mice
- **LC:** Locus coeruleus
- **LFS:** Low frequency stimulation
- **LM:** Light microscopy
- **LPP:** Lateral perforant path
- **LTD:** Long-term depression
- **LTP:** Long-term potentiation

- **MAGL:** Monoacylglicerol lipase
- **MCFL:** Mossy cell fibre layer
- **MCRs**: Metabotropic cannabinoid receptors
- **mGluR:** Metabotropic glutamate receptors
- **mGluR1:** Metabotropic glutamate receptor 1
- **mGluR5:** Metabotropic glutamate receptor 5
- **ML:** Molecular layer
- ***ML:** Mediolateral axis in stereotaxic surgery
- **MML:** Middle molecular layer
- **MPP:** Medial perforant pathway
- **mRNA:** Messenger ribonucleic acid

- **NAc:** Nucleus accumbens
- **NADA:** N-arachidonoyl dopamine
- **NAPE:** N-acylphosphatidyl ethanolamine
- **NAPE-PLD:** N-acyl phosphatidyl ethanolamine hydrolyzing phospholipase D
- **NMDAR:** N-methyl-D-aspartate receptor
- **NORT:** Novel object recognition test
- **NTS:** Nucleus of the solitary tract

- **OB:** Olfactory bulb
- **OLM:** Oriens-lacunosum-moleculare

- **OML:** Outer molecular layer
- **OT:** Olfactory tubercle

- **PAG:** Periaqueductal gray
- **PB:** Phosphate buffer
- **PBS:** Phosphate buffered saline
- **PKA:** Protein kinases type A
- **PLC:** Phospholipase C
- **PNS:** Peripheral nervous system
- **PP:** Perforant path
- **PPAR:** Peroxisome proliferator-activated receptor
- **PPR:** Paired-pulse ratio
- **PTX:** Picrotoxin
- **PTZ:** Pentylenetetrazole
- **PVDF:** Polyvinylidene difluoride
- **RS:** Racine's scale
- **RT:** Room temperature
- **RTX:** Resiniferatoxin
- **SC:** Schaffer collateral pathway
- **SDS:** Sodium dodecyl sulfate
- **SE:** Status epilepticus
- **SNc:** Substantia nigra pars compacta
- **SNr:** Substantia nigra pars reticulata
- **SRS:** Spontaneous recurrent seizures
- **S.E.M:** Standar error of the mean

- **TA:** Temporoammonic pathway
- **TBS:** Tris-hydrogen Chloride buffered saline
- **TBS-T**: Tris-hydrogen Chloride buffered saline with Tween-20
- **TF:** Time exploring familiar object
- **THC:** Delta-9-tetrahydrocannabinol
- **tLTP:** Spike-timing-dependent long-term potentiation
- **TN:** Time exploring new object
- **TRP:** Transient receptor potential
- **TRPA:** Transient receptor potential ankyrin
- **TRPC**: Transient receptor potential canonical
- **TRPP:** Transient receptor potential polycystin
- **TRPML:** Transient receptor potential mucolipin
- **TRPM**: Transient receptor potential melastatin
- **TRPV:** Transient receptor potential vanilloid
- **TRPV1:** Transient potential receptors of vanilloid type 1
- **TRPV1-KO:** TRPV1 knockout

- **VTA:** Ventral tegmental area

- **WT:** Wild type
- **WB:** Western blot

- **2-AG**: 2-arachidonoyl glycerol
- **[^{35}S] GTPγS:** [^{35}S] guanosine-5*-O-(3-thiotriphosphate)

1- Introduction

Genetic robustness is the ability of a living organism to keep its viability despite genetic disruptions (El-Brolosy and Stainier, 2017). Variation in genes is present in evolution, as living organisms need compensating systems to ensure similar development despite differences in genetic background or environmental conditions (Mather, 1953; Waddington, 1959).

This concept is partially based in redundant genes, as one gene may compensate the lack of another gene with equivalent functions and distribution pattern. This has been reported for several mutants in different living organisms (Cohen et al., 1987; Hoffman, 1991; Tautz, 1992; Cadigan et al., 1994; Gonzalez-Gaitán et al., 1994; Wang et al., 1996; Von Koch et al., 1997; Nedvetzki et al., 2004; Santamaria et al., 2007). However, the individual compensation of a gene is not the only event giving robustness to the genome, other forms of robustness have been described in tightly regulated cellular networks such as metabolic, transcriptional or signalling circuits. Impairment of a particular gene's function in a network could change the expression of other genes participating in the same network (Barabasi and Oltvai, 2004; Davidson and Levin, 2005).

The recent advances in genetic engineering have allowed a new range of genetic tools to modify genes in living organisms. One of these advantages, the reverse genetic tools indeed, have revealed underlying phenotypic differences between knockouts and knockdowns in a number of different mutant systems. For instance, in mice (De Souza et al., 2006; Young et al., 2009; McJunkin et al., 2011; Daude et al., 2012), Drosophila (Yamamoto, 2014), zebrafish (Law and Sargent, 2014) and in human cell lines (Karakas et al., 2007; Evers et al., 2016; Morgens et al., 2016).

Bearing in mind that these changes could crop up in any mutant, in this study we aimed at determining the changes that could arise in the endocannabinoid system components in mice with a complete genetic deletion of the transient receptor potential vanilloid 1 (TRPV1) receptor.

1.1- Endocannabinoid system (ECS):

Cannabis sativa, better known as marihuana, has been used for medical practice throughout recorded history for long time. The first documents referring to its medical use date from ancient China around 5000 years ago, where herb extracts were used for amelioration of convulsions and pain (Mechoulan, 1986). However, it was not until early 60's that the first light was shed on the matter by the discovery of Delta-9-tetrahydrocannabinol (THC), the main psychoactive

component of approximately more than 70 phytocannabinoids identified in the plant (Gaoni and Mechoulan, 1964; Kunos et al., 2006).

This milestone discovery led to the development of a variety of synthetic cannabinoids with similar or distinct structures to phytocannabinoids, which finally led to the identification and cloning of the cannabinoid receptor type 1 (CB_1R) (Devane et al., 1988; Matsuda et al 1990). Moreover, another cannabinoid receptor was identified and cloned later termed as the cannabinoid receptor type 2 (CB_2R) (Munro et al., 1993).

Despite the fact that one of the major neurotransmitter systems present in the brain was discovered many decades ago, it remained unexplored until the early 1990s. This was due, on one hand, to the lack of research on the plant cannabinoids, made difficult by legal constraints and on the other hand, because even if cannabinoids had therapeutic potential, their psychoactive effects largely limited their use in clinical practice (Zou and Kumar, 2018). Later on, after becoming aware of the major physiological importance exerted by the ECS in body and brain, the chemistry, metabolism, biochemistry, and pharmacology was extensively investigated (Pertwee et al., 2010).

Even though CB_1R and CB_2R are widely-acknowledged as cannabinoid receptors (CBRs), several other receptors, varying from other G protein-coupled receptors (GPCRs) to ion channels and nuclear receptors, have been reported to interact with cannabinoids and therefore also termed by some authors as cannabinoid receptors (Howlet et al., 2002; Kano et al., 2009; De Petrocellis et al., 2017; Zou and Kumar, 2018). As so, it can be concluded that the ECS is composed of cannabinoid receptors, as well as endogenous compounds known as endocannabinoids (eCBs) that can target these receptors and the enzymes responsible for eCB biosynthesis and degradation (Pertwee et al., 2010).

1.2- Cannabinoid receptors:

Due to their lipophilic nature, cannabinoids were initially thought to exert their biological effects through disrupting the cell membrane in a non-specific manner. Nevertheless, after the breakthrough discovery of THC molecule and subsequent development of chemically synthetized cannabinoids, along with the identification and pharmacological characterization of cannabinoids binding sites in the brain, it was revealed the existence of a putative cannabinoid

receptor and its analogy to a GPCR (Gaoni and Mechoulan, 1964; Devane et al., 1988; Matsuda et al 1990; Kunos et al., 2006; Pertwee, 2006).

The two major CBRs that have been expressed functionally (Matsuda, 1997), CB_1R and CB_2R, belong to the GPCR family and are primarily coupled to Gi or Go proteins (Howlet et al., 2002). Their activation inhibits adenylyl cyclase and certain voltage-gated calcium channels, while activates several mitogen-activated protein kinases inwardly rectifying potassium channels, with some variation depending on the cell type in which they are. Activation of these receptors provokes a varied of consequences on cell physiology, including synaptic function modulation, gene transcription and cell motility (Howlet et al., 2002; Lu and Mackie, 2016).

However, in the last years several evidences outlined that many of the CBR-mediated actions, both at central or peripheral levels, could not be purely attached to the activation of CB_1R and CB_2R since several important cannabimimetic actions were found in biological systems lacking genes for these receptors such specific cell lines or transgenic mice (De Petrocellis et al., 2017). For example, peripherally-induced antihyperalgesia persists in CB_1R /CB_2R knockout (KO) mice (Zimmer et al. 1999; Akopian et al. 2008) or the neuroprotective effect of the CB_1R antagonist rimonabant in a model of cerebral ischemia independent of GPCRs (Pegorini et al. 2006).

The actions that could not be explained by classical processes of GPCRs led to the recognition of a second family of CBRs (Akopian et al., 2009). Among these receptors, the family of transient receptor potential channels (TRP channels) plays a key role. These channels compose a broad family of ligand-gated ion channels that mediate the transmembrane flux of cations down their electrochemical gradients leading to an increase of intracellular calcium and sodium concentration (Montell, 2005).

1.2.1- Main cannabinoid receptors:

These were the first cannabinoid receptors being identified and included CB_1R, CB_2R, GPCR55 and peroxisome-proliferator-activated receptors (PPARs) (Matsuda, 1997; Sun and Bennett, 2007; Ryberg et al., 2007). In the brain, CB_1R is primarily through the receptor that cannabinoids exert their known actions.

1.2.1.1- CB_1 receptor:

CB_1R was first discovered in the brain. Later, by using autoradiography, in situ hybridization, and immunohistochemistry, CB_1R resulted to be the most widely expressed GPCR in the brain (Mackie, 2005; Kano et al., 2009). Within it, the CB_1R is highly expressed in the olfactory bulb, hippocampus, basal ganglia and cerebellum, moderately expressed in the cerebral cortex, septum, amygdala, hypothalamus, parts of the brainstem and the spinal cord dorsal horn, and very low expressed in the thalamus and the spinal cord ventral horn (Mackie, 2005) (figure 1).

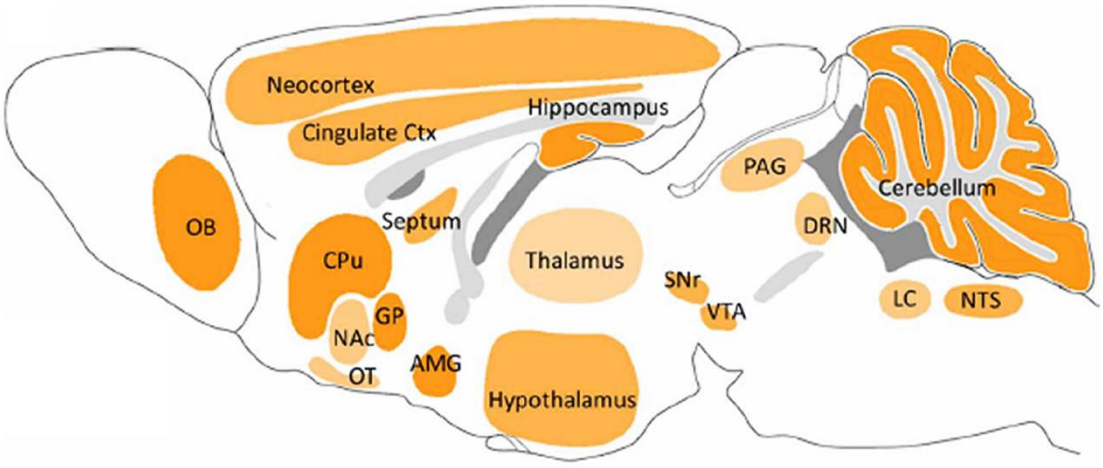

Figure 1: Schematic representation of the main areas expressing CB_1R. AMG, amygdala; CPu, caudate putamen; Ctx, cortex; DRN, dorsal raphe nucleus; GP, globus pallidus; LC, locus coeruleus; NAc, nucleus accumbens; NTS, nucleus of the solitary tract; OB, olfactory bulb; OT, olfactory tubercle; PAG, periaqueductal gray; SNr, substantia nigra pars reticulata; VTA, ventral tegmental area. Obtained from Flores et al., 2013.

CB_1Rs are highly concentrated in presynaptic terminals, which are activated by endocannabinoids acting as retrograde signalling molecules travelling from postsynaptic localizations to suppress the release of GABA, glutamate or other neurotransmitters (Tsou et al. 1998; Katona et al., 1999; Gerdeman et al., 2001). This has been proposed as a plausible mechanism of the CB_1R-mediated neuroprotection against excitotoxicity in neurological disorders such as epilepsy and neurodegenerative diseases (Marsicano et al., 2003; Katona and Freund, 2008; Chiarlone et al., 2014). Even though, the possible existence of the receptor in postsynaptic sites is not fully excluded, as functional studies have shown self-inhibition of neocortical neurons by endocannabinoids (Marinelli et al., 2008; Marinelli et al., 2009; Castillo et al., 2012).

Aside from the well-known plasma membrane localization of the CB_1R, intracellular localizations in transfected non-neuronal cells, undifferentiated neuronal cells and cultured hippocampal

cells have been reported (Rozenfeld, 2011). Probably, part of the intracellular pool represents the constitutive and agonist-induced internalization of CB_1Rs located at plasma membranes (Leterrier et al., 2004). Besides, a distinct pool of intracellular CB_1Rs in acid-filled endo/lysosomes does not contribute to the subpopulation expressed at the cell surface (Rozenfeld and Devi, 2008; Grimsey et al., 2010) and is in charge to augment calcium release from the endoplasmic reticulum and lysosomes upon receptor activation (Brailoiu et al., 2011).

Another CB_1R subpopulation is expressed in organelles such as mitochondria. Previous studies have reported the effect of THC on mitochondrial-associated enzymatic activity, and have demonstrated the presence of the receptor and its direct involvement in cellular respiration in hippocampal neurons (Bénard et al. 2012; Hebert-Chatelain et al. 2014a, b).

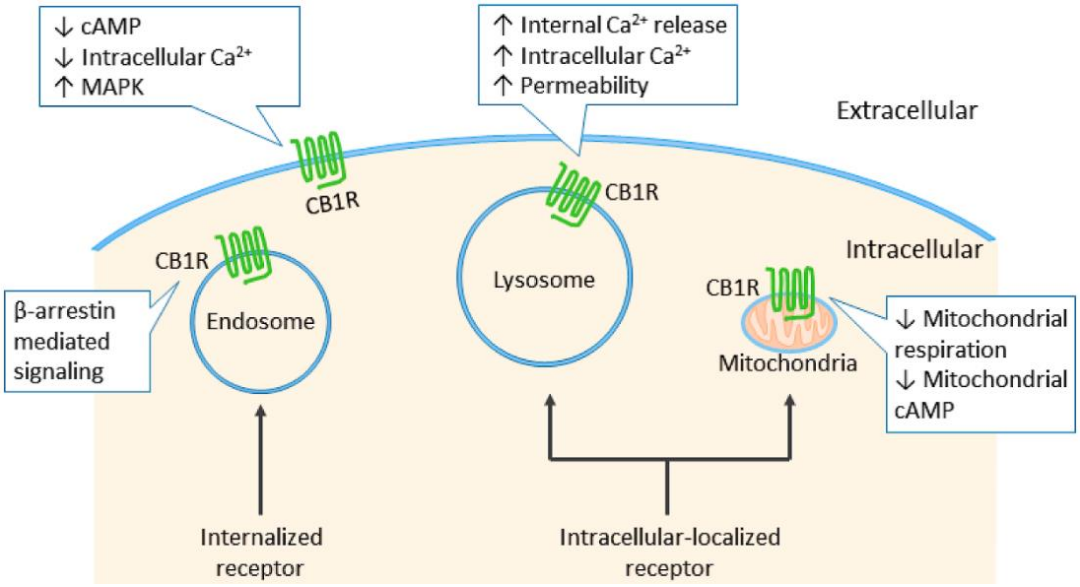

Figure 2: Subcellular localization of the CB_1R. Typically, the CB_1R is located at cell surface and inhibits cyclic adenosine monophosphate (cAMP) formation and calcium influx upon activation. Constitutive and ligand-induced internalized CB_1Rs mediate signalling pathways through β-arrestin. Intracellular-localized CB_1Rs do not translocate to plasma membrane. Instead, they form a subpopulation with pharmacological properties distinct from their plasma membrane-localized counterparts. CB_1Rs located on lysosomes can increase intracellular calcium concentrations through the release of internal calcium stores, and increase the permeability of lysosomes. Mitochondrial CB_1Rs inhibit mitochondrial cellular respiration and cAMP production, hence regulating cellular energy metabolism. Obtained from Zou and Kumar, 2018.

In addition to neurons, CB_1Rs are expressed, although to a much lower extent, in glial cells like astrocytes and oligodendrocytes, where modulate synaptic transmission (Navarrete and Araque 2008; 2010; Stela, 2009; 2010; Castillo et al., 2012; Gutierrez-Rodriguez et al., 2017). Moreover, CB_1Rs are also in astrocytic mitochondria where they seem to regulate astroglial glucose metabolism and social interactions (Gutierrez-Rodriguez et al., 2018; Jimenez-Blasco et al., submitted to Nature).

Because of the widespread distribution of the CB_1R in the human body, it participates in a broad spectrum of physiological functions (Pacher et al., 2006; Kano et al., 2009; Macarrone et al., 2015; Di Marzo et al., 2015) and is involved in central neural processes and disorders, including appetite, learning and memory, anxiety, depression, schizophrenia, stroke, multiple sclerosis, neurodegeneration, epilepsy or addiction (Iversen, 2003; Pacher et al., 2006; Kano et al., 2009; Di Marzo et al., 2015).

Concerning the intracellular signalling of CB_1Rs, these were shown to be mainly coupled to Gαi/o proteins. The activation of these receptors inhibits adenylyl cyclase (AC)/cAMP/PKA/ERK signalling (Jung et al., 1997; Demuth and Molleman, 2006). In addition, CB_1R has been proved to activate Gαs proteins, and stimulate cAMP production (McAllister and Glass, 2002) and to stimulate calcium release from internal stores in astrocytes and endothelial cells (Fimiani et al., 1999). Phospholipase C and downstream cascades through the coupling of CB_1R with Gq/11 proteins likely regulate this (Lauckner et al., 2005).

Whereas CB_1R signalling through G-protein mediated pathways has been extensively investigated, other putative CB_1R-binding proteins, classified as scaffolding or regulatory proteins, have been identified as potential modulators of CB_1R activity (Smith et al., 2010). Cannabinoid receptor interacting protein 1a (CRIP1a) was discovered by the Deborah Lewis laboratory when deleting the distal C-terminal amino acids which resulted in the enhancement of the CB_1R constitutive inhibition of the voltage-dependent calcium current in superior cervical ganglion neurons. This finding suggested that the distal C-terminal domain was involved in an inhibitory function (Nie and Lewis, 2001a; 2001b). Since the C-terminal binds to a regulatory protein, the Lewis laboratory performed a yeast two-hybrid screen that identified CRIP1a as a novel CB_1R-associated protein (Niehaus et al., 2007).

1.2.1.2- CB_2 receptor:

Few years after the discovery of the first receptor, another GPCR was identified to interact with cannabiboids in the spleen macrophages, CB_2R (Munro et al., 1993). Follow up studies revealed a predominant expression of this receptor in immune cells and a moderate expression in other peripheral tissues, including the cardiovascular system, gastrointestinal (GI) tract, liver, adipose tissue, bone and reproductive system. In opposition, the presence of the CB_2R was not observed in the central nervous system (CNS), therefore this was referred as “the peripheral CBR” (Howlet et al., 2002). Nevertheless, this has been challenged recently by numerous studies

demonstrating the expression of the CB_2R in the brain, even if to a much lower extent in comparison to the one found in immune system or compared to the expression of CB_1R (Gong et al., 2006). Although the expression of the CB_2R in the CNS and peripheral nervous system (PNS) is comparatively limited, it is certain that the CB_2R plays an active function in neurological processes, such as nociception, drug addiction and neuroimflamation (Atwood and Mackie, 2010; Dhopeshwarkar and Mackie, 2014). Furthermore, recent studies discovered the intracellular presence of CB_2R in prefrontal cortical pyramidal neurons where it regulates neuronal excitability through the modulation of calcium activated chloride channels (Den Boon et al., 2012).

1.2.2- Other cannabinoid receptors:

In the last decade, some of the mammalian TRP channels have been linked to cannabinoid system as pharmacological evidence has suggested that cannabinoids and endocannabinoids target more than the classical metabotropic cannabinoid receptors (Morales et al., 2017a; Morales and Reggio, 2017b; 2018) .

TRP channel superfamily (figure 3) consists of six subfamilies: canonical (TRPC), vanilloid (TRPV), polycystin (TRPP), mucolipin (TRPML), ankyrin (TRPA) and melastatin (TRPM) (Winter et al., 2013). Despite the fact that 28 channels compose this family, just six of them can be activated by a variety of endogenous, plant-derived or synthetic cannabinoids, apart from other physical and chemical stimulus. These channels, that include TRPV1-TRPV4, TRPA1, and TRPM8, are termed as the ionotropic cannabinoid receptors (ICR) (Muller et al., 2019). Among endogenous and exogenous non-cannabinoid compounds that activate TRP channels there can be found natural compounds like capsaicin and allicin, from chili peppers and garlic respectively.

Inside the cannabinoid molecules that counteract with these channels, the endocannabinoid anandamide (AEA) was the first endogenous TRPV1 agonist identified during a study of the vasodilator action of AEA (Zygmunt et al., 1999). N-arachidonyl dopamine (NADA) and AEA were identified as the first endogenous antagonists of TRPM8 (De Petrocellis et al., 2007). THC acts most potently at TRPV2; moderately modulates TRPV3, TRPV4, TRPA1, and TRPM8; but does not appear to modulate TRPV1 (De Petrocellis et al., 2011). Cannabidiol (CBD) that has been shown to have many beneficial properties, including anti-inflammatory action, has little affinity for the CB_1 and CB_2 receptors, but is reported to be most potent at TRPV1 and TRPM8 channels (De Petrocellis et al., 2011). Synthetic cannabinoids also act through these receptors, for instance, a

CB_1R agonist, WIN55,212-2, has been found to exert analgesic effects by desensitizing both TRPV1 and TRPA1 (Ruparel et al., 2011).

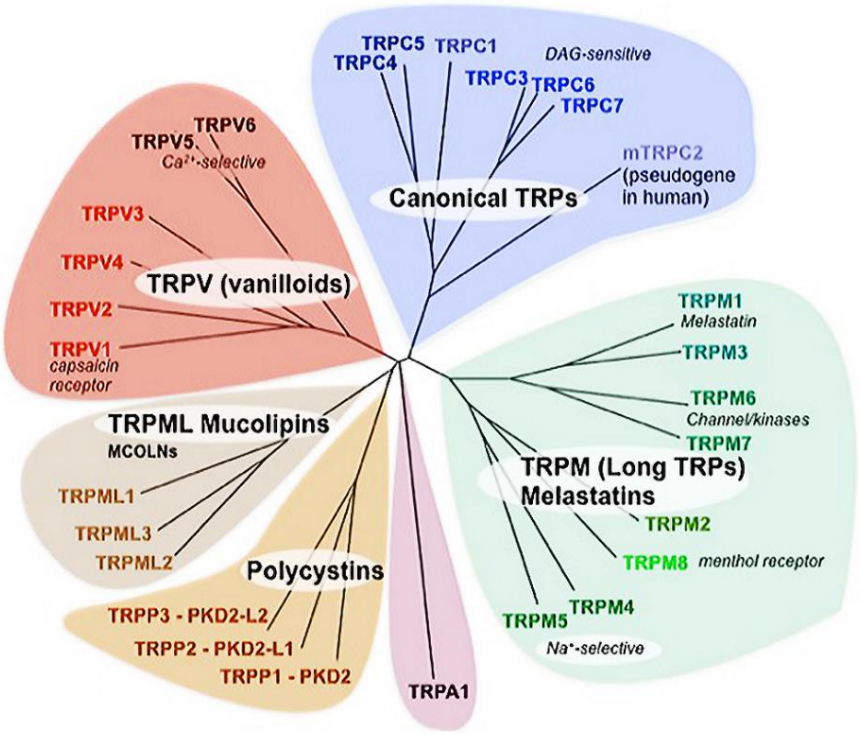

Figure 3: Mammalian TRP family tree. Obtained from Clapham 2003.

1.2.2.1- TRPV1

TRPV1 also known as the capsaicin receptor because of its affinity for this compound, is a polymodal, non-selective cation channel expressed by major classes of nociceptive neurons in PNS and is important for the detection of noxious stimuli (Vay et al., 2012; Caterina, 2014). Ion channels, including TRPV1, are typically found in the plasma membrane and form a passage from outer side of the membrane to inner one (De Petrocellis et al., 2017). After being activated, the transmembrane pore of TRPV1 opens and allows cations to pass from one side to the other. TRPV1 can be activated by a number of endogenous and exogenous stimuli including heat, low pH, N-acyl amides, arachidonic acid (AA) derivatives, vanilloids, capsaicin, protons and, of course, cannabinoids (De Petrocellis et al., 2017), although in the CNS under physiological conditions TRPV1 is unlikely to be activated by heat or low pH.

Capsaicin and resiniferatoxin (RTX), two agonists that strongly activate TRPV1, evoke strong burning sensations. Upon activation, calcium moves through the pore and enters the cell. This stimulates a series of calcium-dependent processes that finally lead to desensitization of the

channel. In this period, the channel enters a refractory period in which it can no longer respond to further stimulation, leading to the paradoxical analgesic effect of these compounds (Iannotti et al., 2014).

Respect to its distribution in the PNS, TRPV1 is present in about half of all somatic and visceral sensory neurons, restricted to neurons of small to medium size in the dorsal root, trigeminal and vagal ganglia (Caterina et al., 1997; Helliwell et al., 1998). TRPV1 is also expressed in the central projections of sensory neurons in the dorsal horn of the spinal cord, trigeminal nucleus caudalis and the nucleus of the solitary tract (Tominaga et al., 1998; Szallasi and Blumberg, 1999).

Even if it was controversial, TRPV1 has been shown to be also present in the CNS, notably in the preoptic area of the hypothalamus, where it is essential for thermoregulatory responses to avoid hyperthermia (Jancso-Gabor et al., 1970; Szolcsanyi et al., 1971). In situ hybridization has further indicated the presence of TRPV1 in several brain nuclei (Mezey et al., 2000). Moreover, specific antibodies and mRNA approaches revealed TRPV1 expression in many cells and brain areas, such as dopaminergic neurons of the substantia nigra, cortical and hippocampal pyramidal neurons, the hypothalamus and the locus coeruleus, olfactory cortex or lateral and dorsal septal nuclei (Mezey et al., 2000; Cortright et al., 2001; Sanchez et al., 2001; Szabo et al., 2002; Roberts et al., 2004; Tóth et al., 2005; Cristino et al., 2006) (figure 4). Apart from being localized in neuronal membranes, the expression of TRPV1 channels has also been reported in astrocytes (Doly et al., 2004; Chen et al., 2009; Huang et al., 2010; Ho et al., 2012; Mannari et al., 2013). Furthermore, it was reported to be in rodent and human microglial cells but mainly located in the hippocampus, cortex, hypothalamus, cerebellum, substantia nigra, olfactory system, mesencephalon, and hindbrain (Tóth et al., 2005; Sun et al., 2013; Hironaka et al., 2014; Huang et al., 2014; 2015; Marrone et al., 2017).

TRPV1 functions were also described in intracellular organelles, including the mitochondria, endoplasmic reticulum (ER), lysosomes, and Golgi apparatus (Huang et al., 2010, Miyake et al., 2015; Stueber et al., 2017). At the ultrastructural level, it was confirmed the expression of the receptor mostly at postsynaptic sites of glutamatergic and GABAergic synapses in the molecular layer of the hippocampal dentate gyrus (Puente et al., 2015; Canduela et al., 2015) and at the excitatory Schaffer collateral terminals in the CA1 hippocampus (Bialecki et al., 2020) .

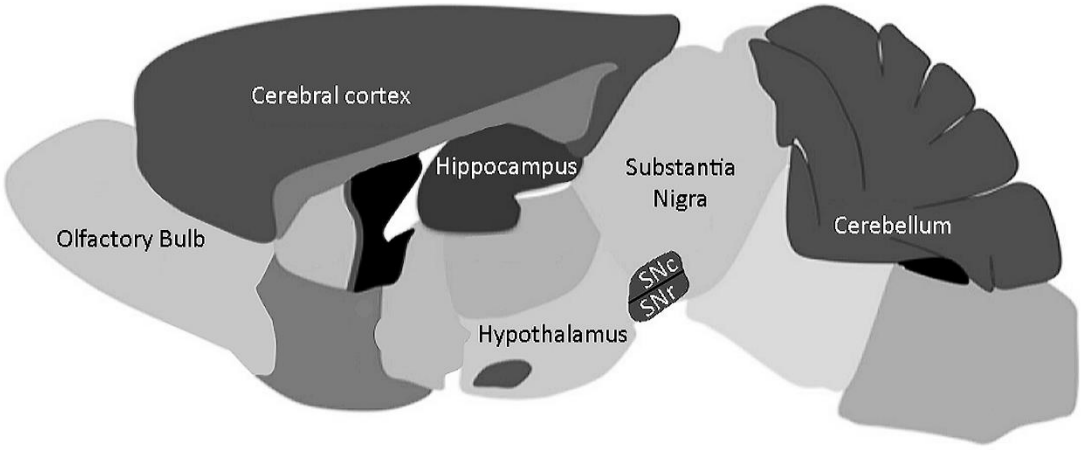

Figure 4: Schematic representation of the main areas expressing TRPV1. SNc, substantia nigra pars compacta; SNr, substantia nigra pars reticulata. Modified from Silvin et al., 2018.

With regard to its functionality, as it is primarily present in the peripheral sensory nerve terminals, this receptor acts as a polymodal receptor that modulates synaptic transmission at the first sensory synapse (Tominaga et al., 1998). Several studies focus the attention on the function of TRPV1 channels in the brain and on their role in the regulation of synaptic transmission, since activation of TRPV1 has been shown to regulate synaptic transmission by pre- and postsynaptic mechanisms. For instance, the activation of presynaptically located TRPV1 on afferents to the locus coeruleus potentiates the release of glutamate and adrenaline/noradrenaline (Marinellli et al., 2002) and the effect on glutamatergic transmission was also shown to be presynaptic in striatum (Musella et al., 2009). Presynaptic TRPV1 has been proved to mediate glutamate release at the Schaffer collaterals synapses in CA1 hippocampus as this effect was absent in TRPV1-KO and prevented by capsazepine (Bialecki et al., 2020). In contrast, TRPV1 suppressed the excitatory transmission in rat and mouse dentate gyrus via postsynaptic calcium-calcineurin and clathrin dependent internalization of AMPA receptors (Chávez et al., 2010). In the nucleus accumbens, TRPV1-mediated depression of the excitatory transmission is also due to a postsynaptic endocytosis of AMPA receptors (Grueter et al., 2010).

Apart from being implicated in glutamatergic transmission, TRPV1 has been proved to be also involved in the modulation of GABAergic transmission (Drebot et al., 2006). Channel activation by either capsaicin or AEA has been shown to depress inhibitory GABAergic transmission in the dentate gyrus by a postsynaptic mechanism (Chávez et al., 2014). Furthermore, TRPV1 participates in spike-timing-dependent long-term potentiation (tLTP) in neocortical pyramidal cells, suggesting that this receptor may be of importance for acquiring new associative memories (Cui et al., 2018). On the other hand, the TRPV1 block resulted in a reduction of

glutamatergic inputs to oriens-lacunosum-moleculare (OLM) interneurons in the hippocampus (Hurtado-Zavala et al., 2017).

TRPV1 is present in a number of areas related to pain like primary afferent neurons, dorsal root ganglia (DRG) and the dorsal horn of the spinal cord. However, in terms of pain modulation, it is notable that this channel is not the only player as numerous evidence indicate complex interactions with cannabinoid and opioid receptors. These interactions with other neuromodulatory systems can be bidirectional, inhibitory or excitatory, acute or chronic and can arise structurally and functionally at the molecular level in physiological or pathological processes (Zador and Wollemann, 2015).

Regarding its function in the PNS, even though TRPV1 involvement is compelling in thermal sensory perception, its distribution in regions not specifically involved in temperature regulation indicates that this receptor plays a role in other functions too. Thus, TRPV1 expression in the smooth muscle of blood vessels and bronchi causes vasodilatation and bronchoconstriction (Mitchell et al., 1997; Zygmunt et al., 1999), while its presence in the urothelium supports its role in micturition (Birder et al., 2002). It has also been proposed that the temperature-sensitive property of TRPV1 may play an important role in regulating cough reflex (Lee et al., 2011) and airway disease (Wortley et al., 2016).

1.3- Endocannabinoids (eCBs):

The successful identification and cloning of the CB_1R elicited the discovery of its first endogenous agonist, N-arachidonoylethanolamine, better known as anandamide or AEA (Devane et al., 1992). Followed by the discovery of another cannabinoid receptor interacting endogenous molecule, 2-arachidonoylglycerol or 2-AG, as AEA could not fully reproduce the effects induced by THC administration (Sugiura et al., 1995; Mechoulam et al., 1995). The majority of the studies on the ECS focuses its attention on these two eCBs, despite the existence of other CB_1R interacting peptides and a series of AA derivatives that generate endocannabinoid-like effects (Di Marzo and De Petrocellis, 2012).

These two well-studied eCBs have been pharmacologically characterized and were found to own distinct properties towards CB_1R. AEA yielded to be a high-affinity molecule, that acts as partial agonist of CB_1R, and almost inactive at CB_2R; whereas 2-AG acts as a full agonist at both receptors with moderate to low affinity (Pertwee, 2010; Di Marzo and De Petrocellis, 2012).

Interestingly, both eCBs counteract with many other receptors. Among those, TRPV1 receptor, which is activated by AEA, is the best documented for its significant role in synaptic transmission and pain regulation, whereas the interaction of 2-AG and non-cannabinoid receptors has emerged more recently (Di Marzo and De Petrocellis, 2012).

Even though, these two eCBs have significant differences in terms of receptor selectivity, both are produced on demand in the postsynaptic zone in response to an increased intracellular calcium concentration (Katona and Freund, 2008; Kano et al., 2009; Castillo et al., 2012). Nonetheless, AEA and 2-AG are synthesized, transported and metabolized on a different way. The biosynthesis of AEA from its precursor, N-arachidonoyl-phosphatidylethanolamine (NAPE), is launched upon neuronal depolarization or activation of ionotropic receptors, and is catalysed from NAPE by a specific phospholipase D (NAPE-PLD). 2-AG, in contrast, is originated from the metabolism of triacylglycerols by the activity of diacylglycerol lipase (DAGL) α or β, in response to activation of metabotropic receptors coupled to the 1-Phosphatidylinositol-4,5-bisphosphate phosphodiesterase beta enzyme (PLCβ) such as group I metabotropic glutamate receptors (mGluR1/5) or muscarinic acetylcoline type 1 (M1) or type 3 (M3) receptors (Araque et al., 2017). Formation of NAPE and DAG precursors is the calcium-sensitive and restricting step in eCB production. These compounds are converted from phosphatidyl-ethanol-amine by N-acyltransferase and phosphoinositides by phospholipase C, respectively (Pacher et al., 2006; Murataeva et al., 2014).

Once synthetized, the eCBs are released from postsynaptic neurons to the synaptic cleft but due to their uncharged hydrophobic nature, endocannabinoids are unable to diffuse freely like other neurotransmitters, and although it has not been yet identified, several models have been proposed to elucidate the transport of AEA (Nicolussi and Gertsch, 2015). For instance, simple diffusion generated by differences in concentration gradients generated from enzymatic degradation, endocytosis involving caveolae/lipid rafts or through transport proteins such as fatty acid binding proteins or heat shock protein 70 (HSP70) (Kano et al. 2009). For the case of 2-AG, same transport systems as AEA have been proposed, but it is not well understood either (Huang et al., 2016). After eCBs are taken up by neurons, these can be metabolized through hydrolysis or oxidation. AEA is degraded by fatty acid amide hydrolase (FAAH) into free AA and ethanolamine (Ahn et al., 2008; Di Marzo, 2009), while 2-AG is mostly hydrolyzed by monoacylglycerol lipase (MAGL) into arachidonic acid and glycerol (Blankman et al., 2007; Rouzer and Marnett, 2011). Other enzymes like α/β-Hydrolase domain-containing 6 (ABHD6) are also involved but in a minor proportion (Dinh et al., 2002; Marrs et al., 2010).

As mentioned before, eCBs are synthetized on demand in postsynaptic neurons in response to physiological or pathological stimuli (Kano et al., 2009; Castillo et al., 2012; Katona and Freund, 2012; Araque et al., 2017). Even though, there is also evidence that both 2-AG activating postsynaptic CB_1R or CB_2R and AEA through TRPV1 can act in a non-retrograde manner (Castillo et al., 2012). Furthermore, eCBs released by neurons can modulate presynaptic and postsynaptic circuits through the activation of CB_1R expressed on astrocytes (Navarrete et al., 2014; Metna-Laurent and Marsicano, 2015) (figure 5).

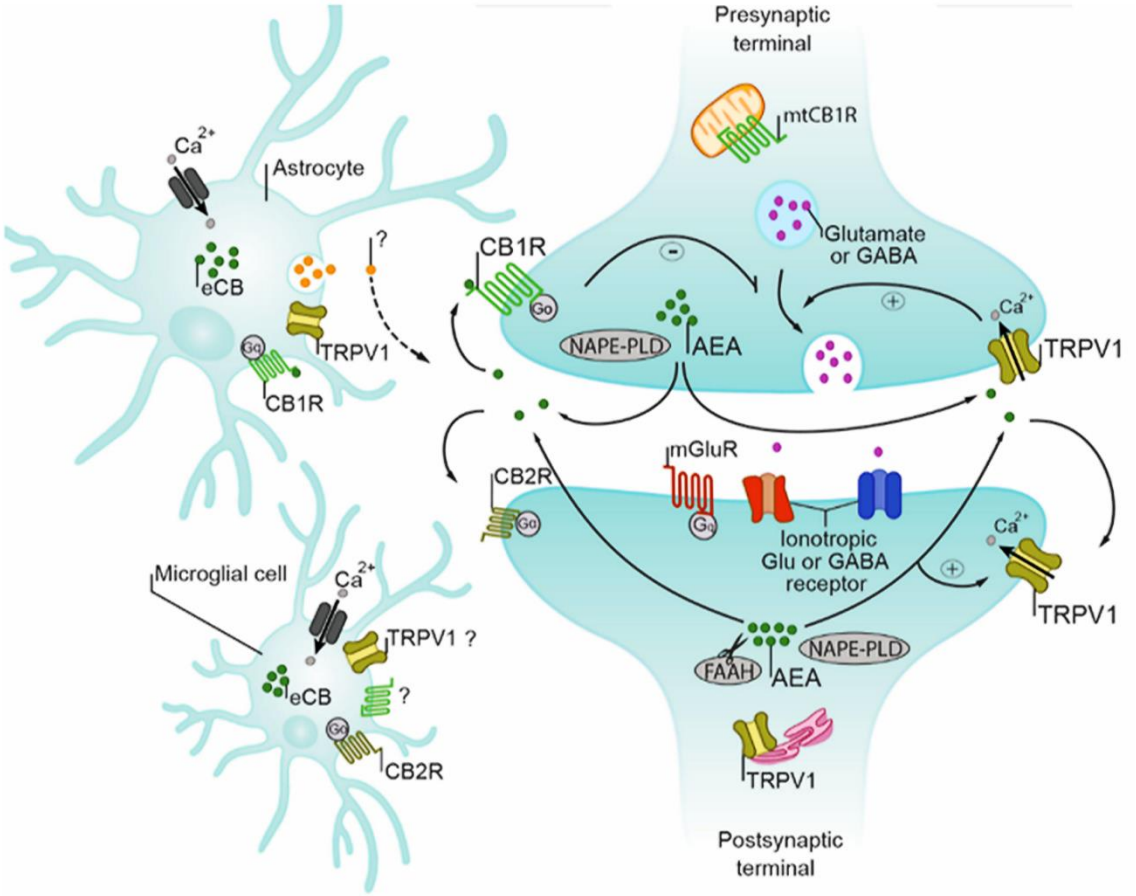

Figure 5: Representative image of ECS compounds distribution in neurons and glial cells. Arrows represent the role of TRPV1 in eCB signalling. AEA may serve as an endogenous ligand for both CB_1R and TRPV1, with activation of CB_1R on presynaptic terminals leading to attenuated transmitter release. Activation of TRPV1 leads to enhanced transmitter release (if expressed presynaptically) or promotes depolarization of the postsynaptic terminal (if expressed postsynaptically). The relative roles of TRPV1 and CB_1R on glutamatergic versus GABAergic terminals may depend on the concentration of the ligand. Obtained from Patel et al., 2017.

1.4- Hippocampal formation:

The hippocampal formation (HF) consists of the hippocampus proper and the neighbouring areas from the brain cortex that connect with it. The hippocampus proper includes the 'cornu ammonis' (CA) fields: the most studied are CA1 and CA3 fields and the smaller, less investigated, CA2 field. Altogether, the hippocampal formation is formed by the entorhinal cortex (EC),

divided into lateral and medial EC, dentate gyrus (DG), CA1, CA2, CA3, subiculum, presubiculum and parasubiculum.

The hippocampal formation and its connections are quite unique and allowed a good identification of the elements present in the circuitry (Cajal, 1955). When compared with neocortex, the simplicity of the hippocampus encouraged the early researchers of memory to study synaptic plasticity (Bliss and Lomo, 1973) and functional capacities (Marr, 1971; Gardner-Medwin, 1976). Remarkably, one of the features that makes unique this structure is that it contains largely unidirectional projections, a crucial detail for those early experiments (Andersen et al., 2006) (figure 6). The main projection from cortical areas that enters the information into the hippocampus comes from the superficial layers of the EC forming the well-known perforant path (PP), whereas the deep layers and the subiculum provide the necessary output from the hippocampus to the rest of the brain (Harley et al., 2014).

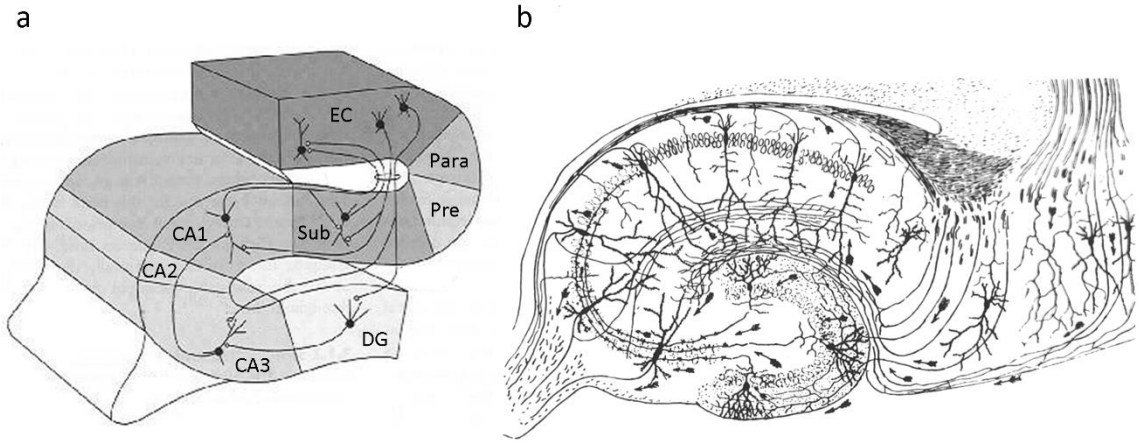

Figure 6: Representatives images of the hippocampal organization. a) Schematic representation of the hippocampal main connectivity. b) Cajal's drawing of the human hippocampus. Modified from Hippocampus anatomy by David S. Touretzky, 2015.

The PP is commonly subdivided in the lateral perforant path (LPP) and the medial perforant path (MPP) that project from the lateral and medial EC, respectively (Hjorth-Simonsen, 1972) (figure 7). These two PP parts show differences in the anatomical organization. Hence, Timm's stained brain sections showed denser staining in the LPP than MPP (West and Andersen, 1980; Fredens, 1981) and Witter and colleagues (1989) found differences in physiology and histochemical organization.

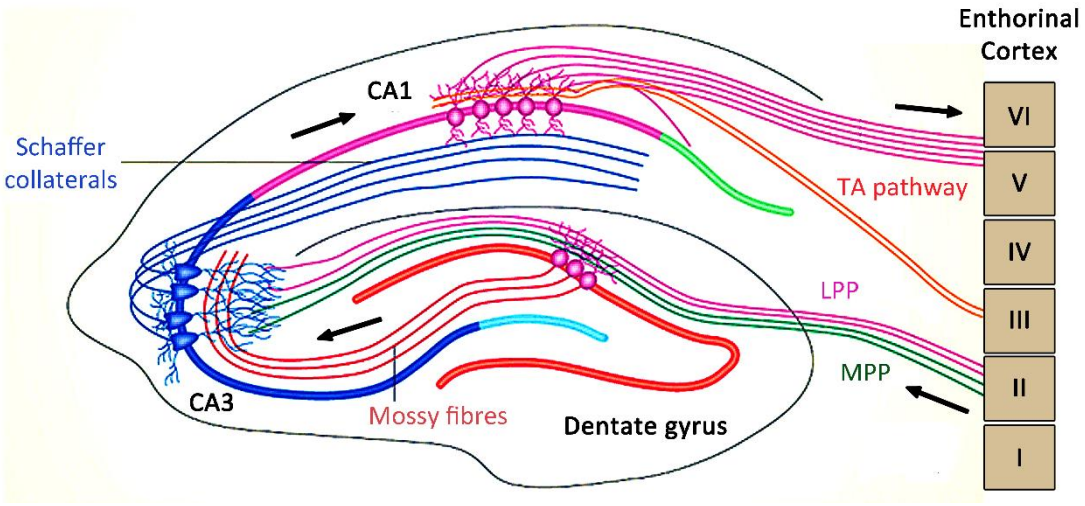

Figure 7: The hippocampal circuitry. The dentate gyrus (DG) receives most of its inputs from layer II of the entorhinal cortex through the medial and lateral perforant path (MPP and LPP, respectively). The axons of the granule cells extend towards the pyramidal cells of the cornu ammonis (CA) 3 region, forming the glutamatergic mossy fibres. The projections of the CA3 pyramidal cells form the Schaffer collaterals, which make excitatory synapses with CA1 pyramidal cell dendritic spines. Finally, CA1 neurons complete the hippocampal circuitry by projecting their axons to the deep layers of the entorhinal cortex. CA1 also receives direct input from layer III of the entorhinal cortex through the temporoammonic pathway (TA). Obtained from Pinar et al., 2017.

1.4.1- ECS and dentate gyrus:

The dentate gyrus (DG) is composed primarily of the glutamatergic granule cells (GC), and differs from other hippocampal areas because it contains an additional glutamatergic cell type, the mossy cells. Mossy cells are termed for their characteristic 'mossy' appearance after being stained with the Golgi technique, which also reveals clusters of complex spines on their proximal dendrites, known as thorny excrescences. Mossy cells have been shown to be implicated in numerous pathological conditions, but their physiological functions remain unclear (Scharfman, 2016).

The granule cells are oriented in a stereotypical manner. Thus, their dendrites are in the molecular layer (ML) and their cell bodies form the adjacent granule cell layer (GCL). Between the GCL and CA3, there is a polymorphic layer called the hilus, which contains the mossy cells. The molecular layer is subdivided into the outer molecular layer (OML), the middle molecular layer (MML) and the inner molecular layer (IML). This anatomical organization is similar in rodents and primates (Scharfman, 2016). The main cortical input that enters into the DG comes from the glutamatergic PP arising in the entorhinal layer II. This projection is responsible for most of the afferent inputs to the OML (LPP) and MML (MPP) (Steward and Scoville, 1976; Amaral et al., 2007; Witter, 2007). Furthermore, the axons of the hilar mossy cells are the

primary afferents to the IML (Ribak et al., 1985; Buckmaster et al., 1996; Scharfman and Myers, 2013). The GC axons (mossy fibres) project to the CA3 pyramidal neurons and send collaterals to the mossy cells (Amaral et al., 2007).

Concerning the ECS, several studies have demonstrated the immunohistocheminal localization of the major metabotropic and ionotropic receptors in the brain and appear to be co-expressed in membranes of cell bodies, axons and dendrites of several brain regions. Indeed, two general patterns of neuronal CB_1/TRPV1 localization were observed, one in which both receptors expression is overlapped in plasma membranes and perinuclear compartments, and another where the two receptors are co-expressed on perikaryal membranes and cell processes (perisomatic and axonal labelling). The first pattern was in interneurons of the hippocampal formation, thalamic and hypothalamic neurons and in neurons of the cerebellar nuclei. The second distribution pattern was usually found in hippocampal pyramidal neurons, basal ganglia neurons, Purkinje cells and ventral periaqueductal gray (PAG) neurons (Cristino et al., 2006). The HF is one of the structures with the highest CB_1R immunoreactivity in the brain. Several studies have described the CB_1R pattern in the hippocampus (Herkenham et al., 1990; Mailleux and Vanderhaeghen, 1992; Matsuda et al., 1993; Tsou et al., 1998; Marsicano and Lutz, 1999; Egertova and Elphick, 2000; Katona et al., 2006; Kawamura et al., 2006; Ludanyi et al., 2008; 2011; Katona and Freund, 2008; 2012; Steindel et al., 2013; Hu and Mackie, 2015). CB_1R localization is mostly, but not exclusively, in membranes of GABAergic and glutamatergic presynaptic axon terminals (Gutierrez-Rodriguez et al., 2017), being highly expressed in the glutamatergic mossy cell terminals in the IML and to a lesser extend in the rest of the ML (Kawamura et al., 2006; Monory et al., 2006; Katona and Freund, 2008; 2012). Also, CB_1Rs are localized in astrocytic processes (Bosier et al., 2013; Gutierrez-Rodriguez et al., 2018) and mitochondrial membranes of the hippocampus (Benard et al., 2012; Hebert-Chatelain et al., 2014a,b).

With respect to TRPV1, immunohistocheminal studies revealed its localization in synapses mainly, but not exclusively, in postsynaptic dendritic spines of several rat central neurons (Tóth et al., 2005). Furthermore, using a highly sensitive preembedding immunogold method for electron microscopy, TRPV1 was shown at inhibitory and excitatory synapses in the dentate gyrus (Canduela et al., 2015; Puente et al., 2015). Hence, about 30% of the inhibitory synapses are TRPV1 immunopositive in the ML being mostly localized perisynaptically at postsynaptic dendritic membranes receiving symmetric synapses in the IML (Canduela et al., 2015). As to its presence at excitatory synapses, TRPV1 immunopaticles are highly concentrated in postsynaptic

dendritic spines receiving PP synaptic terminals in the outer 2/3 of the ML (Puente et al., 2015). Finally, our laboratory has very recently demonstrated the presence TRPV1 in presynaptic CA1 Schaffer collateral terminals (Bialecki et al., 2020) which confirms previous reports describing similar presynaptic TRPV1 localization in other brain areas (Marinelli et al., 2002; Musella et al., 2009; Kawahara et al., 2011). Also, we observed a high accumulation of TRPV1 particles in the cytoplasm of granule cells (Canduela et al., 2015) as shown in several brain regions (Tóth et al., 2005; Cristino et al., 2006; 2008). However, it is not yet clarified the role of intracellular TRPV1: there might be involved in calcium release from intracellular stores required for glutamatergic synaptic plasticity (Chávez et al., 2010) and mitochondrial viability (Athanasiou et al., 2007).

Concerning possible functional interactions between CB_1 and TRPV1 receptors, some authors have previously shown functional cross talks between both receptors when they are expressed in the same cell. For example, CB_1 and TRPV1 activation exerts opposing effects on intracellular calcium concentrations (Szallasi and Di Marzo, 2000). Thus, some dual agonists, like AEA or NADA, can cause opposite effects on neurotransmitter release depending on the activated receptor. This has been already demonstrated in the substantia nigra pars compacta for glutamate release (Marinelli et al., 2003). In the hippocampus, activation of CB_1 and TRPV1 receptors also elicits opposing effects on both excitatory and inhibitory neurotransmission in principal neurons and interneurons, respectively (Tahmasebi et al., 2015). The data suggest that the opposing actions occur for GABA in the context of paired-pulse depression (Al-Hayani et al., 2001). *In vivo* administration of AEA and NADA can also produce similar behavioural effects through both receptors, i.e., hypolocomotion due to the co-localization of CB_1 and TRPV1 receptors in the basal ganglia (Di Marzo et al., 2001; de Lago et al., 2004). The co-localization of both receptors in brainstem nuclei controlling emesis (area postrema and nucleus of the solitary tract) may explain the potent anti-emetic effects of dual agonists (Sharkey et al., 2007).

It is likely, therefore, that interactions between CB_1 and TRPV1 receptors expressed in the same cell might promote reciprocal influences on gene expression. In fact, TRPV1 expression decreased in the DG and increased in the cerebellar granule cell layer in CB_1R-deficient mice (Cristino et al., 2006) suggesting that CB_1Rs exert a basal regulation over TRPV1 expression.

1.5- ECS and synaptic plasticity:

Synaptic plasticity is an essential process occurring in the brain for the adaptation and learning relative to experiences of neuronal circuits. It is also an indicative of normal brain functioning. From embryonic phase to adulthood, environmental stimuli provoke changes of synaptic function and individual experiences are imperative for learning new memories, develop new abilities or generate new conducts that would end in a better adaptation. The ECS has demonstrated to participate as a key modulator of synaptic transmission; thus, its participation in synaptic plasticity is undeniable.

Synaptic transmission regulation produced by eCB mobilization occurs both in the short and long term. Those synaptic changes that occur within seconds are eCB-mediated short-term changes and include depolarization-induced suppression of excitation (DSE) and inhibition (DSI) depending on whether eCBs affect glutamatergic or GABAergic terminals, respectively (Kano et al., 2009; Castillo et al., 2012). Long-term synaptic changes, those occurring from minutes to hours, can occur in response to different forms of pre- or postsynaptic activity also in both types of terminals (Araque et al., 2017). Therefore, eCBs are powerful mediators of synaptic function through the brain and have proved to be able to modulate a number of brain functions, including cognition, motor control, emotion, reward and feeding behaviours. Dysregulation of the ECS has been linked to neuropsychiatric disorders, such as depression, autism, schizophrenia, addiction, stress or anxiety (Hillard et al., 2012; Mechoulam and Parker, 2013; Parsons and Hurd, 2015; Volkow et al., 2017).

eCBs regulate synaptic function through activating CB_1Rs in GABAergic and glutamatergic terminals (Kano et al., 2009; Castillo et al., 2012). Within the HF, as CB_1Rs are mostly expressed at inhibitory terminals (Freund et al., 2003), eCBs exert a robust effect on inhibition, decreasing GABA release in a short-term (Wilson and Nicoll, 2001) or long-term manner by triggering long-term depression (LTD) of inhibition (iLTD) (Chevaleyre and Castillo, 2003). This inhibition of GABA release can profoundly affect the excitatory-inhibitory balance in the circuitry and contribute to associative learning (Letzkus et al., 2015). When interneuron are inhibited, eCBs facilitate the generation of excitatory long-term potentiation (LTP) at Schaffer collateral (SC)-CA1 pyramidal cell synapses (SC-CA1) (Carlson et al., 2002; Chevaleyre and Castillo, 2004).

In the circuit formed between the EC and the HF, eCBs have been implicated in input-timing-dependent plasticity (Xu et al., 2012; Basu et al., 2013), a form of heterosynaptic plasticity at SC-

CA1 synapses that is generated by pairing SC and PP inputs from the EC (Dudman et al., 2007). This plasticity involves both eCB-iLTD from cholecystokinin (CCK) positive interneuron (CB_1 positive) and the previously mentioned SC-CA1 LTP (Carlson et al., 2002; Chevaleyre and Castillo, 2004; Basu et al., 2013). Precise timing of both SC inputs onto CCK interneurons and PP inputs to postsynaptic CA1 pyramidal cells is needed for this plasticity. Presynaptic eCB-iLTD of feedforward inhibition in CCK interneurons may facilitate activation of CA1 pyramidal cells (Basu et al., 2013). In the mouse neocortex, eCBs mediate spike timing-dependent LTD at excitatory synapses (eLTD), which is typically induced by pairing induction protocols (Caporale and Dan, 2008; Heifets and Castillo, 2009). A form of eCB mediated LTD was also found in the nucleus accumbens (Grueter et al., 2010) and in the bed nucleus of the stria terminalis (BNST) (Puente et al., 2011). eCB-mediated short-term plasticity (DSI/DSE) is based on the CB_1R-mediated inhibition of presynaptic calcium influx through voltage-gated calcium channels (Kano et al., 2009).

How CB_1R activation leads to long-lasting suppression of transmitter release (eCB-LTD) still needs to be understood (Castillo et al., 2012; Araque et al., 2017). In the mouse DG, our group recently found a long-lasting CB_1R-dependent depression of MPP-GC excitatory synapses (Peñasco et al., 2019). The stimulation protocol used for eCB-eLTD induction in this work was previously used to consistently induce eCB-dependent eLTD in other brain regions such as prefrontal cortex or BNST (Lafourcade et al., 2007; Puente et al., 2011). In this form of plasticity, the magnitude of eCB-eLTD was unchanged after bath application of the NMDA receptor antagonist D-APV. This suggests that, unlike in other synapses, NMDA receptors are not involved in this form of eCB-eLTD at the MPP synapses (Bender et al., 2006; Sjöström et al., 2003). We further found that this LTD was 2-AG dependent through activation of presynaptic CB_1Rs located on excitatory terminals (Peñasco et al., 2019). Interestingly, although the CB_1R expression in the IML is very high in glutamatergic terminals due to the excitatory input coming from the hilar mossy cells (Katona et al., 2006; Kawamura et al., 2006; Monory et al., 2006; Gutiérrez-Rodríguez et al., 2017), the stimulation protocol inducing eCB-eLTD at the MPP synapses was unable to induce eCB-eLTD at mossy cell-granule cell synapses (Chiu and Castillo, 2008; Peñasco et al., 2019).

Within the DGML, other forms of synaptic plasticity have been characterized. For instance, the TRPV1-dependent LTD at the MPP synapses was shown to require mGluR5 activation, but not mGluR1, increased AEA synthesis and involved postsynaptic AMPA receptor internalization

(Chávez et al., 2010). A similar TRPV1-LTD was induced by the same stimulation protocol in the BNST, which also required activation of postsynaptic mGluR5 receptors (Puente et al., 2011).

Studies have shown that eCBs can also mediate LTP by unconventional mechanisms in both the hippocampus and neocortex. Thus, at the SC-CA1 synapses, eCBs trigger LTP of glutamate release through stimulation of the astrocyte-neuron signalling (Navarrete and Araque, 2008; Gomez-Gonzalo et al., 2015). In the DG, high frequency LPP stimulation *in vitro* triggers a presynaptic form of LTP that requires postsynaptic NMDAR and mGluR5-dependent calcium rise, postsynaptic 2-AG mobilization and activation of presynaptic CB_1Rs (Wang et al., 2016). How exactly CB_1R activation leads to a long-lasting increase in glutamate release is unclear but it could involve reorganization of the presynaptic actin cytoskeleton in LPP terminals (Wang et al., 2018).

Species	Synapse type	Induction protocol	Induction requirement	Reference
Rat	MCF inputs to dentate granule cells (DGC)/ (MCF-DGC synapses)	Depolarization step (from −70 mV to o mV) of 3-s	eCB-DSE, calcium-dependent, modulated by cholinergic and group I mGluRs, DAGL independent	Chiu and Castillo-2008
Rat	MCF inputs to DGC/(MCF-DGC synapses)	Theta-burst stimulation or high frequency stimulation or spike-timing dependent plasticity	No eCB-LTD	Chiu and Castillo-2008
Rat	GABAergic inputs to DGC/(GABAergic-DGC synapses)	Depolarizing step of 1–3 s or a series of short (500 ms) repetitive depolarizations	eCB-DSI, calcium dependent, involves ryanodine receptor (RyR)-mediated Ca2+ release	Isokawa and Alger-2005
Rat	GABAergic inputs to hilar mossy cells (HMC)/ (GABAergic-HMC synapses)	Depolarization step of 5-s	eCB-DSI, confined to very small spaces (e.g., ≤20 µm), Ca2+ dependent and facilitated by activation of mAChRs	Hofmann et al. (2006)
Rat, mouse	MPP inputs to DGC/(MPP-DGC synapses)	Brief postsynaptic depolarizations (1 Hz)	Anandamide-mediated TRPV1-LTD in a CB1 receptor-independent manner, Ca2+ calcineurin and clathrin-dependent internalization of AMPA receptors	Chávez et al., (2010)
Rat, mouse	LPP inputs to DGC/(LPP-DGC synapses)	2 trains of 100 Hz, each lasting 1s	2-AG-mediated CB1-LTP via small GTPases and the assembly of latrunculin A-sensitive actin filaments	Wang et al. (2016)
Rat, mouse	LPP inputs to DGC/(LPP-DGC synapses)	1 or 2 trains of 100 Hz, lasting 1s	2-AG-mediated CB1-LTP involving β1 integrins and presynaptic actin regulatory signaling	Wang et al. (2018)
Mouse	MPP inputs to DGC/(MPP-DGC synapses)	1 train of 10 Hz, lasting 10 min	eCB-LTD, is group I mGluR-dependent and requires intracellular calcium influx and 2-AG synthesis	Peñasco et al. (2019)

Table 1: Different forms of eCB dependent-synaptic plasticity in DG glutamatergic and GABAergic synapses. Adapted from Peñasco et al., 2019.

1.6- ECS and epilepsy:

Epilepsy is a common neurological condition that affects approximately 1 % of the adult population (Hauser and Hesdorffer, 1990) and diverse groups of seizure disorders are included, varying in their onset region, age, pathophysiological symptoms, and underlying mechanisms. Generally, half of the epileptic disorders are classified as acquired epilepsy (AE), where an insult in the brain, such as stroke, status epilepticus (SE) or head trauma, results in a permanent neuronal plasticity shift (Hauser and Hesdorffer, 1990). Although epilepsies can be subdivided into many different pathological disorders, all of them come along with spontaneous recurrent seizures (SRS) discharges, resulting from the synchronous firing of a certain neuronal population due to an imbalance between excitatory and inhibitory neuronal transmission (Lothman et al., 1991; Scharfman, 2007; Badawy et al., 2009a; 2009b). In recent years, although there are a wide range of antiepileptic drug (AED) treatments available, it has been predicted that between 25% and 40% of newly diagnosed epileptic patients will suffer from refractory seizures resistant to current therapies (Schmidt and Sillanpaa, 2012). This is the reason why it is emphasized the need for new therapeutic targets in this disease for a better control of seizures (Wilcox et al., 2013). As already stated before, ECS plays a key role in the brain through its modulation of several processes in both physiological and pathological conditions (Di Marzo et al., 1998; Alger, 2006; Mackie and Stella, 2006; Kano et al., 2009; Castillo et al., 2012). Taking into account that SRS display intermittent activity, it is suggested that a transient dysregulation of synaptic transmission within either a certain brain region (focal seizures) or affecting more than one brain region (generalized seizures) takes place. Many studies have focused their attention on understanding the potential role that the ECS function and dysfunction could have controlling or provoking epileptic seizure discharge (Blair et al., 2015).

Animal models have demonstrated that activation of CB_1Rs decreases seizure severity. Conditional mutant mice lacking CB_1Rs in principal forebrain excitatory neurons (but not in interneurons) showed more severe kainate (KA)-induced seizures compared to wildtype controls (Marsicano et al., 2003). In the hippocampus, CB_1R expression in hippocampal glutamatergic, but not GABAergic inputs, was necessary and sufficient to protect against KA-induced seizures (Monory et al., 2006). Furthermore, overexpressing CB_1Rs with viral vectors resulted in a reduced KA-induced seizure severity in the hippocampus and reduced mortality (Guggenhuber et al., 2010). Together, these results demonstrate that CB_1Rs could control epileptic seizures and protect neurons from resulting cell death and reactive gliosis (Rosenberg et al., 2015). In addition, TRPV1 activation was found to inhibit calcium influx and decrease GABA

release from hippocampal synaptosomes, consequently increasing the excitability of pyramidal cells (Kofalvi et al., 2006; Gibson et al., 2008). However, activation of presynaptic TRPV1 inhibited CA1 pyramidal neurons by enhancing the GABAergic trasnsmission (Al-Hayani et al., 2001; Kofalvi et al., 2006). The increased epileptiform activity and hyperexcitability in the hippocampus after TRPV1 agonist stimulation was suppressed by vanilloid receptor antagonists (Chen et al., 2007; Bhaskaran and Smith, 2010; Gonzalez-Reyes et al., 2013). Furthermore, the pro-convulsant activity of the TRPV1 agonist capsaicin (CAP) was blocked by the antagonist capsazepine (CPZ) which was also able to prevent pentylenetetrazole (PTZ)-induced seizures (Manna and Umathe, 2012) as it occurs in TRPV1 knockout (TRPV1-KO) mice (Kong et al., 2014). Interestingly, the TRPV1 expression significantly increased in the hippocampus and cortex of rodents and patients with temporal lobe epilepsy (Bhaskaran and Smith, 2010; Sun et al., 2013). Altogether, these data suggest that hippocampal TRPV1 plays an important role in epilepsy with TRPV1 activation accelerating epileptogenesis while TRPV1 antagonism having beneficial effects (Fu et al., 2009).

2- Working hypothesis

More than two decades have passed since the two main cannabinoid receptors (CB_1R and CB_2R) and their mediating pharmacological mechanism were identified (Matsuda, 1997; Howlet and Mukhopadhyay, 2000). In addition, numerous cannabinoid effects have been described and well characterized, both at central and peripheral tissues. Nevertheless, some of the pharmacological actions could not be explained only by the activation of these two receptors, since in cell lines or mutant mice lacking genes of one or both receptors, several cannabinoid-like actions were found. In line with this, cannabinoids have been shown to modulate ligand-gated ion channels and ion-transporting membrane proteins (De Petrocellis et al., 2017), thereafter been named as ionotropic cannabinoid receptors (ICRs) (Akopian et al., 2009).

Within ionotropic cannabinoid receptors (ICRs), the members from the family of transient receptor potential (TRP) channels play a major role compared to others, including channels from TRPV, TRPM and TRPA subfamilies (De Petrocellis et al., 2017). These channels regulate the transmembrane flux of cations throw electrochemical gradients, increasing intracellular concentrations of calcium and sodium (Montell, 2005). One of the first channels identified in mammalian cells, and therefore one of the most extensively investigated, was TRPV1 (Nilius and Szallasi, 2014). Numerous evidence have outlined the complexity of the interactions between this channel and the cannabinoid receptors, defining them as bidirectional, inhibitory or excitatory, acute or chronic, that happen at the ultrastructural level affecting also functionality (Zador and Wollemann, 2015).

In the dentate gyrus molecular layer, CB_1 receptors are present in glutamatergic and GABAergic synaptic terminals, mainly presynaptically but not exclusively, and in astrocytes (Gutierrez-Rodriguez et al., 2017; Bonilla-Del Río et al., 2019), and TRPV1 receptors are mainly postsynaptic at glutamatergic and GABAergic synapses (Puente el al., 2015; Canduela et al., 2015). Moreover, both CB_1 and TRPV1 receptors mediate different types of synaptic plasticity in DGML (Chavéz et al., 2011; 2014; Peñasco et al., 2019). Taking into account that also both receptors interact with some same molecules, our working hypothesis in this thesis work was that the absence of either receptor should be accompanied by some compensatory mechanisms in the structure of the endocannabinoid system that should have an impact on the information processing by neural circuits in physiological conditions.

We tested this hypothesis in a mouse model carrying the genetic deletion of TRPV1. We have made use of biochemical tools to determine protein expression of the endocannabinoid system, immunohistochemical analysis for keeping up ultrastructural rearrangements in CB_1 receptor

distribution, electrophysiological evaluation of synaptic transmission and plasticity, and behavioural tests to assess hippocampal-linked behaviours. Finally, we have also evaluated the response of the TRPV1-KO mice to the KA-induced model of epilepsy.

3- Objectives

The main goal of this work was to determine the impact of the genetic ablation of the TRPV1 receptor on the CB_1R expression and function in the DGML. For this investigation, we planned an interdisciplinary strategy combining a wide range of techniques of molecular biology, biochemistry, anatomy, electrophysiology and behaviour.

The specific objectives of the doctoral thesis were to:

1. Analyse the overall expression pattern of compounds of the endocannabinoid system in the hippocampus of TRPV1-KO mice by an immunoperoxidase method for light microscopy and western blot analysis.
2. Establish the CB_1R distribution in cellular and subcellular locations in the dentate gyrus molecular layer of TRPV1-KO mice by means of an immunogold method for electron microscopy.
3. Characterize changes in synaptic plasticity and their mechanisms in the dentate gyrus molecular layer of TRPV1-KO mice by field excitatory post-synaptic currents electrophysiology.
4. Assess hippocampal-related behaviours in TRPV1-KO mice by behavioural tests.
5. Evaluate the effect of the kainic acid model of excitotoxic seizures in TRPV1-KO mice.

4- Materials and Methods

4.1- Animals:

The experiments were performed in the *Laboratory of Ultrastructural and Functional Neuroanatomy of the Synapse*, Department of Neurosciences, University of the Basque Country UPV/EHU. All protocols were approved by the Committee of Ethics for Animal Welfare of the University of the Basque Country (CEEA/M20/2015/105; CEIAB/M30/2015/106) and were in accordance to the European Communities Council Directive of 22nd September 2010 (2010/63/EU) and Spanish regulations (Real Decreto 53/2013, BOE 08-02-2013). All efforts were made to minimize pain and suffering and to reduce the number of animals used. Adult male TRPV1$^{-/-}$ mice aged 6–8 weeks and their wild type littermates (WT) were used to perform experiments. These mice were derived from heterozygous breeding pairs generated by crossing of B6.129X1-Trpv1tm1Jul/J mice (The Jackson Laboratory) with C57BL/6j mice (Janvier-labs) in the animal facilities located in the campus of Leioa (EHU/UPV). Every animal used was genotyped in the General Service "Genomics and Proteomics" of the University.

Mice were housed in pairs or groups of maximum three littermates in standard Plexiglas cages (17 cm × 14.3 cm x 36.3 cm) and before experiments were conducted, they were allowed to acclimate to the environment for at least 1 week. Animals were maintained at standard conditions with food and tap water ad libitum throughout all experiments and in a room with constant temperature (22 °C). Mice were kept in a 12 h: 12 h light/dark cycle with lights off at 9 p.m. Behavioural experiments were conducted during the light phase of mice between 9:30 a.m. and 3 p.m.

4.2- Antibodies:

The primary antibodies were used in combination with the corresponding secondary antibodies for the techniques of: immunoperoxidase for light microscopy (LM); combined preembedding silver intensified immunogold and immunoperoxidase for electron microscopy (EM) and western blotting (W.B).

4.2.1- Primary antibodies: (TABLE 1)

Antibody	[Concentration]	Manufacturer; species; catalogue number; RRID
Anti-cannabinoid receptor type-1 (CB_1)	2 µg / ml IHC	Frontier Institute co., ltd; goat polyclonal; CB1-Go-Af450; AB_2571592
Anti-cannabinoid receptor type-1 (CB_1)	0.2 µg / ml W.B	Frontier Institute co., ltd; rabbit polyclonal; CB1-Rb-Af380; AB_2571591
Anti-glial fibrillary acidic protein (GFAP)	20 ng/ ml IHC	Sigma-Aldrich; mouse monoclonal; G3893; AB_257130
Anti-Gephyrin	4 µl/ ml IHC	Synaptic Systems; mouse monoclonal; 147021; AB_2232546
Anti-monoacylglycerol lipase (MAGL)	2 µg/ ml IHC 0.2 µg/ ml W.B	Frontier Institute co, ltd; rabbit polyclonal; MGL-Rb-Af200; AB_2571798
Anti-diacylglycerol lipase alpha (DAGLα)	2 µg/ ml IHC 0.2 µg/ ml W.B	Frontier Institute co, ltd; rabbit polyclonal; DGLa-Rb-Af380; AB_2571691
Anti- N-acetylphosphatidylethanolamine-hydrolysing phospholipase D (NAPE-PLD)	4 µg/ ml IHC 0.2 µg/ ml W.B	Frontier Institute co, ltd; guinea pig polyclonal; NAPE-PLD-Gp-Af720; AB_2571806
Anti-fatty acid amide hydrolase (FAAH)	1 µg/ ml IHC 0.2 µg/ ml W.B	Cayman Chemical; rabbit polyclonal; 101600-1; AB_327842
Anti-CNRIP1 (Y-12)	0.4 ng / µl W.B	Santa Cruz Biotechnology; rabbit polyclonal; sc-137401; AB_10709018
Anti-Go	0.04 ng/ µl W.B	Santa Cruz Biotechnology; rabbit: K-20; AB_2314438
Anti-Gi1	0.2 ng/ µl W.B	Santa Cruz Biotechnology; rabbit polyclonal; sc-391, AB_2247692

Anti-Gi2	0.2 ng/ µl W.B	Santa Cruz Biotechnology; rabbit polyclonal; sc-7276, AB_2111472
Anti-Gi3	4 pg/ µl W.B	Santa Cruz Biotechnology; rabbit polyclonal; sc-262, AB_2279066
Anti-actin	0.2 µg/ ml W.B	Sigma-Aldrich; rabbit polyclonal; A2066; AB_476693
Anti-PLC β	42 pg/ µl W.B	BD Biosciences; mouse monoclonal; 610924, AB_398239

4.2.2- Secondary antibodies: (TABLE 2)

Antibody	[Concentration]	Manufacturer; species; catalogue number; RRID
Biotinylated anti-mouse secondary antibody	7.5 µg/ ml ICH	Vector Labs; BA-2000; AB_2313581
Biotinylated anti-goat secondary antibody	7.5 µg/ ml ICH	Vector Labs; BA.5000; AB_2336126
Biotinylated anti-rabbit secondary antibody	7.5 µg/ ml ICH	Vector Labs; BA-1000; AB_2313606
1.4 nm gold-conjugated anti-goat IgG (Fab' fragment) antibody	0.8 µg/ ml ICH	Nanoprobes Inc; rabbit polyclonal; Cat-2005; AB_2617133
Goat anti-guinea pig IgG HRP conjugated	1 ng/ ml W.B	Bioss; bs-0358G; AB_10860553
Goat anti-rabbit IgG HRP conjugated	1 ng/ ml W.B	Cell Signalling Technology; 7074; AB_2099233
Rabbit anti-goat IgG HRP conjugated	1 ng/ ml W.B	Sigma-Aldrich; rabbit polyclonal; A5420, AB_258242
Sheep anti-mouse IgG HRP conjugated	1 ng/ ml W.B	GE Healthcare; sheep; NA9310, AB_772193

4.3- Drugs:

All drugs for electrophysiology were dissolved in dimethyl sulfoxide (DMSO; Sigma-Aldrich) and were added at the final concentration to the superfusion medium (Table 3).

Kainic acid (KA) was dissolved in 0.9% sodium chloride (saline) for dosage preparation in intrahippocampal administrations.

4.3.1- Electrophysiology drugs: (TABLE 3)

Drug	Description	Concentration of use	Incubated time	Supplier
Picrotoxin (PTX)	$GABA_A$ receptor antagonist	[100 µm]	All recording	Tocris BioScience (Bristol, United Kingdom)
AM251	Potent CB_1 antagonist and GPR55 agonist	[4 µm]	20 min of additional incubation	Tocris BioScience (Bristol, United Kingdom)
WIN 55.212-2	Potent cannabinoid receptor agonist	[5 µm]	20 min of additional incubation	Tocris BioScience (Bristol, United Kingdom)
CP 55.940	Non-selective, potent cannabinoid receptor agonist	[10 µm]	All recording	Tocris BioScience (Bristol, United Kingdom)
JZL 184	Potent and selective MAGL inhibitor	[50 µm]	1 h of additional pre-incubation	Tocris BioScience (Bristol, United Kingdom)
URB597	Potent and selective FAAH inhibitor	[2 µm]	20 min of additional incubation	Tocris BioScience

				(Bristol, United Kingdom)
THL	Potent inhibitor of DAGLα	[10 µm]	20 min of additional incubation	Santa Cruz Biotechnology Inc (Spain)
AMG9810	TRPV1 receptor antagonist	[3 µm]	All recording	Tocris BioScience (Bristol, United Kingdom)
D-APV	Potent, selective NMDA antagonist; an active form of DL-APV	[50 µm]	All recording	Tocris BioScience (Bristol, United Kingdom)
Latrunculin A	G-actin monomer polymerization blocker	[0.5 µm]	20 min of additional incubation	Tocris BioScience (Bristol, United Kingdom)
LY 354740	Potent mGluR-II agonist	[100 µm]	All recording	Tocris BioScience (Bristol, United Kingdom)

4.4- Immunohistochemical procedures:

4.4.1- Preservation of mouse brain tissue:

Mice, TRPV1-KO and WT littermates (at least three of each condition), were deeply anesthetized by intraperitoneal administration of a mixture of ketamine/xilacine (80/10mg/kg body weight).

They were transcardially perfused through the left ventricle at room temperature (RT) with phosphate buffered saline (0.1 M PBS, pH 7.4) for 20 seconds, followed by the iced-cooled fixative solution made up of 4% formaldehyde (freshly depolymerized from paraformaldehyde),

0.2% picric acid and 0.1% glutaraldehyde in phosphate buffer (0.1 M phosphate buffer, pH 7.4) for 10-15 minutes or 250 ml for each mouse.

Then, brains were carefully removed from skull and post-fixed in the fixative solution for 1 week at 4°C. After, brains were stored in 0.1 M phosphate buffer (PB) diluted fixative solution (1:10) containing 0.025% sodium azide at 4°C until use.

4.4.2- Avidin-biotin peroxidase method for light microscopy:

This indirect immunohistochemical method uses avidin-biotin complex (ABC) to amplify the signal of biotinylated secondary antibody that has previously added to recognize the primary antibody used to identify the protein of interest.

This ABC consists of biotin associated with peroxidase and avidin mixture in a proportion that some avidin-biotin binding sites are left free. The biotin of the secondary antibody binds to the free valences of the avidin and forms AB complexes. These complexes bind to each other in succession in order to enhance this signal. 3,3'-diamenobenzidine (DAB) was used for revealing this signal. This chromogen is oxidized in a medium containing hydrogen peroxide and gives a reddish-brown precipitate when the peroxidase in the ABC catalyses the decomposition reaction of hydrogen peroxide and forms free oxygen species. To discard false positives, negative controls were run simultaneously in each experiment.

This is the protocol in detail:

1. Brain was cut into 50 µm-thick coronal vibrosections (Leica VT 1000s) and collected in 0.1 M phosphate buffer (PB, pH 7.4) at RT.
2. Hippocampal vibrosections were pre-incubated in a blocking solution of 10% bovine serum albumin (BSA), 0.1% sodium azide and 0.5% triton X-100 prepared in Tris-hydrogen chloride buffered saline (TBS 1X, pH 7.4) for 30 min at RT.
3. They were incubated in the corresponding primary antibody (TABLE 1), prepared in the blocking solution, and was kept shaking gently for 2 days at 4°C. Negative controls were incubated only in blocking solution.
4. Tissue was rinsed several times in a washing solution composed of 1% BSA and 0.5% triton-X100 in TBS 1X for 30 min to remove excess of antibody.
5. Sections were incubated with biotinylated antibody (1:200) (TABLE 2) prepared in the washing solution for 1h on a constant movement at RT.
6. Tissue was washed several times in washing solution.

7. Sections were incubated in avidin-biotin complex (1:50; avidin-biotin peroxidase complex, Elite, Vector Laboratories, Burlingame, CA, USA) prepared in washing solution for 1h at RT.
8. Tissue was washed several times in washing solution and then last washes were made with 0.1 M PB and 0.5% triton X-100.
9. Slices were incubated in 0.05% DAB and 0.01% hydrogen peroxide prepared in 0.1 M PB and 0.5% triton X-100.
10. They were washed several times in 0.1 M PB and 0.5% triton X-100.
11. They were mounted in previously gelatinized slides.
12. Sections were dehydrated in graded alcohols, 5 minutes each (50°, 70°, 96° and 100°).
13. They were cleared in Xilol (3 X 5 min).
14. Sections were coverslipped with DPX mountain solution.
15. Finally, they were studied and photographed with a Zeiss Axiocam light microscope coupled to Zeiss AxioCamHRc camera.

4.4.3- Single pre-embedding immunogold and combined pre-embedding immunogold and immunoperoxidase method for electron microscopy:

This technique has been used for ultrastructural localization of proteins with nanogold particles (Baude et al., 1993; Lújan et al., 1997; Mateos et al., 1999; Elezgarai et al., 2003; Puente et al., 2010a, 2010b; Reguero et al., 2011, 2014; Gutiérrez-Rodríguez et al. 2017, 2018; Puente et al., 2019). In my thesis work, the preembedding immunogold was used for the cellular and subcellular localization of CB_1R in DGML. In the case of double immunostainings, one of the secondary antibodies was a Fab' fraction conjugated to a 1.4 nm gold particle, and the other secondary was a biotinylated antibody. The small size of gold particles allowed a greater penetration into the tissue increasing the sensitivity of the method, while the simultaneous labelling of a second epitope permitted the co-localization of two proteins, which resulted in a better identification of cells such as astrocytes and microglia (figure 1). Furthermore, the preembedding method preserved antigen-antibody reaction better than other EM methods, as this happened before osmium tetroxide exposure and resin polymerization at high temperatures. Negative controls were run simultaneously in each experiment.

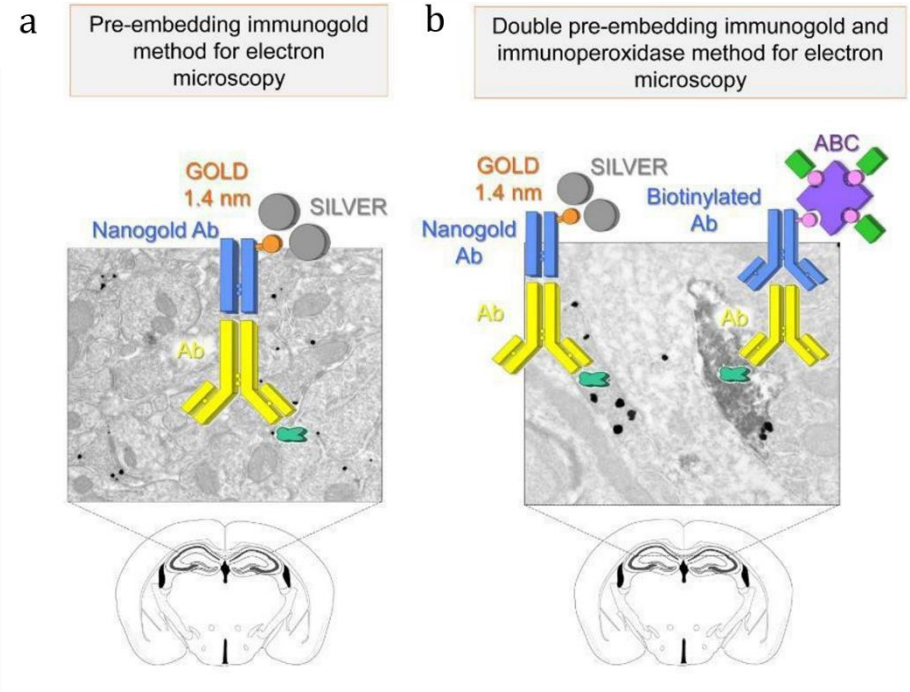

Figure 1: Cartoon of how antibody reaction works on single (a) and combined (b) preembedding immunogold method for electron microscopy. Adapted from Puente et al., 2019.

The following protocol was applied (figure 2):

1. Brain was cut into 50 µm-thick coronal vibrosections (Leica VT 1000S) and collected in 0.1 M phosphate buffer (PB, pH 7.4) at RT.
2. Hippocampal vibrosections were pre-incubated in a blocking solution of 10% bovine serum albumin (BSA), 0.1% sodium azide and 0.02% saponin prepared in Tris-hydrogen Chloride buffered saline (TBS 1X, pH 7.4) for 30 min at RT.
3. Sections were incubated in the primary antibodies: goat polyclonal anti-CB_1R antibody (1:100) alone or with mouse monoclonal anti-gephyrin (1:300) or mouse monoclonal anti-GFAP (1:1000) for double immunostaining, prepared in blocking solution of 10% bovine serum albumin (BSA), 0.1% sodium azide and 0.004% saponin prepared in TBS 1X (pH 7.4), and were kept shaking gently for 2 days at 4°C. Negative controls were incubated only in blocking solution.
4. Tissue was washed in washing solution composed of TBS 1X and 1% BSA for 30 minutes.
5. Sections were incubated in secondary nanogold antibody (TABLE 2) alone or with a secondary biotinylated antibody for double immunostaining. Both secondary antibodies were prepared in a blocking solution of 1% bovine serum albumin (BSA), 0.1% sodium azide and 0.004% saponin in TBS 1X (pH 7.4) for 3h in the case of single labelling and 4h for double immunostaining, on a shaker at RT.

6. Tissue was washed several times in washing solution (TBS 1X and 1% BSA) for 30 minutes.
7. Sections processed for double immunostaining were incubated with avidin-biotin complex (1:50) prepared in washing solution for 1.5h at RT on a shaker.
8. Tissue was washed several times in washing solution and left in the last wash overnight on a shaker at 4°C.
9. Sections were post-fixed with 1% glutaraldehyde prepared in TBS 1X for 10 minutes at RT.
10. They were washed several times with doubled distilled water for 30 minutes.
11. Gold particles were silver intensified with HQ silver kit (Nanoprobes Inc., Yaphank, NY USA).
12. Sections were washed several times with double distilled water for 10 minutes.
13. They were washed several times in 0.1 M PB (PH 7.4) for 30 minutes.
14. For double immunostaining, sections were incubated in 0.05% DAB and 0.01% hydrogen peroxide prepared in 0.1 M PB for 5 minutes at RT.
15. Stained sections were osmicated with osmium tetroxide in 0.1 M PB for 20 minutes at RT.
16. They were washed several times in 0.1 M PB for 30 minutes.
17. Tissue sections were dehydrated in graded alcohols (50°, 70°, 96° and 100°) to propylene oxide, 5 minutes in each and 15 minutes (3 times 5') in 100°C and propylene oxide.
18. Sectiones were incubated in a mixture of 1:1 Epon resin 812 and propylene oxide on a shaker at RT overnight.
19. They were embedded in Epon resin 812 for 2h on a shaker at RT.
20. Tissue sections were kept in the oven at 60°C for resin polymerization for 48 h.
21. Ultrathin 50 nm-thick sections were cut in an ultramicrotome (RMC Products, PowerTome XL) and collected on mesh nickel grids.
22. Grids were counterstained with 2.5% lead citrate for 20 minutes at RT.
23. Tissue specimens were examined and photographed in the electron microscope. Two electron microscopes were used: Philips EM208S and JEOL JEM 1400 plus. Electron micrographs were taken at 22,000x magnification by using a digital Morada camera from Olympus coupled to the Phillips EM208S electron microscope, the area of each electron micrograph was up to 20 μm^2. The JEOL electron microscope had its own camera incorporated to take snap assemblings at 8,000x magnification covering an area of up to 300 μm^2 corresponding to 15 electron micrographs taken with the Morada camera.

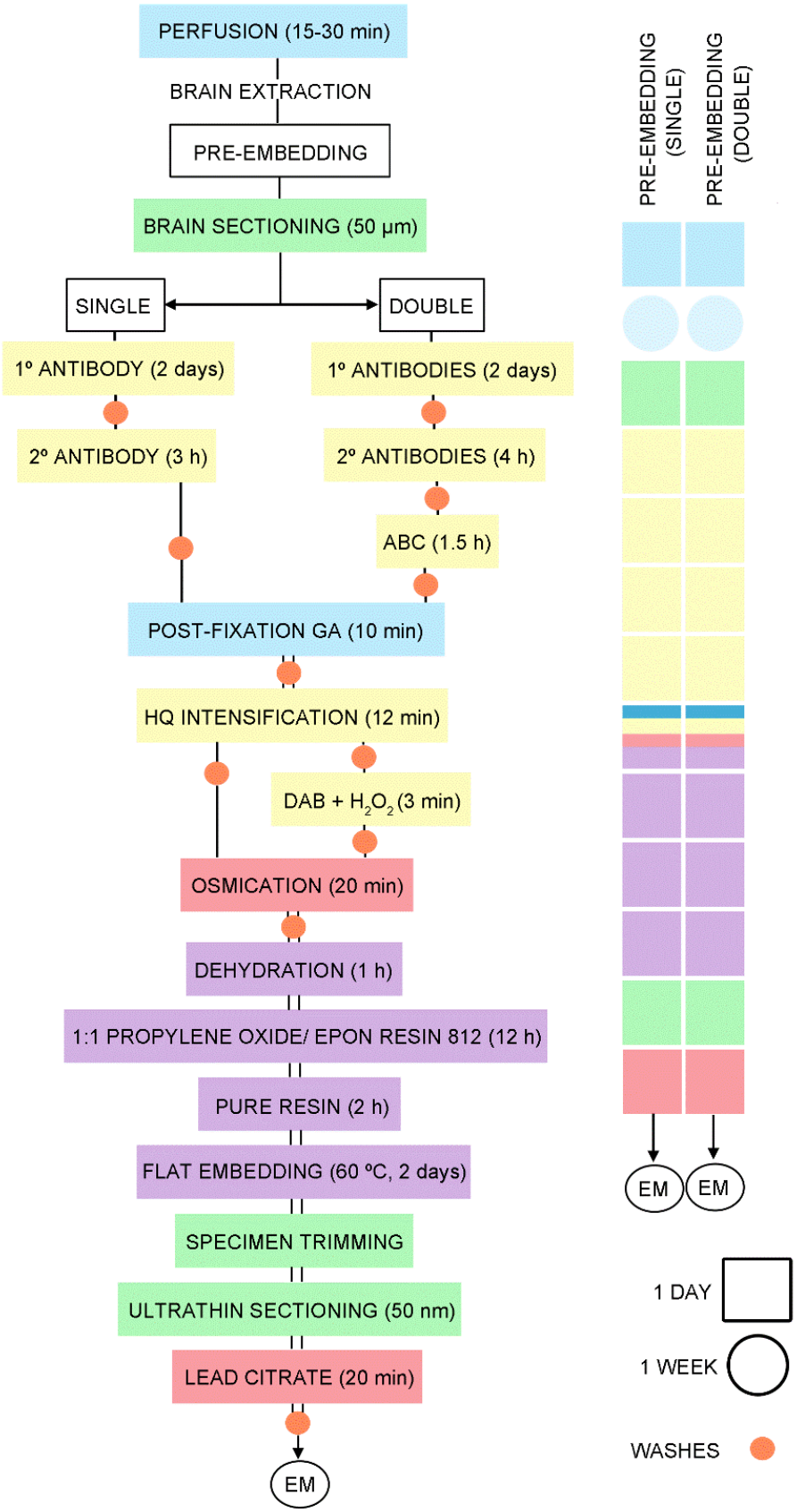

Figure 2: Timeline of the general steps for pre-embedding immunoelectron microscopy techniques. Adapted from Puente and colleagues (2019).

4.4.4- Semi-quantification analysis:

Immunolabelled sections obtained from three different mice of each condition were visualized under the light microscope in order to first dissect the hippocampus, then the DG and further the IML and the outer 2/3 of the DML, which corresponds, with the termination zone of the PP.

Chosen zones contained a good and reproducible CB_1R, GFAP and gephyrin immunolabelling and conserved good ultrastructure for a reliable quantification. Moreover, to further standardize the conditions of the analysis, only the first 1.5 µm from the surface of the tissue was snapped. Metal particles were counted on presynaptic terminal membranes, mitochondrial outer membranes and astrocytic membranes. Sampling was always performed accurately in the same way for all studied mice.

For identification of the synaptic terminals, ultrastructural and chemical features were taken considered. Hence, glutamatergic synapses were identified by their characteristic asymmetric synapses with thick postsynaptic densities and presynaptic buttons containing clear, spherical and abundant synaptic vesicles. Inhibitory synapses formed symmetric synapses and exhibited gephyrin immunoreaction product (only present in this type of synapses); also, the inhibitory terminals had typical pleomorphic synaptic vesicles.

To determine the proportion of CB_1R labelled terminals in each condition, a synaptic button was considered positive when at least one gold particle was on the presynaptic membrane or within about 30nm from the plasma membrane. Astrocytes were identified when GFAP immunoreaction product was found inside cellular profiles (then considered as GFAP positives). Image J (FIJI) free software was used to measure the following parameters: percentage of CB_1R-positive terminals; percentage of CB_1R-positive mitochondria; percentage of CB_1R-positive astrocytic processes; density of CB_1R particles in membranes of terminals and astrocytes; terminals perimeter; number of terminals and astrocytic processes per area and proportion of CB_1R immunoparticles in terminal membranes versus total CB_1R expression in cell membranes. The statistical significance of differences was analysed by Student's t-test or Mann-Whitney test. Results were displayed as mean ± S.E.M. using a statistical software package (GraphPad Prism, GraphPad Software Inc, San Diego, USA). Values of $p < 0.05$ were considered statistically significant.

4.5- Molecular biology methods:

4.5.1- Western blotting of whole hippocampal homogenates:

Mice (7-8 per group) were deeply anaesthetised by inhalation of isoflurane (2-4%) before decapitation. Hippocampi from both hemisphere were dissected and manually homogenized with a plastic stick in a homogenization lysis buffer composed of 10 mM PB (pH 7.4), 5 mM ethyleneglycol-bis(2-aminoethylether)- N,N,N',N' tetraacetic acid, 5 mM ethylene-diamine-tetra-acetic acid, 1mM dithiotreitol, and the protease inhibitor cocktail (Ref. P-8340, Sigma-Aldrich). Thereafter, samples were kept 30 min on ice and centrifuged for 15 min at 13,000 rpm. The resulting supernatant was used as soluble protein extract and protein concentrations were estimated using Bio-Rad Protein Assay reagent (Ref. 500-0006, Bio-Rad Laboratories SA). The same amount of protein (15 μg) was loaded onto any kDa polyacrylamide gel (Ref. 456-9036, Bio-Rad Laboratories Inc.). After electrophoresis (150 V for 60 min), samples were transferred for 3 min to a polyvinylidene difluoride (PVDF) membrane (Ref. 170-4157, Transfer Pack Trans-Blot Turbo, Bio-Rad Laboratories Inc., Spain) using the Trans-Blot Turbo System (Bio-Rad). Membranes were then blocked for 2h in TBS-T buffer (Tris-hydrogen Chloride buffered saline (10 mM Tris-HCl pH 7.6, 150 mM NaCl) and 0.1% Tween-20) containing 5% non-fat dry milk (Sveltesse, Nestle) and incubated overnight with primary antibody at 4°C (anti-CB_1; anti-MAGL and anti-FAAH) used at 1:1000 dilution.

After several washes, membranes were incubated for 1h with corresponding horseradish peroxidase-conjugated secondary antibody used at 1:2000 dilution. Immunoblot was visualized by chemiluminescence (Ref. Li-Cor, Bonsai Advanced Technologies SL) and quantified by densitometry using Image Studio Lite 4.0 (Li-Cor, Bonsai Advanced Technologies SL). To ensure equal protein loading, stripping buffer (100 mM glycine, pH 2.3) was applied to blots, washed, and incubated with anti-actin antibody (1:2000). The statistical significance of differences between both mice was analysed by Student's t-test or Mann-Whitney test. Statistical significance was set at the 95 % confidence level. Results were displayed as mean ± S.E.M using a statistical software package (GraphPad Prism, GraphPad Software Inc, San Diego, USA). Values of $p < 0.05$ were considered statistically significant.

For studying more in depth the effects of the genetic deletion of TRPV1 receptor on the ECS, the following techniques were applied in collaboration with the laboratory of Dr. Joan Sallés Alvira (Department of Pharmacology, Faculty of Pharmacy, University of the Basque Country UPV-EHU,

Vitoria-Gasteiz, CIBERSAM). They performed western blotting analysis of CB_1R, MAGL, FAAH, DAGLα, NAPE-PLD, CRIP1a and Gi/o α subunits in hippocampal membranes (P2 fraction) and synaptosomes, as well as [^{35}S] $GTP_\gamma S$ binding assays in synaptosomes. The results obtained are described here with the permission of Dr. Joan Sallés Alvira, Dr. Gontzal Garcia del Caño and Miquel Saumell Esnaola.

4.5.2- Western blotting of hippocampal synaptosomes:

Hippocampal synaptosomes were prepared as previously described by Dodd et al. (1981) with slight modifications (Garro et al., 2001) from mice 8 weeks old of both conditions (WT and TRPV1-KO). Mice were anaesthetised with isoflurane and decapitated; right after brains were removed and placed on ice-cold 0.32 M sucrose, pH 7.4, containing 80 mM Na2HPO4 and 20 mM NaH2PO4 (sucrose phosphate buffer) with protease inhibitors (Iodoacetamide 50 µM, PMSF 1 mM). The tissue was minced and homogenized in 10 volumes of sucrose/phosphate buffer using a motor-driven Potter Teflon glass homogenizer (motor speed 800 rpm; 10 up and down strokes; mortar cooled in an ice-water mixture throughout). The homogenate was centrifuged at 1.000x g for 10 min and obtained pellet (P1) was re-suspended and pelleted. The supernatants (S1 + S1') were pelleted at 15.000 x g (P2) and re-suspended in the homogenization buffer to a final volume of 16 ml. This P2 fraction is a heterogeneous population including myelin fragments, synaptosomes and free mitochondria. The suspension was layered directly onto tubes containing 8 ml 1.2 M sucrose phosphate buffer, and centrifuged at 180.000 x g for 20 min. The material retained at the gradient interface (synaptosome + myelin + microsome) was carefully collected with a Pasteur-pipette and diluted with ice-cold 0.32 M sucrose/phosphate buffer to a final volume of 16 ml. The diluted suspension was then layered onto 8 ml of 0.8 M sucrose phosphate buffer, and centrifuged as described above. The obtained pellet was re-suspended in ice-cold phosphate buffer, pH 7.5 and aliquoted in microcentrifuge tubes. Aliquots were then centrifuged at 40,000 x g for 30 min, the supernatants were aspirated and the pellets correspond to the nerve terminal membranes were stored at -80°C. Protein content was determined using the Bio-Rad dye reagent with bovine γ-globulin as standard.

Western blotting was performed as previously described with minor modifications (Garro et al., 2001; López de Jesús et al., 2006). Briefly, hippocampal synaptosome fractions were boiled in urea-denaturing buffer [20 mM Tris-HCl, pH 8.0, 12 % glycerol, 12 % Urea, 5 % dithiothreitol, 2 % sodium dodecyl sulfate (SDS), 0.01 % bromophenol blue] for 5 min. Denaturized proteins were resolved by electrophoresis on SDS–polyacrylamide (SDS-PAGE) gels and transferred to

nitrocellulose or PVDF membranes at 30 V constant voltage overnight at 4°C. Blots were blocked in 5 % non-fat dry milk/phosphate buffered saline containing 0.5 % BSA and 0.1 % Tween for 1h, and incubated with the antibodies overnight at 4°C. Blots were washed and incubated with specific horseradish peroxidase conjugated secondary antibodies diluted in blocking buffer for 1.5h at RT. Immunoreactive bands were incubated with the ECL system according to the manufacturer instructions. In these experiments, differences between the relative expressions of proteins were analysed by regression line slopes comparison method by a statistical software package (GraphPad Prism, GraphPad Software Inc, San Diego, USA).

4.5.3- Agonist stimulated [^{35}S] GTPγS binding assays:

The [^{35}S] GTPγS binding assays were performed following the procedure described elsewhere (Barrondo and Sallés, 2009; Casado et al., 2010). Briefly, hippocampal synaptosomal membranes were thawed, and incubated at 30°C for 2h in [^{35}S] GTPγS-incubation buffer (0.5 nM [^{35}S] GTPγS, 1 mM EGTA, 3 mM $MgCl_2$, 100 mM NaCl, 0.2 mM DTT, 50 µM GDP, BSA 0.5 % and 50 mM Tris-HCl, pH 7.4). The CB_1R agonist CP 55.940 (10^{-9} - 10^{-5} M) was added to determine receptor-stimulated [^{35}S] GTPγS binding. Nonspecific binding was defined in the presence of 10 µM unlabelled GTPγS. Basal binding was assumed to be the specific [^{35}S] GTPγS binding in the absence of agonist. Reactions were stopped by rapid vacuum and filtration through Whatman GF/B glass fibre filters and the remaining bound radioactivity was measured by liquid scintillation spectrophotometry.

For data analysis of [^{35}S] GTPγS binding assays, individual CP 55.940 concentration-response curves were fitted by nonlinear regression to the four parameter Hill equation.

$$E = Basal + E_{max} - Basal/1 + 10 (Log\ EC_{50} - Log\ [A])\ nH$$

Where E denotes effect, log [A] the logarithm of the concentration of agonist, nH the midpoint slope, Log EC_{50} the logarithm of the midpoint location parameter, and E_{max} and basal the upper and lower asymptotes, respectively.

All [^{35}S] GTPγS binding assays experiments were performed in triplicate and the results were obtained from three independent experiments. Data are expressed as the mean ± S.E.M. Experimental data were analysed using a computerized iterative procedure (GraphPad Prism version 6.0) by directly fitting the data to the mathematical model described above. The

statistical significance of differences between E_{max} and between pEC_{50} values was analysed by paired two-tailed Student's t-test followed by the Tukey–Kramer multiple comparison tests. Statistical significance was set at the 95 % confidence level. A statistical software package was used (GraphPad Prism, GraphPad Software Inc, San Diego, USA).

4.6- *In vitro* electrophysiology:

4.6.1- Slice preparation:

Mice were anaesthetised with isoflurane (2-4 %) and decapitated. Brains were quickly removed and deposited in a sucrose-based solution at 4°C consisted of (in mM): 87 NaCl, 25 glucose, 75 sucrose, 7 MgCl2, 0.5 CaCl2, 2.5 KCl and 1.25 NaH2PO4. Vibratome was used for sectioning the brain into coronal sections (300 µm thick, Leica Microsistemas S.L.U.); slices were collected and recovered at 32-35°C, before being placed in the recording chamber and superfused (2 ml/min) with artificial cerebrospinal fluid (aCSF) containing (in mM): 130 NaCl, 23 NaHCO3, 11 glucose, 1.2 MgCl2, 2.4 CaCl2, 2.5 KCl and 1.2 NaH2PO4, equilibrated with 95 % O2 // 5 % CO2. All experiments were carried out at 32–35°C and Picrotoxin (PTX; 100 µM, Tocris Bioscience UK) was added to the aCSF in order to block $GABA_A$ receptors.

4.6.2- Extracellular field recordings:

Field fEPSPs were recorded in hippocampal DGML. The stimulation electrode (borosilicate glass capillaries, Harvard apparatus UK capillaries 30-0062 GC100T-10) was placed in the MCFL, in the MPP or in the LPP and the glass-recording pipette, filled with aCSF, always in the MCFL. To ensure the right location of the electrodes in the MPP, the potent mGluR2 agonist LY354740 was applied as it has been previously shown to selectively depress MPP synapses in the DML (Chávez et al., 2010). To evoke field excitatory postsynaptic potential responses (fEPSPs), repetitive control stimuli were applied at 0.1 Hz (Stimulus Isolater ISU 165, Cibertec, Spain; controlled by a Master-8, with an isolation unit A.M.P.I.). An Axopatch-200B (Axon Instruments/Molecular Devices, Union City, CA, USA) was used to record the data filtered at 1-2 kHz, digitized at 5 kHz on a DigiData 1440A interface collected on a PC using Clampex 10.0 and analysed using Clampfit 10.0 (all obtained from Axon Instruments/Molecular Devices, Union City, CA, USA). In the beginning of each experiment, an input-output curve was established. Stimulation intensity was chosen for baseline measurements that yielded between 40 and 60 % of the maximal amplitude response.

To induce a presumable eCB driven eLTD of glutamatergic inputs, a low frequency tetanic stimulation (LFS, 10 min at 10 Hz) protocol was applied following recording of a steady baseline as previously described (Robbe et al., 2002; Puente et al., 2011; Peñasco et al., 2019, 2020).

4.6.3- Data analysis:

The magnitude of the fEPSP area for eCB-eLTD after tetanic stimulation was calculated as the percentage change between baseline area (averaged excitatory responses for 10 min before LFS) and last 10 min of stable responses, recorded 30 min after the end of the LFS. At least three mice were used for each experimental condition. WT and TRPV1-KO littermates were intermixed during experiments.

The paired-pulse ratio (PPR) was calculated by averaging the ratio of the fEPSP initial slopes (P2/P1) of 30 pairs of pulses (50 msec interpulse interval), where P2 corresponded to fEPSP2 slopes (2^{nd} evoked responses) and P1 to fEPSP1 slopes (1^{st} evoked responses).

4.7- Behavioural studies:

Behavioural tests were conducted in 7-8-week-old mice (10-11 per each condition). They were kept in a temperature- and air flux-controlled room 30 minutes before starting the trial; tests were performed in the same conditions. They were carried out in the same room, always in the light phase and the same time period. Two blinded observers monitored all tests and used at least one stopwatch. All experiments were recorded using a digital camera (Panasonic Lumix). To avoid olfactory cues, maze and objects were cleaned with 70 % EtOH and then rinsed with water before each trial.

4.7.1- Novel object-recognition test (NORT):

It was used to assess non-spatial recognition memory. This behaviour depends on hippocampal function and is based on the tendency of rodents to explore more objects that are new rather than familiar ones.

The test was performed in an L-shape maze made of white Plexiglas with two corridors (30 cm and 35 cm long, respectively, 4.5 cm wide and 15-cm high walls) set at a 90° angle and under a weak light intensity (50 Lux). It consisted of three consecutive trials (9 minutes each) in 3 days.

The first was the habituation day where mice were placed at the intersection of the two arms and were let explore freely both arms. On the second day, two identical objects were placed at the end of each arm. Mice were let explore the objects. Last day, a new object replaced one of the identical objects. This object was different in shape, colour and texture and was placed in the position of the replaced one; the familiar object remained unchanged. The position of the novel object and the pairings of novel and familiar objects were randomized.

At least one experienced observer blinded to the genotypes (WT and TRPV1-KO) scored each mouse exploration. Exploration was considered the time the mouse spent with the nose pointing to the object at a distance no more than 1 cm; climbing on or chewing the object was not assessed. To evaluate memory performance, the discrimination index was calculated as the difference between the time spent exploring the novel (TN) and the familiar object (TF) divided by the total exploration time (TN+TF): discrimination index = (TN−TF)/(TN+TF) (Puighermanal et al. 2009).

4.7.2- Barnes-maze spatial-memory and strategy test (BM test):

It is a dry-land based behavioural test to study spatial memory in mice (Bach et al., 1995). This memory task is hippocampal-dependent and mice learn the relationship between spatially placed visual cues in the surrounding environment and a fixed escape box.

We used an adapted protocol for BM based on Rueda-Orozco et al., 2008. Thus, an elevated circular platform with 20 spaced holes around the perimeter was used. Escape box was fixed under one hole and pointed with two visual clues of different shape and colour while the remaining 19 holes were left empty. As bright light and high open spaces are aversive to mice, the height layout of the maze and the lighting source above were motivating factors to induce escape. The escape box and visual clues were maintained at a fixed location for the whole duration of the test consisisting of four daily trials during five days. Mice typically use a sequence of three different search strategies (random, serial, and spatial) to learn the location of the escape box.

During the daily trials, at least two blinded experienced observers scored the strategies displayed by the mice and measured the time taken to complete each task. First, mice were placed in the escape box for 1 minute, then were placed in the centre of the maze and let them explore freely for 4 minutes to find the escape box. The results were scored in the following

manner: 1) no strategy (NS): the escape box was not found during the exploration period; 2) random strategy (RM): the escape box was found after random search through different holes; serial strategy (SE): the escape box was found following serial holes with no turns back; spatial strategy (SP): the animal aimed at the escape box right straight from the centre. The time taken to enter into the escape box was measured in each trial. The statistical significance of differences between WT and TRPV1-KO mice was analysed by Two-Way ANOVA test. Results were displayed as mean ± S.E.M. using a statistical software package (GraphPad Prism, GraphPad Software Inc, San Diego, USA). Values of $p < 0.05$ were considered statistically significant.

4.8- Kainic acid model of excitotoxic seizures:

The kainic acid model of excitotoxic seizures is widely used to simulate temporal lobe epilepsy. This model has contributed to the understanding of the molecular, cellular and pharmacological mechanisms underlying epileptogenesis since it displays neuropathological and electroencephalographic features that are seen in patients with temporal lobe epilepsy (Lévesque and Avoli, 2013).

4.8.1- Intrahippocampal administration of kainic acid (KA):

KA (20mM) was administered intrahippocampally based on the protocol described by Sierra et al. 2015.

Six-week-old male mice (n = 15 WT and TRPV1-KO each) were used. They were anaesthetised by intraperitoneal injection of ketamine/xilacine (100/10mg/kg body weight), then were placed in the stereotaxic frame and the craniotomy was performed. After setting the injector (Nanoject II Auto-Nanoliter injector, Drummond Scientific Company) in the stereotaxic arm, KA was injected in the dorsal hippocampus according to the coordinates: anteroposterior (AP) − 1.7, mediolateral (ML) + 1.6mm, dorsoventral (DV) − 1.9mm. Fifty nanolitres (11 × 4.6 nL, every 10 s) of 20mM KA were delivered into the right hippocampus using the Nanoject controller. After 2 minutes, the injector needle was removed to avoid backflow of the fluid. Mice were taken out from the stereotaxic frame, incision stitched, and placed on a heat pad until recovery from anaesthesia.

4.8.2- Behavioural scoring of seizure severity:

Mice were scored during 4 hours after surgery. The severity of the behavioural seizures was rated every 30 minutes according to a modified Racine's scale (1972). Racine developed a scale (RS) to score seizures in the amygdala-kindling model by establishing the relationship between EEG changes and the development of motor seizures. Nowadays, RS is still in use and often adapted for fitting better in a wide variety of seizure and epilepsy models (Clement et al. 2003; Vinogradova and van Rijn, 2008; Lüttjohann et al., 2009).

Seven stages of intensity were defined in the modified Racine's scale based on the behavioural symptoms displayed by the animals during the seizures after being recovered from the effects of the anaesthesia: "staring and immobility" (stage 1); "tail extension and forelimb clonus" (stage 2); "rearing and repetitive movements" (stage 3); "rearing and falling" (stage 4); "continuous rearing and falling" (stage 5); "tonic-clonic seizures with loss of posture, jumping and wild running" (stage 6); "death" (stage 7). The maximum score reached by each animal in each period was taken for the analysis. The statistical significance of differences between WT and TRPV1-KO mice was analysed by Two-Way ANOVA test. Results were displayed as mean ± S.E.M. using a statistical software package (GraphPad Prism, GraphPad Software Inc, San Diego, USA). Values of $p < 0.05$ were considered statistically significant.

5- Results

5.1- Expression pattern of components of the ECS in the WT and TRPV1-KO mice hippocampus.

5.1.1- Immunohistochemistry of CB_1R and endocannabinoid enzymes in WT and TRPV1-KO mouse hippocampus.

The immunostaining patterns of CB_1R and the main enzymes for synthesis and degradation of the two main endocannainoids, 2-AG and AEA, were analysed in WT and TRPV1-KO by an immunoperoxidase method for light microscopy (LM) (figure 1).

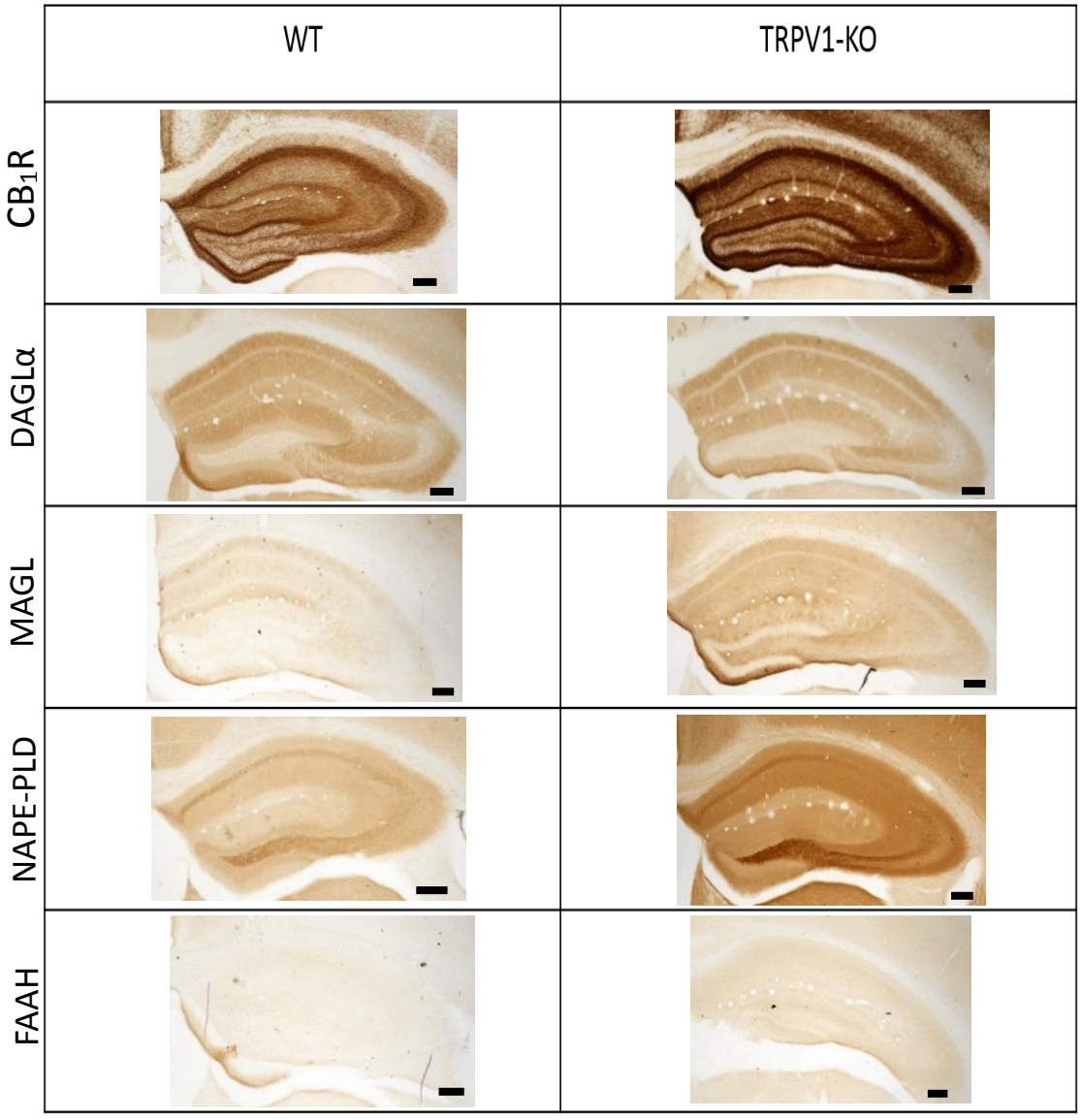

Figure 1: Expression patterns of components of the ECS in the hippocampus of WT and TRPV1-KO mice. Immunoperoxidase method for LM. Immunostaining for CB_1R; DAGLα enzyme; MAGL enzyme; NAPE-PLD enzyme and FAAH enzyme. Note a general increase in protein staining (though FAAH is very poor) except for DAGLα which shows a discreet decrease overall but particularly in CA1 stratum lacunosum moleculare. Scale bars: 500 µm.

First, a change in the expression pattern was observed in the hippocampus of TRPV1-KO compared to WT. Thus, an increase was found for CB_1R, MAGL, NAPE-PLD and FAAH, whereas DAGLα expression seemed to lightly decrease.

All micrographs were taken with the same light intensity and exposure time in order to allow comparisons. The staining obtained for MAGL and FAAH was faint in the hippocampus of WT and TRPV1-KO mice compared to the other stainings. MAGL, FAAH and NAPE-PLD showed a general increase throughout the entire hippocampus of TRPV1-KO. MAGL expression increased more than FAAH and NAPE-PLD remarkably increased in the hilus and CA3 stratum lucidum, the termination zone of the mossy fibres. CB_1R expression noticeably increased overall being particularly strong in the DGML, CA3 stratum radiatum and CA1 stratum pyramidale.

5.1.2- Expression of CB_1R and endocannabinoid enzymes in whole hippocampal homogenates and synaptosomes of WT and TRPV1-KO hippocampus.

The expression of CB_1R, DAGLα, FAAH and MAGL were analysed in whole homogenate extracts obtained from hippocampi of WT and TRPV1-KO (figure 2). CB_1R increased 27.5 % in TRPV1-KO (values: control vs 127.5 ± 23.83 %; p = 0.301 ns; n= 8) but was not statistically significant (figure 2a). However, FAAH significantly increased (56 %) in the TRPV1-KO (values: control vs 156.3 ± 23.52 %; p = 0.0467 *; n= 8) (figure 2b). As to the 2-AG related enzymes, DAGLα remained unchanged (values: control vs 109.5 ± 7.5 %; p = 0.2476 ns; n= 2) (figure 2c) but a greatly significant increase (~288 %) was found in MAGL expression in TRPV1-KO relative to WT (values: control (100 %) vs 388.1 ± 54.7 %; p = 0.0001 ***; n= 8) (figure 2d).

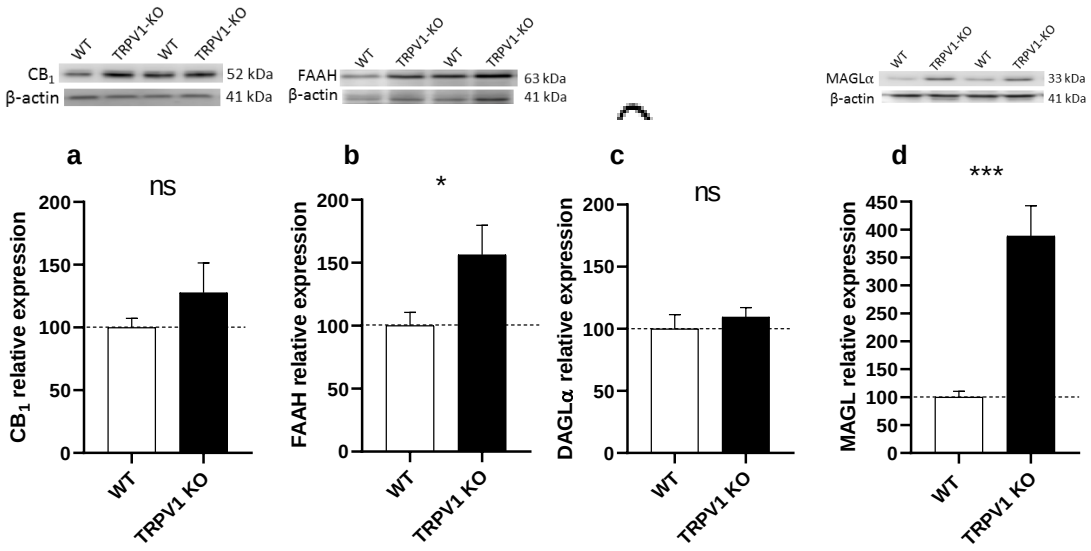

Figure 2: Relative expression of CB_1R and endocannabinoid enzymes in whole hippocampal whole homogenates from WT and TRPV1-KO mice. a) Immunoblot for CB_1R. The increase observed in TRPV1-KO is not significant. B) Immunoblot for FAAH. There is a significant increase in TRPV1-KO versus WT. c) Immunoblot for DAGLα. No changes are observed in its expression. d) Immunoblot for MAGL. The enzyme increases outstandingly in TRPV1-KO. Data were analyzed by means of non-parametric or parametric tests (Mann–Whitney U test or unpaired t-test); *p < 0.05; ***p < 0.001. Data are expressed as mean ± S.E.M.

However, doubts existed as global detection of CB_1R expression might be masking underlying differences in specific ultrastructural compartments. To figure it out, homogenates were purified to P2 fractions where all the cellular and subcellular membranes were separated from the cytosolic fraction. Again, there was not found any significant change in the CB_1R expression between TRPV1-KO and WT (values: control vs 96.18 ± 16.38 %; p = 0.8213; ns) (figure 3).

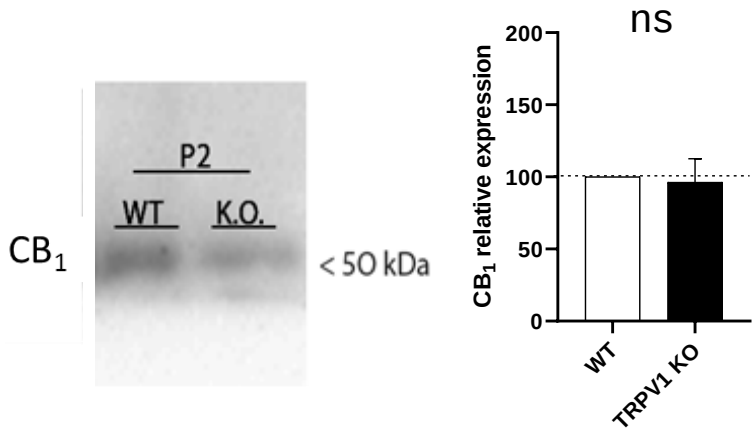

Figure 3: Immunoblot and relative expression of CB_1R in P2 extract of raw membranes from WT and TRPV1-KO mice hippocampi. Not significant changes in CB_1R expression are detected in TRPV1-KO versus WT. Unpaired t test. p > 0.05. Data are shown as mean ± S.E.M.

Then, synaptosomal fractions were extracted from homogenates to study the expression of endocannabinoid-related proteins in synaptic terminals (figure 4).

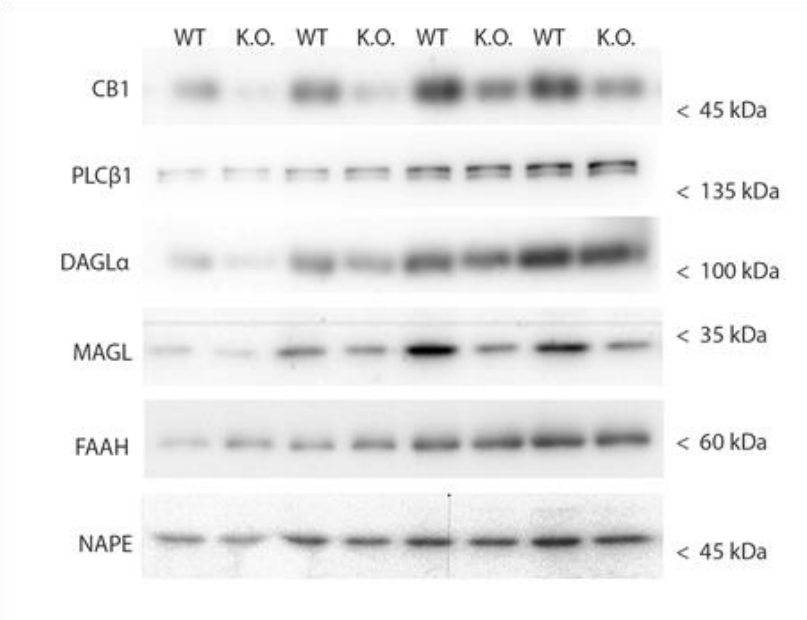

Figure 4: Immunoblots of CB_1R, PLCβ1, DAGLα, MAGL, FAAH and NAPE-PLD in synaptosomes from WT and TRPV1-KO mice hippocampus. See the text for values details.

Synaptosomal fractions revealed a significant decrease in CB_1R and MAGL in TRPV1-KO compared to WT. Thus, CB_1R dropped about 45 % (WT slope values: 5.878 ± 0.5065; TRPV1-KO: 3.214 ± 0.8289 (p = 0.0092; **) (figure 5a) and the decrease in MAGL was about 42 % (WT slope values: 6.512 ± 1.381; TRPV1-KO: 3.763 ± 1.161 (p = 0.0431; *) (figure 5b). Also, a moderately decrease in ~ 28 % was observed in NAPE-PLD in the TRPV1-KO (3.499 ± 1.268 (p = 0.4186; ns) relative to WT (4.836 ± 0.8018) (figure 5c). Finally, the expression of DAGLα (WT: 6.498 ± 0.5544; TRPV1-KO: 5.724 ± 0.2046 (p = 0.3194; ns) (figure 5d); FAAH (WT: 6.419 ± 0.7261; TRPV1-KO: 5.973 ± 0.3228 (p= 0.607; ns) (Figure 5e) and PLCβ (WT: 7.569 ± 0.5175; TRPV1-KO: 7.231 ± 0.6894 (p= 0.6343; ns) (figure 5f) did not change.

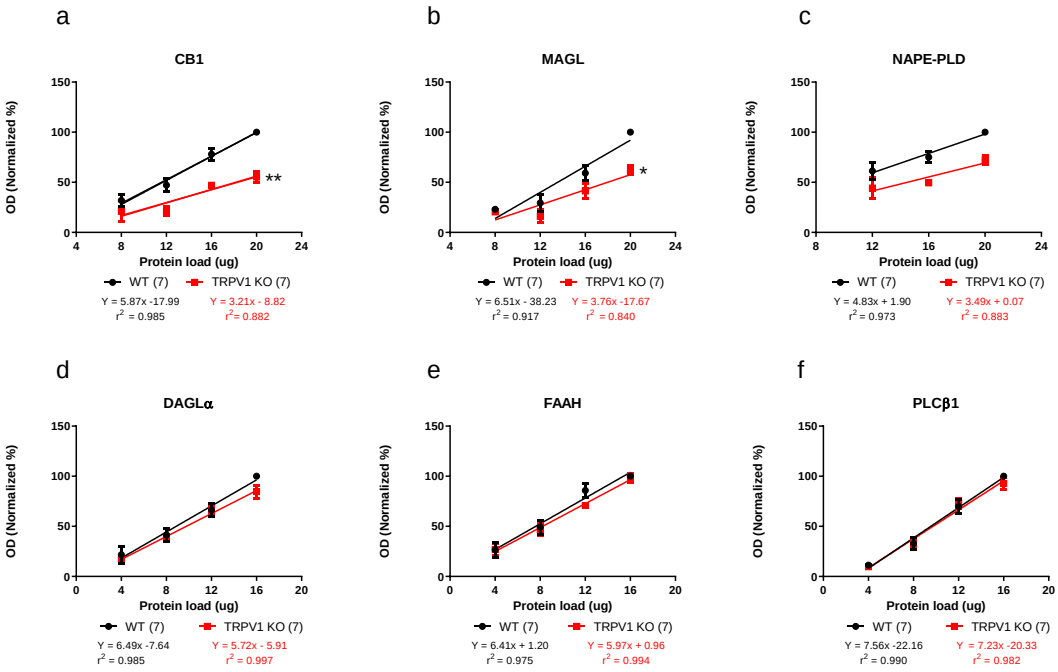

Figure 5: Linear regression analysis of the relative expression of CB_1R and enzymes of the ECS in synaptosomal extracts from WT and TRPV1-KO mice hippocampus. a) CB_1R. b) MAGL enzyme. c) NAPE-PLD enzyme. DAGLα enzyme. e) FAAH enzyme. Fisher's exact test. $p > 0.05$; *$p < 0.05$; **$p < 0.005$. Data are displayed as mean ± S.E.M.

5.1.3- CP 55.940 stimulated [^{35}S] $GTP_\gamma S$ binding assays in synaptosomal fractions from WT and TRPV1-KO mice hippocampus.

[^{35}S] $GTP_\gamma S$ binding assays were performed with the CB_1R agonist CP 55.940 in synaptosomal extracts obtained from the hippocampi of WT and TRPV1-KO mice. Hence, CP 55.940 stimulated [^{35}S] $GTP_\gamma S$ binding in both WT and TRPV1-KO in a concentration dependent manner (figure 6a). However, there was a significant increase in the maximum efficacy (E_{max}) in TRPV1-KO (193.70 ± 12.21 % over the basal activation) with respect to WT (maximum efficacy: 176.20 ± 9.73 % over the basal activation) ($p < 0.05$; *) (figure 6a). Furthermore, there were not changes in the potency (EC_{50}) of the CP 55.940 stimulation (EC_{50} in WT: -6.47 ± 0.14; in TRPV1-KO: -6.58 ± 0.01 ($p = 0.5139$; ns) (figure 6a), but a decrease in the basal activation in TRPV1-KO (86.25 ± 1.02 %) compared to WT (100 ± 1.76 %) ($p = 0.0203$; *) was found (figure 6b).

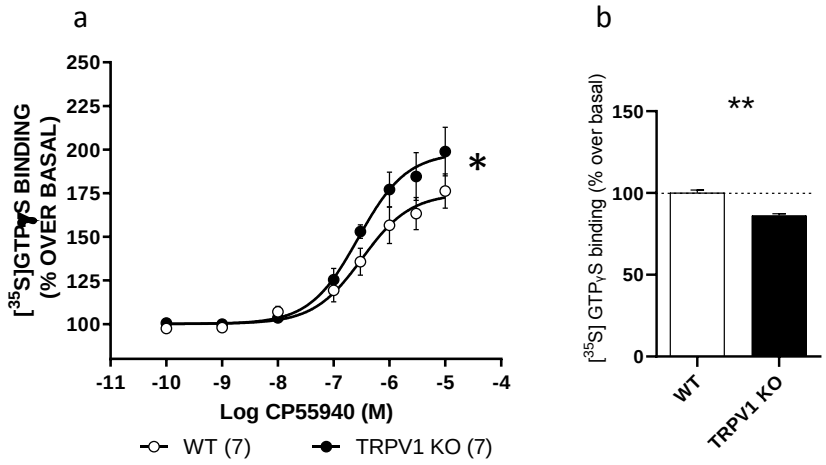

Figure 6: Effect of genetic TRPV1 deletion in CB_1R functionality. a) Representative image of CP 55.940-stimulated [^{35}S] GTP$_\gamma$S binding assay in hippocampal synaptosome fractions from WT and TRPV1-KO mice. Concentration curves were constructed using mean values ± S.E.M. from four different experiments performed in triplicates. Unpaired t test; *$p < 0.05$; b) Bar graph representing the relative percentage of [^{35}S] GTP$_\gamma$S basal binding levels in WT and TRPV1-KO. Unpaired t test; **$p < 0.005$. Data are represented as mean ± S.E.M.

5.1.4- Intracellular CB_1R-related protein expression in synaptosomes of WT and TRPV1-KO hippocampus.

The Gα subunit proteins (o, i1, i2, i3) and the cannabinoid receptor interaction protein 1a (CRIP1a) were analysed (figure 7).

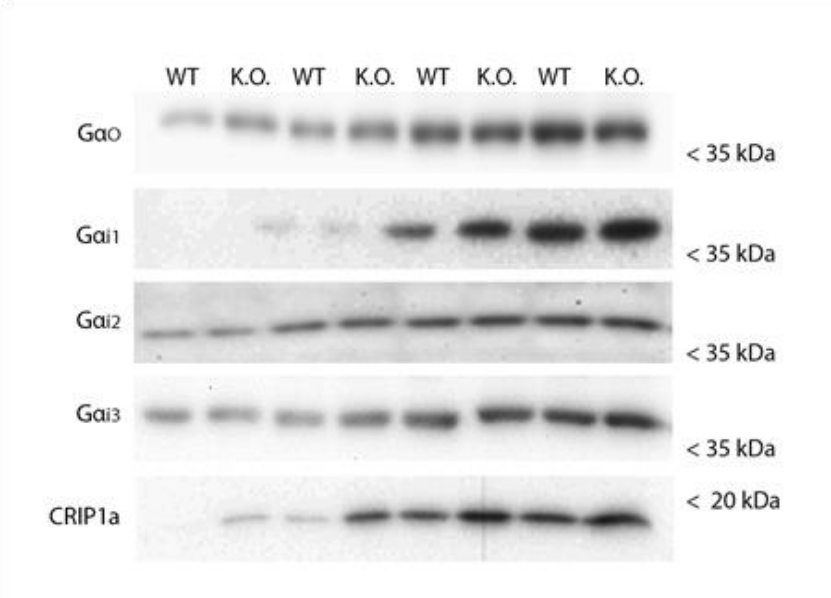

Figure 7: Immunoblot of CB_1R interacting proteins in synaptosomal extracts from WT and TRPV1-KO mice hippocampus. Expression of Gαo, Gαi different subunits (1, 2, 3) and CRIP1a in synaptosomes.

In TRPV1-KO versus WT, there were not changes in Gαo (WT: 7.008 ± 0.998; TRPV1-KO: 6.695 ± 0.6674 (p = 0.7853; ns) (figure 8a) but a significant increase was observed in Gα1 (WT: 8.14 ± 0.1228; TRPV1-KO: 12.66 ± 0.0789 (p = 0.03808;*) (figure 8b), Gα2 (WT: 8.101 ± 0.2337; TRPV1-KO: 11.2 ± 0.7939 (p = 0.0463; *) (figure 8c), Gα3 (WT: 6.135 ± 1.489;TRPV1-KO: 11.43 ± 0.685 (p < 0.0001; ****) (figure 8d) and CRIP1a (WT: 8.481 ± 1.324; TRPV1-KO: 18.41 ± 1.89 (p = 0.0006; ***) (figure 8e).

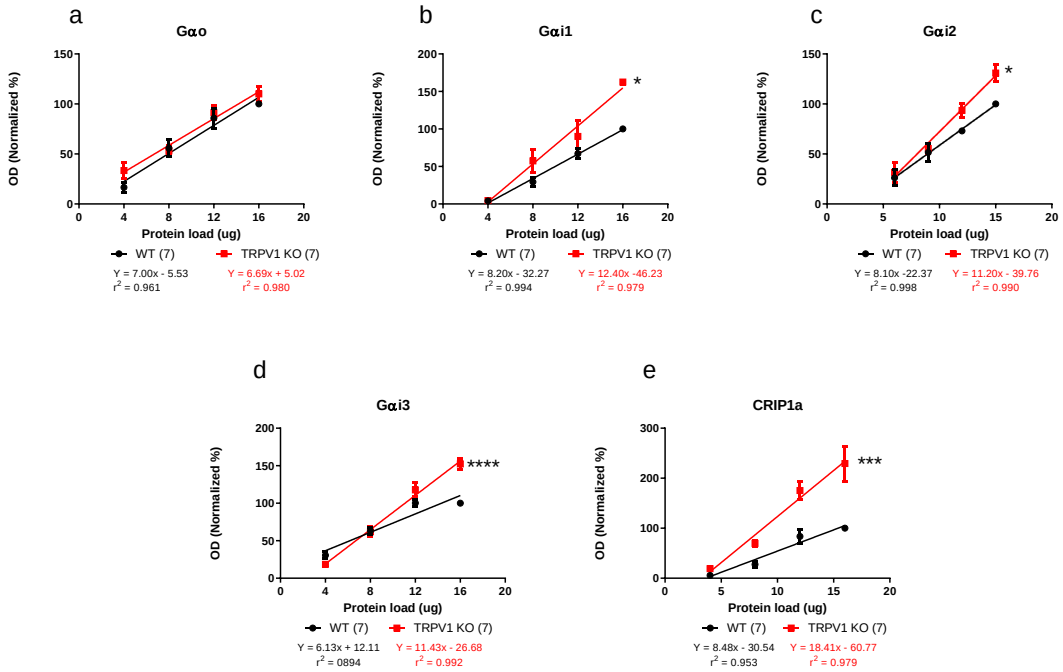

Figure 8: Linear regression analysis of the relative expression CB_1R interacting proteins in synaptosomal extracts from WT and TRPV1-KO mice hippocampus. a) Gαo subunit (n=7). b) Gαi1 subunit (n=7). c) Gαi2 subunit (n=7). d) Gαi3 subunit (n=7). e) CRIP1a protein (n=7). Fisher's exact test. p > 0.05; *p < 0.05; ***p < 0.001; ****p < 0.0001. Data are expressed as mean ± S.E.M.

Protein expression analysis in P2 and synaptosomal fractions, as well as [^{35}S] $GTP_\gamma S$ binding assays were performed by Mikel Saumell in the laboratory of Dr. Joan Sallés Alvira (Department of Pharmacology, University of the Basque Country).

5.2- Cellular and subcellular localization of CB_1R in the hippocampus of TRPV1-KO mice. High-resolution electron microscopy.

The attention was focused on the dentate gyrus (figure 9) since the presence of TRPV1 and CB_1 receptors and their role in functional plasticity have been described in the dentate molecular layer (Chavéz et al., 2011; 2014; Puente el al., 2015; Canduela et al., 2015; Gutiérrez-Rodríguez et al., 2017; Wang et al., 2016; 2018; Bonilla-Del Río et al., 2019; Peñasco et al., 2019).

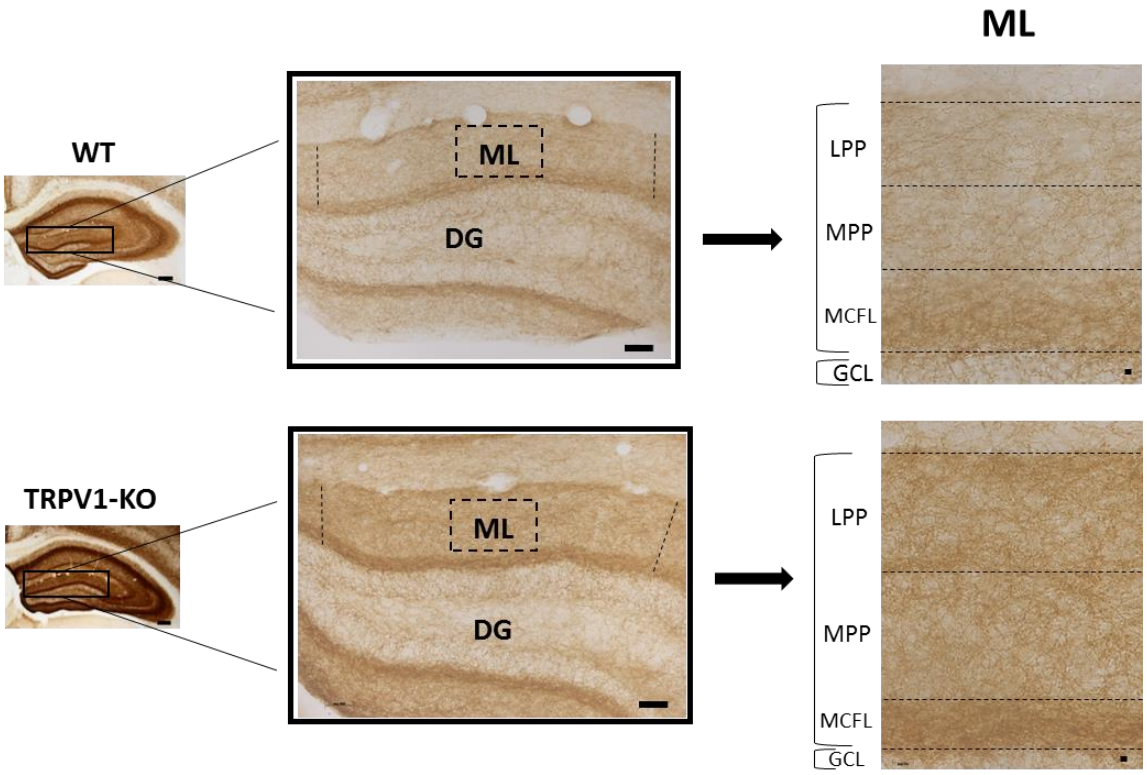

Figure 9: Representative light microscopy images of CB_1R immunolabelling in the dentate molecular layer of WT and TRPV1-KO mice. In the WT molecular layer (ML), CB_1R immunoreactivity is strong in a fibre meshwork in the inner 1/3 of the layer which corresponds to the termination zone of the glutamatergic mossy cell axons (MCFL). And weaker but yet conspicuous in fibrous profiles distributed in the outer 2/3 of the ML targeted by the medial (MPP) and lateral perforant path (LPP). In TRPV1-KO, the same but stronger CB_1R immunoreactive pattern is observed overall ML. DG: dentate gyrus; MCFL: mossy cell fibre layer; GCL: granule cell layer. Scale bars: 200 µm.

For a better identification of the astrocytes and the GABAergic synapses in the electron microscope, an immunoperoxidase method was applied together with a preembedding immunogold method for electron microscopy. Thus, in the ML of WT and TRPV1-KO, abundant CB_1R immunoparticles were localized, as expected, in GABAergic axon terminal membranes making symmetric synapses with postsynaptic dendrites, whereas glutamatergic terminals forming asymmetric synapses with dendritic spines or postsynaptic membranes showed a few

CB_1R immunoparticles. In both types of synapses, CB_1R particles were located in the perisynaptic and extrasynaptic domains of the terminals. CB_1R labelling was also present in astrocytic processes and mitochondrial membranes.

5.2.1- Distribution of CB_1R in presynaptic axon terminals in the MCFL.

CB_1R immunoparticles were found in the perisynaptic and extrasynaptic zones of glutamatergic and GABAergic axon terminals in MCFL (figure 10) and in astrocytes (figure 11), showing a similar distribution pattern in WT and TRPV1-KO.

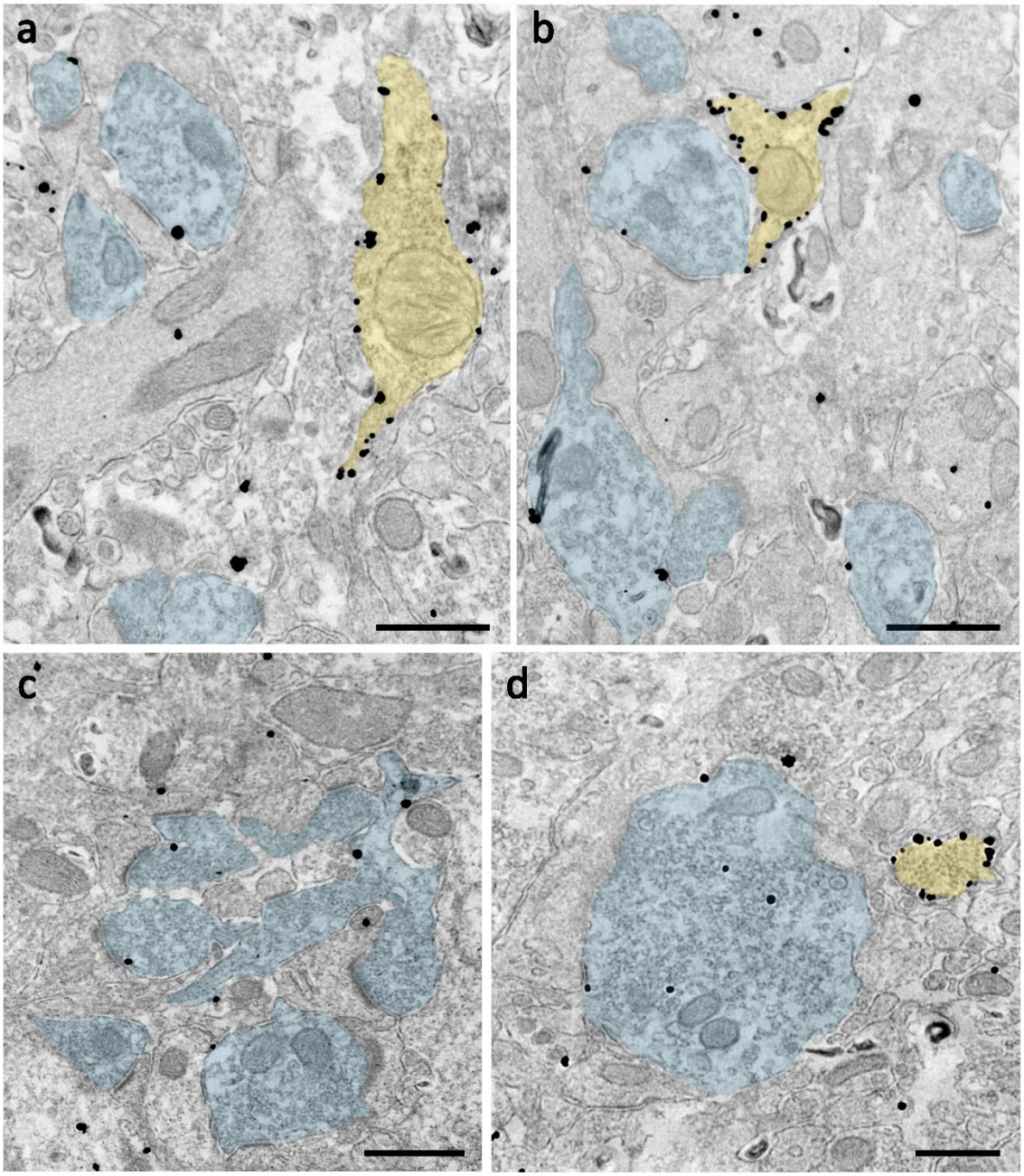

Figure 10. CB_1R distribution in MCFL of WT and TRPV1-KO mice. **Preembedding immunogold method for electron microscopy.** a) & b) WT mice. c) & d) TRPV1-KO mice. Blue: excitatory terminals; yellow: inhibitory terminals; black dots: silver-intensified CB_1R gold particles. CB_1R immunoparticles are abundant in inhibitory terminals and scattered in excitatory boutons. Scale bars: 0.5 µm.

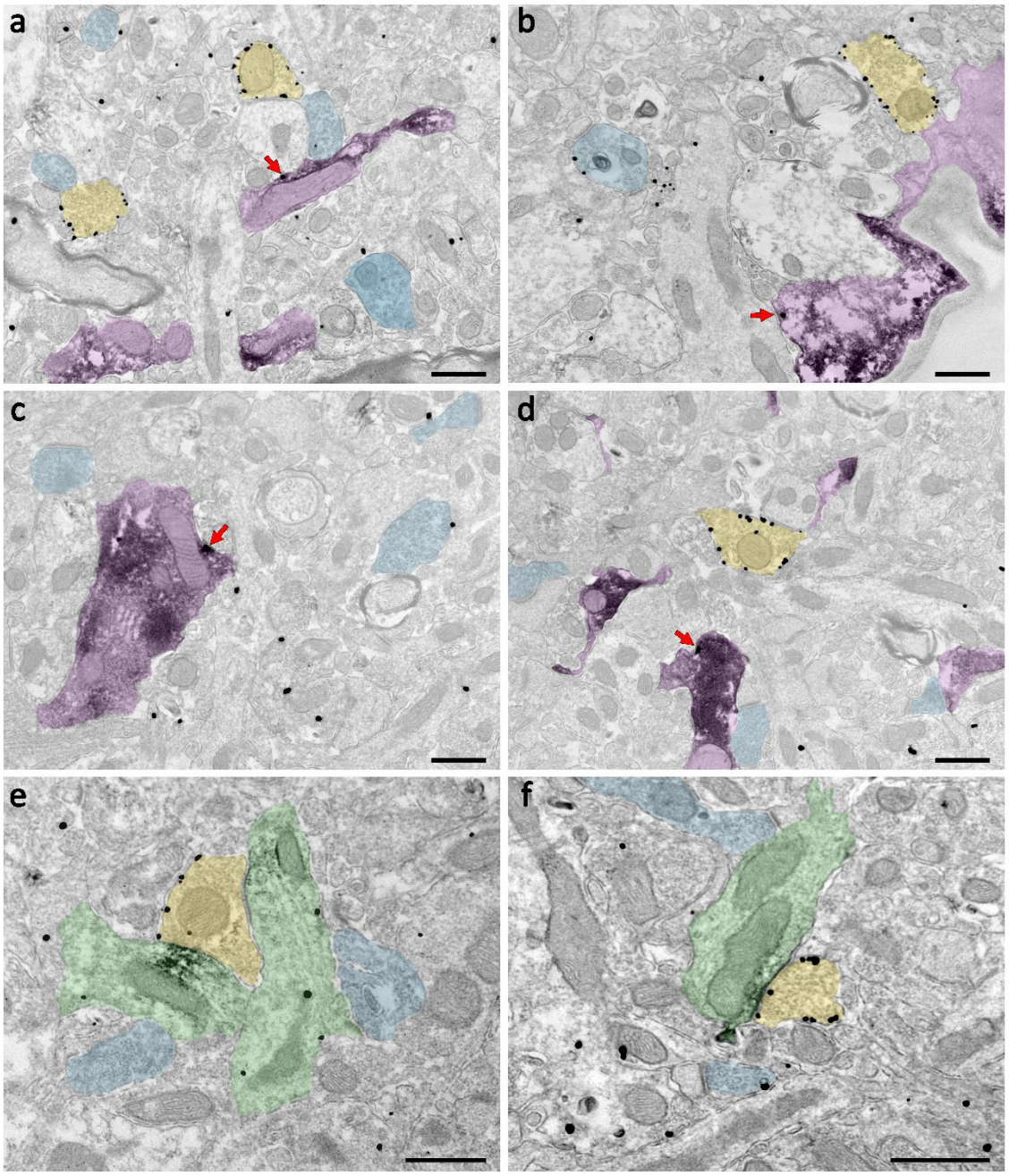

Figure 11: CB_1R in GFAP-positive astrocytes and gephyrin-positive synapses in MCFL. Double preembedding immunohistochemistry for electron microscopy. Immunoreaction product for GFAP is observed in astrocytic profiles and for gephyrin in postsynaptic membranes of inhibitory synapses. a) & c) In WT, CB_1R immunoparticles are in astrocytic membranes in addition to excitatory and inhibitory synaptic boutons. b) & d) Similar distribution pattern is observed in TRPV1-KO. e) In WT, gephyrin immunoreactivity is seen in membranes of two postsynaptic dendrites apposed to a presynaptic bouton CB_1R positive. f) In TRPV1-KO, gephyrin immunodeposits are restricted to a dendritic membrane postsynaptic to a GABAergic terminal loaded with CB_1R particles. Blue: excitatory terminals; yellow: inhibitory terminals; purple: astrocytic processes; green: dendrites; red arrows: astrocytic CB_1R particles. Scale bars: 0.5 µm

A significant increase in the proportion of CB_1R positive excitatory terminals in the MCFL was found in TRPV1-KO (% CB_1R +: 45.48 ± 2.334 % of excitatory axon terminals) versus WT (% CB_1R +: 35.19 ± 2.207 % of total excitatory terminals) (p = 0.0004; ***) (figure 12a). Interestingly, a significant reduction in excitatory terminals per area was observed in TRPV1-KO (3.168 ± 0.1309 terminals/sample area) relative to WT (3.622 ± 2.008 terminals/sample area) (figure 12d) (p = 0.034; *). Finally, there were not significant differences in the excitatory terminals of TRPV1-KO and WT in terms of the number of CB_1R + in 20 μm^2 (figure 12e), perimeter (figure 12c) and density of CB_1R (figure 12b) (Table 4).

As to the inhibitory terminals in the MCFL, there was not any significant change in the features analysed in TRPV1-KO (% CB_1R +, number of inhibitory terminals, number of of CB_1R + in 20 μm^2, axon terminal perimeter, CB_1R density) (Table 4).

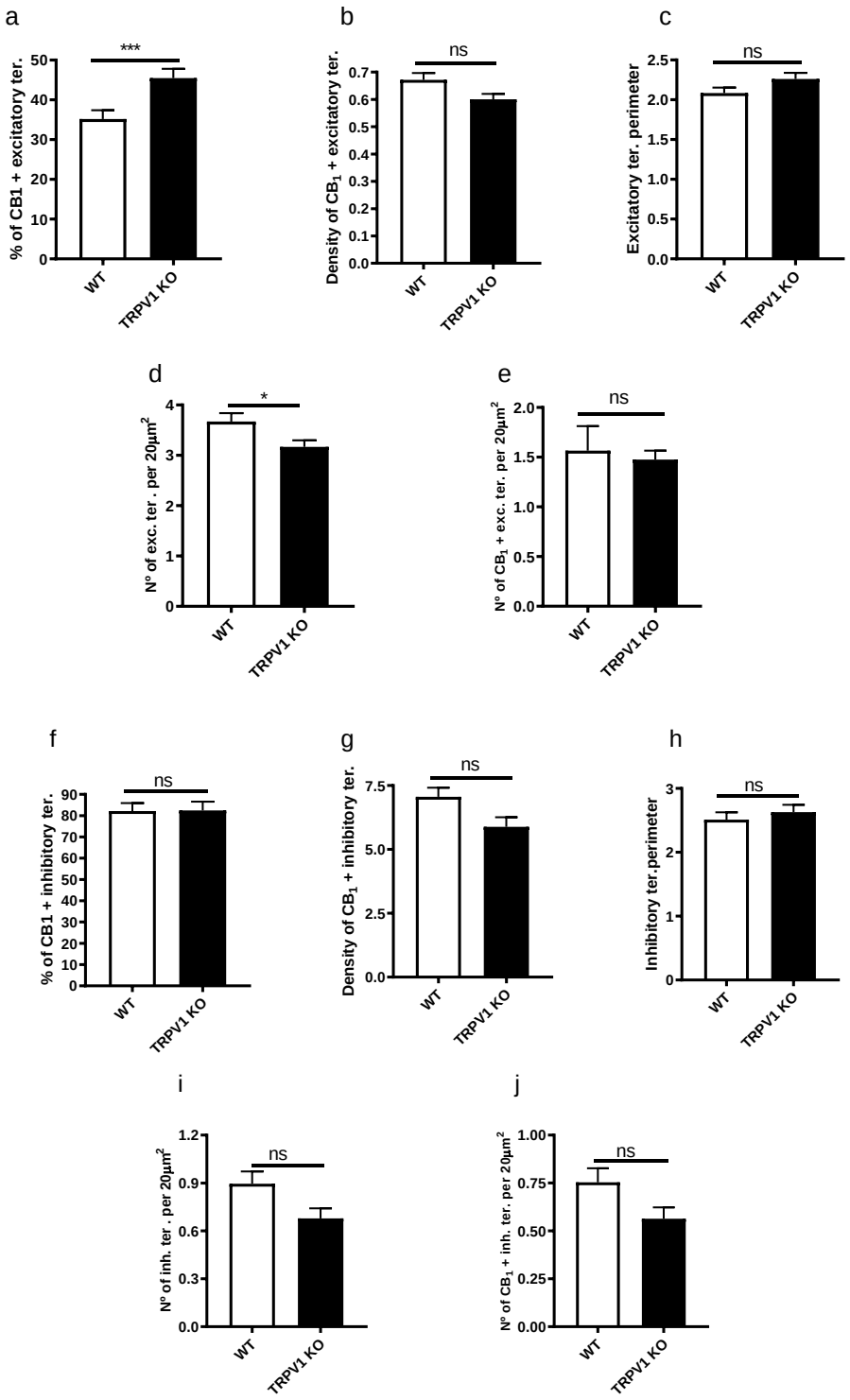

Figure 12: Ultrastructural distribution of CB_1R in the MCFL terminals of WT and TRPV1-KO mice. a) Percentage of CB_1R immunopositive excitatory terminals. b) CB_1R density (particles/µm) in CB_1R immunopositive excitatory terminals. c) Perimeter of excitatory terminals. d) Number of excitatory terminals in 20 μm^2. e) Number of CB_1R immunopositive excitatory terminals in 20 μm^2. f) Percentage of CB_1R immunopositive inhibitory terminals. g) CB_1R density (particles/µm) in CB_1R immunopositive inhibitory terminals. h) Perimeter of inhibitory terminals. i) Number of inhibitory terminals in 20 μm^2. j) Number of CB_1R immunopositive inhibitory terminals in 20 μm^2. Data were analysed by means of non-parametric or parametric tests (Mann–Whitney U test or unpaired t-test); *$p < 0.05$; ***$P < 0.0001$). All data are represented as mean ± S.E.M.

Table 4: Raw values of the parameters analysed in MCFL terminals.

Parameter	WT	TRPV1-KO	p value
Total sample area (µm²)	~ 3000 µm²	~ 3000 µm²	3 mice
% of CB_1R positive excitatory terminals	35.19 ± 2.207 % (224 / 525)	45.48 ± 2.334 % (211 / 453)	**p = 0.0004; *****
Density of CB_1R positive excitatory terminals (particle / µm)	0.6717 ± 0.0251	0.6007 ± 0.0197	p = 0.0635; ns
Excitatory terminals perimeter (µm)	2.084 ± 0.0685	2.261 ± 0.0771	p = 0.0951; ns
Number of excitatory terminals in 20 µm²	3.622 ± 2.008	3.168 ± 0.1309	**p = 0.034; ***
Number of CB_1R positive excitatory terminals in 20 µm²	1.566 ± 0.2476	1.476 ± 0.0903	p = 0.3029; ns
% of CB_1R positive inhibitory terminals	82.18 ± 3 .714 % (107 / 128)	82.43 ± 4.13 % (80 / 97)	p = 0.8141; ns
Density of CB_1R positive inhibitory terminals (particle / µm)	7.058 ± 0.3588	5.886 ± 0.376	p = 0.0578; ns
Inhibitory terminals perimeter (µm)	2.511 ± 0.1159	2.63 ± 0.113	p = 0.3863; ns
Number of inhibitory terminals in 20 µm²	0.8784 ± 0.0754	0.6783 ± 0.0632	p = 0.0892; ns
Number of CB_1R positive inhibitory terminals in 20 µm²	0.7466 ± 0.0719	0.5634 ± 0.0595	p = 0.0985; ns

5.2.2- Subcellular distribution of CB_1R in MCFL mitochondria.

CB_1R immunoparticles were also found to be localized in mitochondrial outer membranes in MCFL. The CB_1R pattern was similar between WT and TRPV1-KO (figure 13). Furthermore, the overall percentage of CB_1R + mitochondria (figure 13a) and the distribution of CB_1R in neuronal mitochondria determined by the proportion of CB_1R + mitochondria in terminals (figure 13b) and dendrites (figure 13c) was not significantly different in TRPV1-KO versus WT (Table 5). The number of mitochondria counted in 20 µm² of MCFL was similar between WT and TRPV1-KO with respect to the total number of analysed mitochondria (figure 13d). However, there was a significant increase in the number of mitochondria in terminals of TRPV1-KO (11.87 ± 0.49) versus WT (9.945 ± 0.43) (p = 0.0028; **) (figure 13e) and a significant reduction in dendritic mitochondria in TRPV1-KO (5.356 ± 0.332) relative to WT (6.725 ± 0.307) (p = 0.0048; **) (figure 13f). (Table 5).

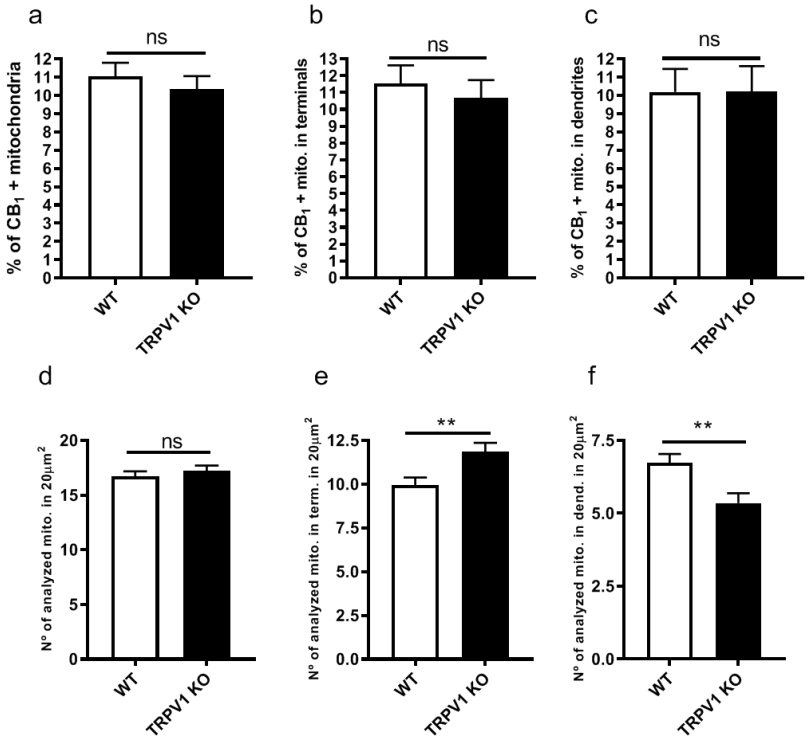

Figure 13: Ultrastructural distribution of CB_1R in MCFL mitochondria of WT and TRPV1-KO mice. a) Percentage of CB_1R immunopositive mitochondria. b) Percentage of CB_1R immunopositive mitochondria in terminals. c) Percentage of CB_1R immunopositive mitochondria in dendrites. d) Number of analysed mitochondria in 20 μm^2. e) Number of analysed mitochondria in terminals per 20 μm^2. f) Number of analysed mitochondria in dendrites per 20 μm^2. Data were analysed by means of non-parametric tests (Mann–Whitney test; **p < 0.005). All data are represented as mean ± S.E.M.

Table 5: Raw values of the parameters analysed in MCFL mitochondria.

Parameter	WT	TRPV1-KO	*p* value
Total sample area (μm^2)	~ 2000 μm^2	~ 2000 μm^2	3 mice
% of CB_1R positive mitochondria	11.06 ± 0.7335 % (164 / 1523)	10.35 ± 0.7164 % (148 / 1550)	p = 0.4208; ns
% of CB_1R positive mitochondria in terminals	11.54 ± 1.076 %	10.7 ± 1.041 %	p = 0.3326; ns
% of CB_1R positive mitochondria in dendrites	10.19 ± 1.264 %	10.23 ± 1.39 %	p = 0.6363; ns
Number of mitochondria in 20 μm^2	16.74 ± 0.431	17.22 ± 0.485	p = 0.3300; ns
Number of mitochondria in terminals in 20 μm^2	9.945 ± 0.43	11.87 ± 0.49	**p = 0.0028; ****
Number of mitochondria in dendrites in 20 μm^2	6.725 ± 0.307	5.356 ± 0.332	**p = 0.0048; ****

5.2.3- Distribution of CB_1R in MCFL astrocytes.

CB_1Rs were also localized in astrocytes in the MCFL (figure 11). The analysis of the CB_1R distribution revealed no statistical differences neither in the proportion of CB_1R + astrocytic processes (figure 14a) nor in the area occupied by the astrocytes between WT and TRPV1-KO (figure 14b) (Table 6).

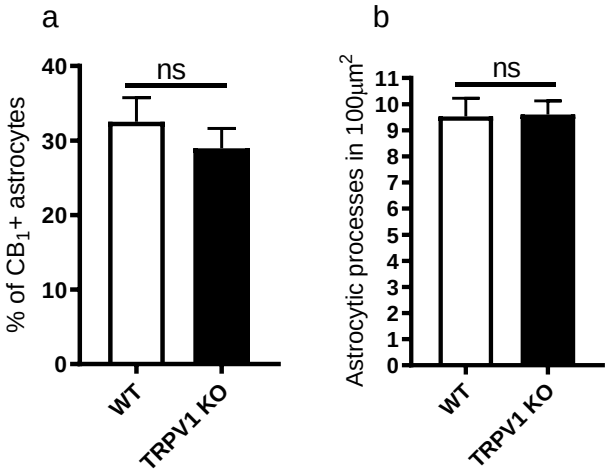

Figure 14: Ultrastructural distribution of CB_1R in MCFL astrocytes of WT and TRPV1-KO mice. a) Percentage of CB_1R immunopositive astrocytic processes. b) Number of astrocytic processes in 100 μm^2. Data were analysed by means of parametric tests (Unpaired t test. $p > 0.05$). All data are represented as mean ± S.E.M.

Table 6: Raw values of the parameters analysed in astrocytes from MCFL.

Parameter	WT	TRPV1-KO	*p* value
Total sample area (μm^2)	~ 3000 μm^2	~ 3000 μm^2	3 mice
% of CB_1R positive astrocytes	32.53 ± 3.235 % (84 / 286)	28.95 ± 2.679 % (97 / 384)	p = 0.39; ns
Area (μm^2) of astrocytic processes in 100 μm^2	9.533 ± 0.696	9.6 ± 0.524	p = 0.8194; ns

5.2.4- CB_1R particle distribution in MCFL.

We next searched for potential changes in the distribution of CB_1R (figure 15). As shown in figures 15a (WT) and figure 15b (TRPV1-KO), there was a change in the distribution of the CB_1R particles between WT and TRPV1-KO in the MCFL. Taken into account, the total number of particles analysed in each compartment (figure 15c), a significant decrease in CB_1R particles was found in inhibitory terminal membranes in TRPV1-KO (122.3 ± 15.53 particles in 100 μm^2) versus WT (230.1 ± 38.15 particles in 100 μm^2) ($p = 0.0070$; **) (figure 15d).

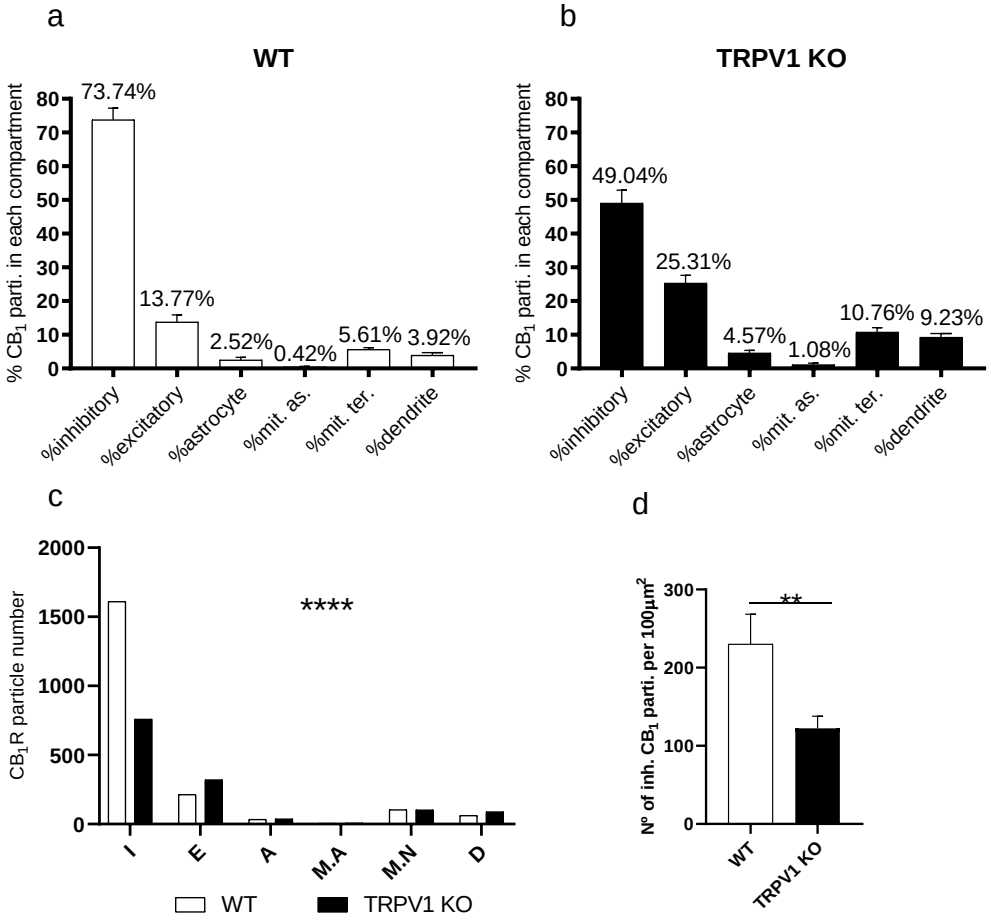

Figure 15: CB_1R distribution in the MCFL of WT and TRPV1-KO mice. a) Proportion of CB_1R labelling in different compartments normalized to the total CB_1R content in WT. b) Proportion of CB_1R labelling in different compartments normalized to the total CB_1R content in TRPV1-KO. c) Number of CB_1R particles in different membranes compartments. Chi square test. ****$p < 0.0001$. d) Number of CB_1R particles localized in inhibitory terminals in 100 μm^2. Unpaired t test. **$p < 0.01$. All data are represented as mean ± S.E.M.

5.2.5- Distribution of CB_1R in the outer 2/3 ML.

As expected, CB_1R immunoparticles were localized in perisynaptic and extrasynaptic sites of glutamatergic and GABAergic axon terminals (figure 16) and in astrocytes (figure 17) located in the outer 2/3 ML of WT and TRPV1-KO. Also, the CB_1R distribution was similar between WT and TRPV1-KO.

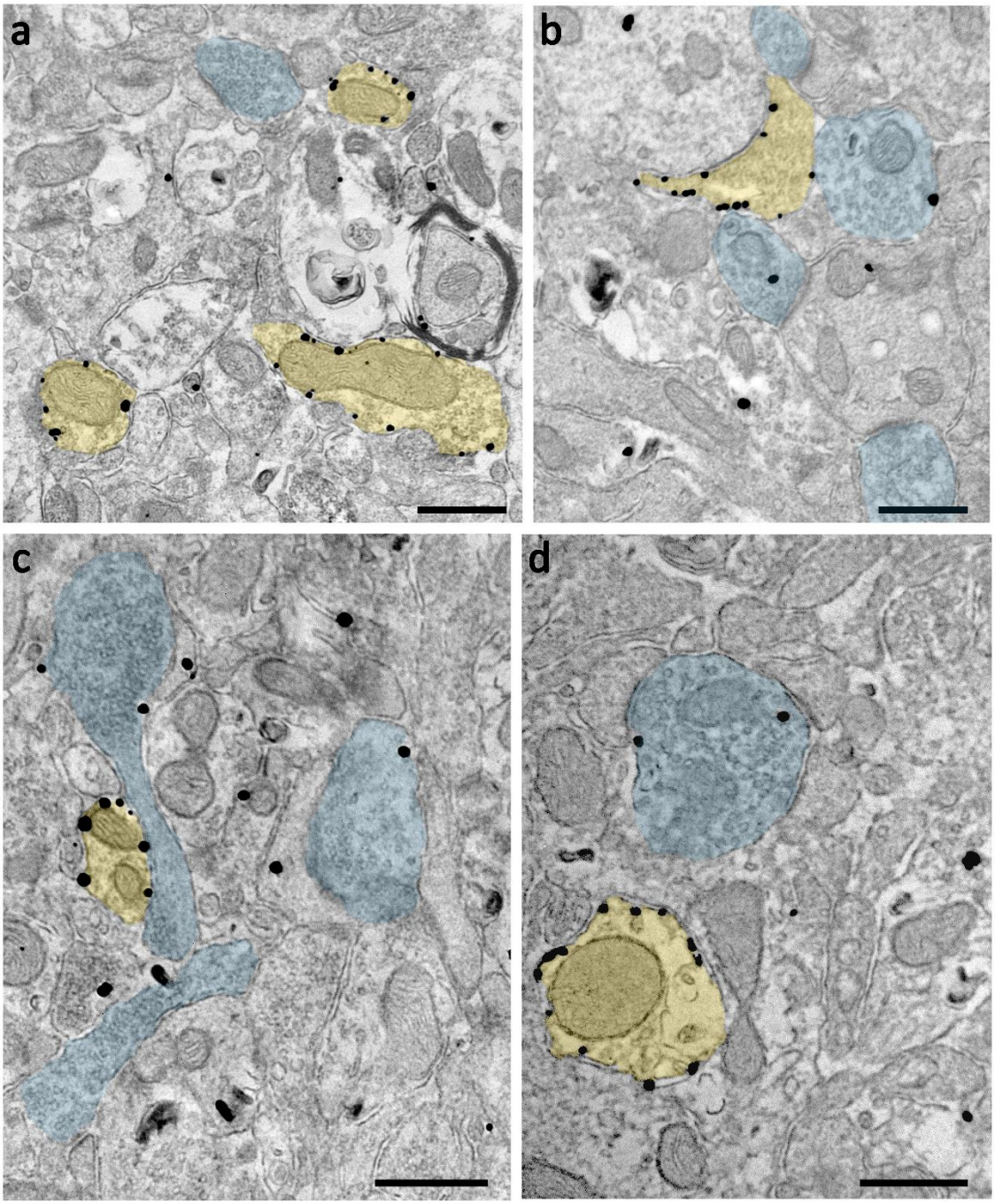

Figure 16. CB_1R localization in synaptic terminals in the outer 2/3 ML of WT and TRPV1-KO mice. **Preembedding immunogold method for electron microscopy.** CB_1R immunoparticles (black dots) are localized to inhibitory (yellow) and excitatory (blue) terminal membranes in WT (a & b) and TRPV1-KO (c & d) mice images. Scale bars: 0.5 μm.

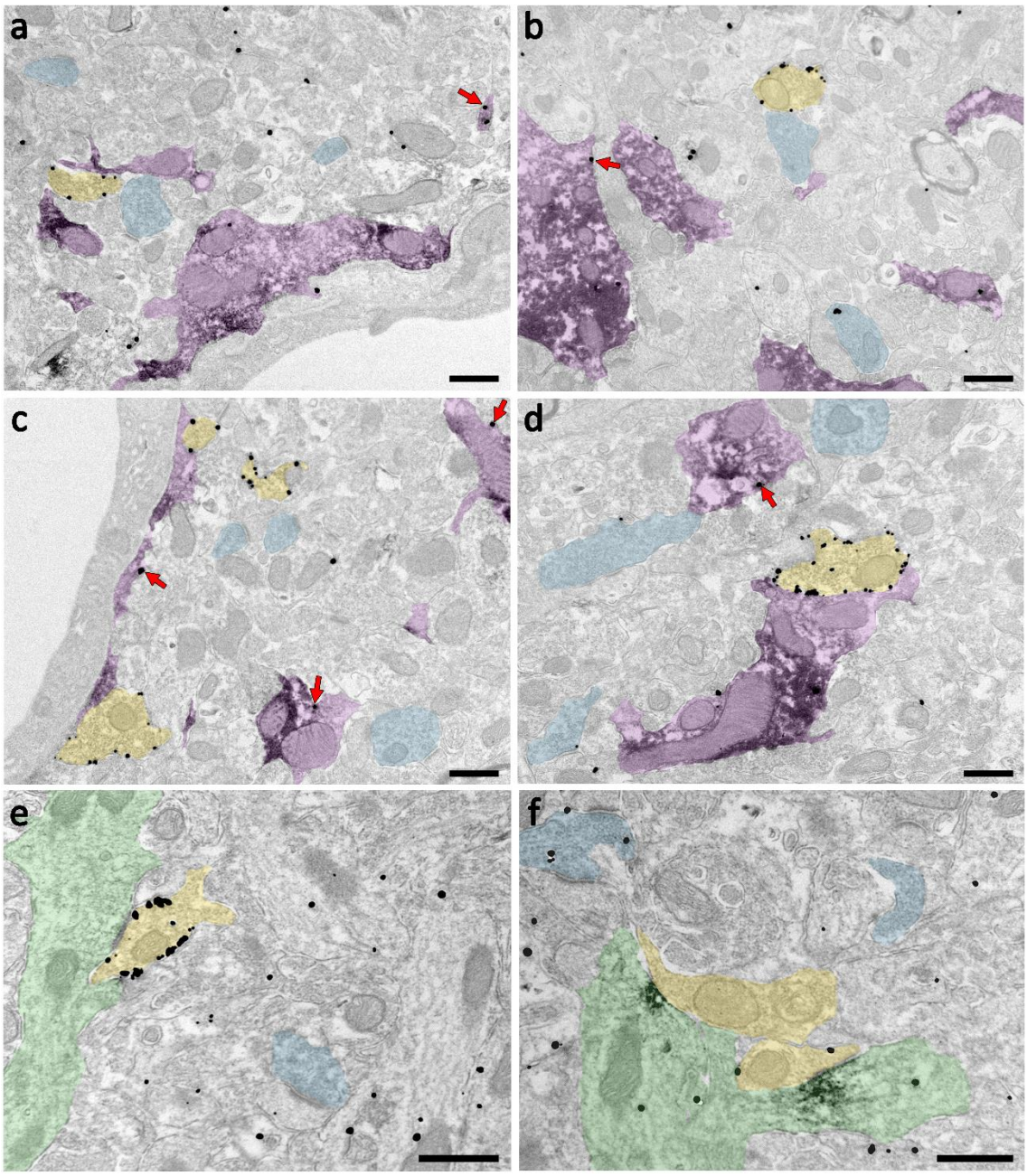

Figure 17: Double immunolabelling to detect CB_1R in astrocites and inhibitory synapses in the outer 2/3 ML of WT and TRPV1-KO mice. Combined preembedding immunoperoxidase and immunogold method for electron microscopy. CB_1R particles (red arrows) are on GFAP+ astrocytic membrane processes (purple) in WT (a & c) and TRPV1-KO (b & d). Gephyrin immunoreaction product is seen at postsynaptic sites of symmetric synapses between inhibitory terminals (yellow) containing CB_1R particles (black dots) and dendrites (green) in WT (e) and TRPV1-KO (f). Blue: excitatory terminals. Scale bars: 0.5 µm

As in the MCFL, we observed a significant increase in the proportion of CB_1R + excitatory terminals, in the outer 2/3 of the ML in TRPV1-KO (31.71 ± 1.441 % of total excitatory terminals) compared to WT (28.03 ± 1.331 % of total excitatory terminals) (figure 18a) (p = 0.0103; *). There was also found a significant reduction in excitatory terminals per area (20 μm^2) in TRPV1-KO (3.73 ± 0.1154 terminals) versus WT (4.333 ± 0.123 terminals) (p = 0.0003; ***) (figure 18d). However, the number of CB_1R + excitatory terminals per area (figure 18e), perimeter of the excitatory terminals (figure 18c) and density of CB_1R in positive excitatory terminals (figure 18b) were similar between TRPV1-KO and WT (Table 7).

As to the inhibitory terminals, there were not significant differences in the percentage of CB_1R + inhibitory terminals (figure 18f), number of inhibitory terminals per 20 μm^2 (figure 18i), number of CB_1R + inhibitory terminals per area (figure 18j), nor in the perimeter of the inhibitory terminals (figure 18h) between TRPV1-KO and WT. However, the density of CB_1R particles significantly decrease in TRPV1-KO (6.0106 ± 0.2148 particle/µm) versus WT (6.639 ± 0.1991 particle/µm) (p = 0.0402; *) (figure 18g) (Table 7).

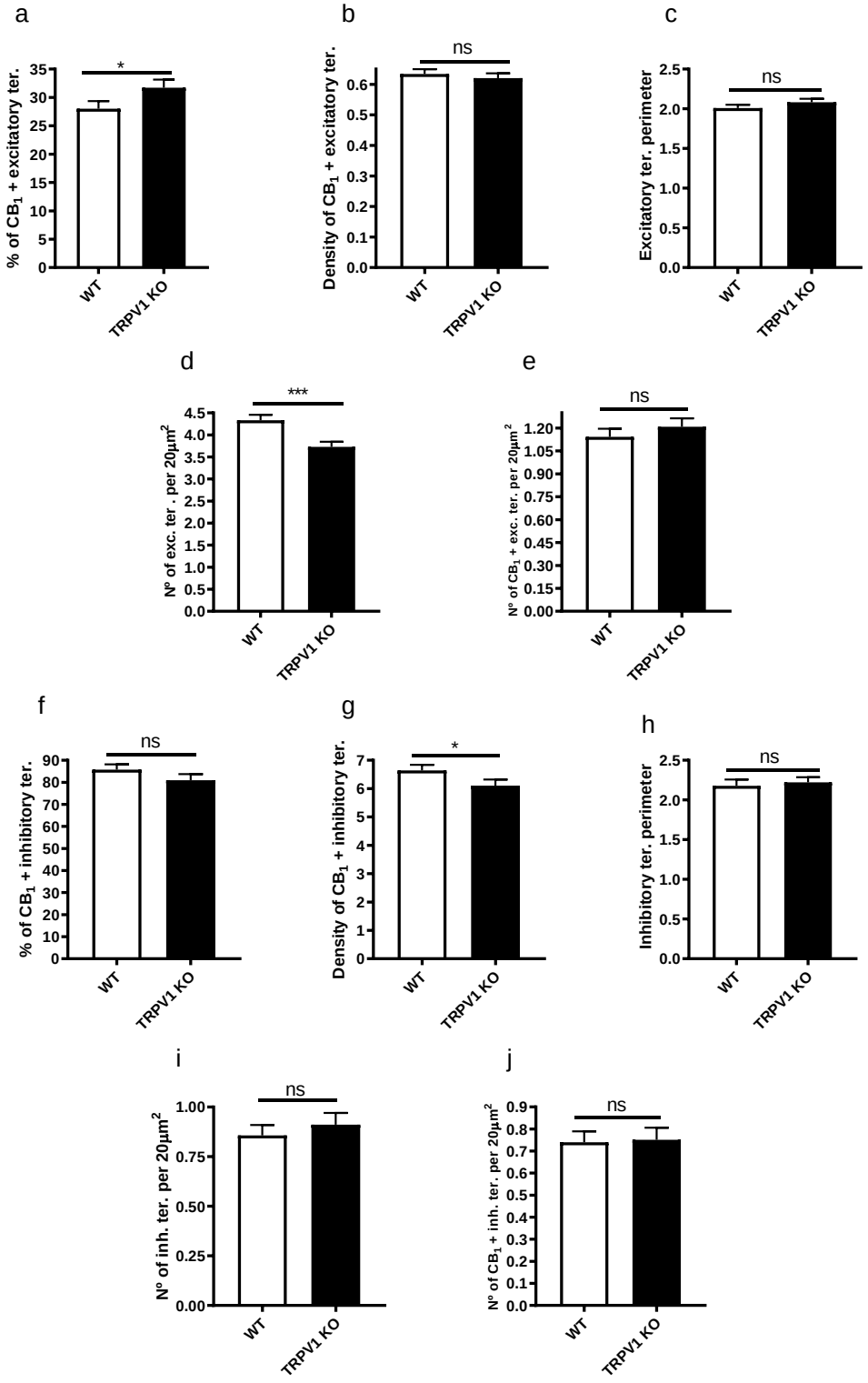

Figure 18: CB_1R distribution in the outer 2/3 ML of WT and TRPV1-KO mice. a) Percentage of CB_1R immunopositive excitatory terminals. b) CB_1R density (particles/µm) in CB_1R immunopositive excitatory terminals. c) Perimeter of the excitatory terminals. d) Number of excitatory terminals in 20 μm^2. e) Number of CB_1R immunopositive excitatory terminals in 20 μm^2. f) Percentage of CB_1R immunopositive inhibitory terminals. g) CB_1R density (particles/µm) in CB_1R immunopositive inhibitory terminals. h) Perimeter of inhibitory terminals. i) Number of inhibitory terminals in 20 μm^2. j) Number of CB_1R immunopositive inhibitory terminals in 20 μm^2. Data were analysed by means of non-parametric or parametric tests (Mann–Whitney U test or unpaired t-test); *$p < 0.05$; ***$P < 0.0001$. All data are represented as mean ± S.E.M.

Table 7: Raw values of the parameters analysed in terminals of the outer 2/3 ML.

Parameter	WT	TRPV1-KO	*p* value
Total sample area (µm²)	~ 6000 µm²	~ 6000 µm²	3 mice
% of CB_1R positive excitatory terminals	28.03 ± 1.331 % (331 / 1272)	31.71 ± 1.441 % (354 / 1093)	**p = 0.0103; ***
Density of CB_1R positive excitatory terminals (particle / µm)	0.6339 ± 0.0157	0.6203 ± 0.01565	p = 0.2772; ns
Excitatory terminals perimeter (µm)	2.008 ± 0.0432	2.083 ± 0.0422	p = 0.1431; ns
Number of excitatory terminals in 20 µm²	4.333 ± 0.123	3.73 ± 0.1154	**p = 0.0003; ***
Number of CB_1R positive excitatory terminals in 20 µm²	1.143 ± 0.0522	1.208 ± 0.0577	p = 0.4078; ns
% of CB_1R positive inhibitory terminals	85.79 ± 2.398 % (214 / 252)	81 ± 2.705 % (220 / 267)	p = 0.1594; ns
Density of CB_1R positive inhibitory terminals (particle / µm)	6.639 ± 0.1991	6.0106 ± 0.2148	**p = 0.0402; ***
Inhibitory terminals perimeter (µm)	2.179 ± 0.0792	2.22 ± 0.637	p = 0.1288; ns
Number of inhibitory terminals in 20 µm²	0.8567 ± 0.0526	0.9113 ± 0.0593	p = 0.7525; ns
Number of CB_1R positive inhibitory terminals in 20 µm²	0.74 ± 0.0494	0.7509 ± 0.0550	p= 0.8098; ns

5.2.6- CB_1R in mitochondria of the outer 2/3 ML.

CB_1R immunoparticles were also localized in mitochondrial outer membranes in the outer 2/3 ML with a similar distribution in WT and TRPV1-KO. Besides, there were not differences in the total proportion of CB_1R + mitochondria (figure 19a), percentage of CB_1R + mitochondria in terminals (figure 19b) and dendrites (figure 19c) between TRPV1-KO and WT (Table 8). However, the total number of analysed mitochondria in TRPV1-KO (18.22 ± 0.375 mitochondria in 20 µm²) was significantly lower than in WT (23.24 ± 0.501 mitochondria in 20 µm²) ($p < 0.0001$; ****) (figure 19d). Furthermore, these significant differences were also observed by neuronal compartments: in terminals (TRPV1-KO: 11.75 ± 0.369 mitochondria; WT: 15.56 ± 0.472 mitochondria in 20 µm²) ($p < 0.0001$; ****) (figure 19e), and in dendrites (TRPV1-KO: 6.452 ± 0.207 mitochondria; WT: 7.638 ± 0.268 mitochondria in 20 µm²) ($p = 0.0029$; **) (figure 19f) (Table 8).

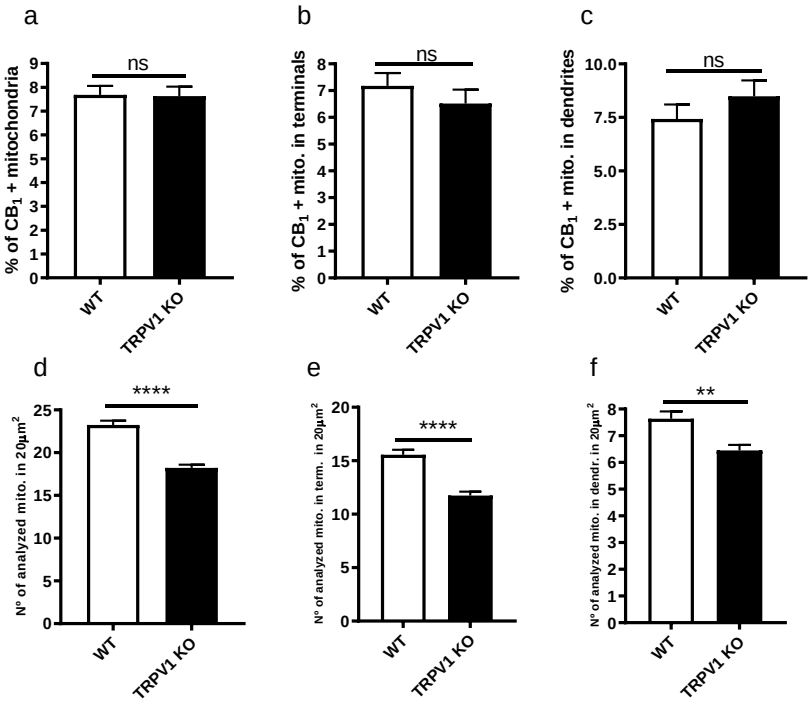

Figure 19: CB_1R distribution in mitochondria of the outer 2/3 ML of WT and TRPV1-KO mice. a) Percentage of CB_1R immunopositive mitochondria. b) Percentage of CB_1R immunopositive mitochondria in terminals. c) Percentage of CB_1R immunopositive mitochondria in dendrites. d) Number of analysed mitochondria per 20 µm². e) Number of analysed mitochondria in terminals per 20 µm². f) Number of analysed mitochondria in dendrites per 20 µm². Data were analysed by means of non-parametric (Mann–Whitney); *p < 0.05; **p < 0.005; ***p < 0.0001. All data are represented as mean ± S.E.M.

Table 8: Raw values of the parameters analysed in mitochondria of the outer 2/3 ML.

Parameter	WT	TRPV1-KO	*p* value
Total sample area (µm²)	~ 4000 µm²	~ 4000 µm²	3 mice
% of CB_1R positive mitochondria	7.68 ± 0.375 % (342 / 4042)	7.63 ± 0.4 % (254 / 3024)	p = 0.8748; ns
% of CB_1R positive mitochondria in terminals	7.175 ± 0.484 %	6.519 ± 0.514 %	p = 0.1452; ns
% of CB_1R positive mitochondria in dendrites	7.432 ± 0.675 %	8.491 ± 0.742 %	p = 0.3711; ns
Number of mitochondria per 20 µm²	23.24 ± 0.501	18.22 ± 0.375	**p < 0.0001; ******
Number of mitochondria in terminals per 20 µm²	15.56 ± 0.472	11.75 ± 0.369	**p < 0.0001; ******
Number of mitochondria in dendrites per 20 µm²	7.638 ± 0.268	6.452 ± 0.207	**p = 0.0029; ****

5.2.7- CB_1R in astrocytes of the outer 2/3 ML.

CB_1Rs were also localized in astrocytes in the outer 2/3 of the ML (figure 17). The analysis of the CB_1R distribution revealed no significant changes in the proportion of CB_1R + astrocytic processes (figure 20a) nor in the area of astrocytes (figure 20b) between WT and TRPV1-KO. In contrast, a significant decrease in CB_1R density was observed in TRPV1-KO (0.2432 ± 0.0405 particles/µm) relative to WT (0.4122 ± 0.0727 particles/µm) (p = 0.0452; *) (figure 20c) (Table 9).

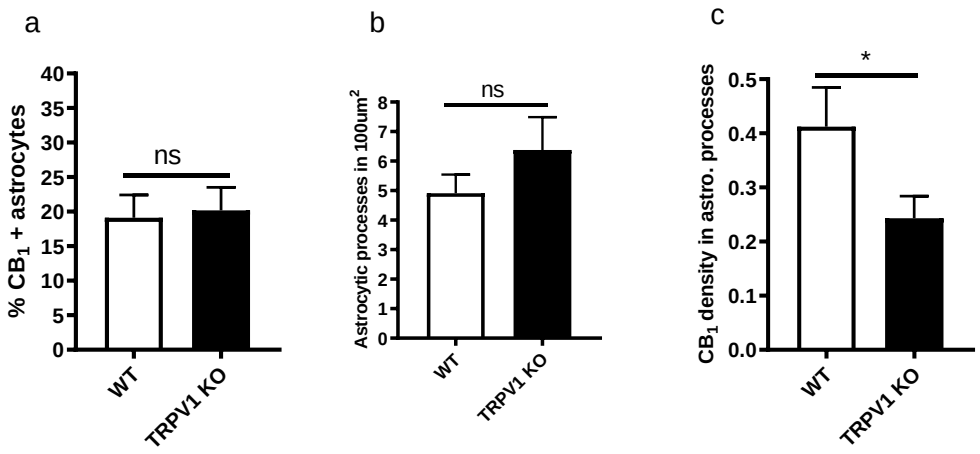

Figure 20: CB_1R distribution in the outer 2/3 ML astrocytes of WT and TRPV1-KO mice. a) Percentage of CB_1R immunopositive astrocytic processes. b) Number of astrocytic processes in 100 µm^2. c) Density of CB_1R immunopositive astrocytic processes. Data were analysed by means of non-parametric or parametric tests (Mann–Whitney U test or unpaired t-test); *p < 0.05. All data are represented as mean ± S.E.M.

Table 9: Raw values of the parameters analysed in astrocytes of the outer 2/3 ML.

Parameter	WT	TRPV1-KO	*p* value
Total sample area (µm^2)	~ 2700 µm^2	~ 2700 µm^2	3 mice
% of CB_1R positive astrocytes	19.1 ± 3.29 % (24 / 127)	20.19 ± 3.31 % (29 / 165)	p = 0.39; ns
Astrocytic processes area (µm^2) in 100 µm^2	5.325 ± 1.008	6.666 ± 1.493	p = 0.3401; ns
CB_1R density in astrocytic processes	0.412 ± 0.0727	0.243 ± 0.0405	**p = 0.0452; ***

5.2.8- CB_1R particle distribution in the outer 2/3 ML.

We next analysed the general CB_1R distribution considering all the particles localized over the identified profiles. As shown in figures 21a (WT) and figure 21b (TRPV1-KO), there was a change in the distribution of the CB_1R particles between WT and TRPV1-KO. Thus, in TRPV1-KO (figure 21b), there was a reduction in the percentage of CB_1R particles in inhibitory terminals as well as there was an increase in the proportion of particles in excitatory terminals, astrocytes, including

mitochondria in astrocytes, and in dendrites. Furthermore, taken into account the total number of particles analysed in each compartment (figure 21c) a change in the CB_1R distribution in terminal membranes was found in TRPV1-KO mice compared to WT.

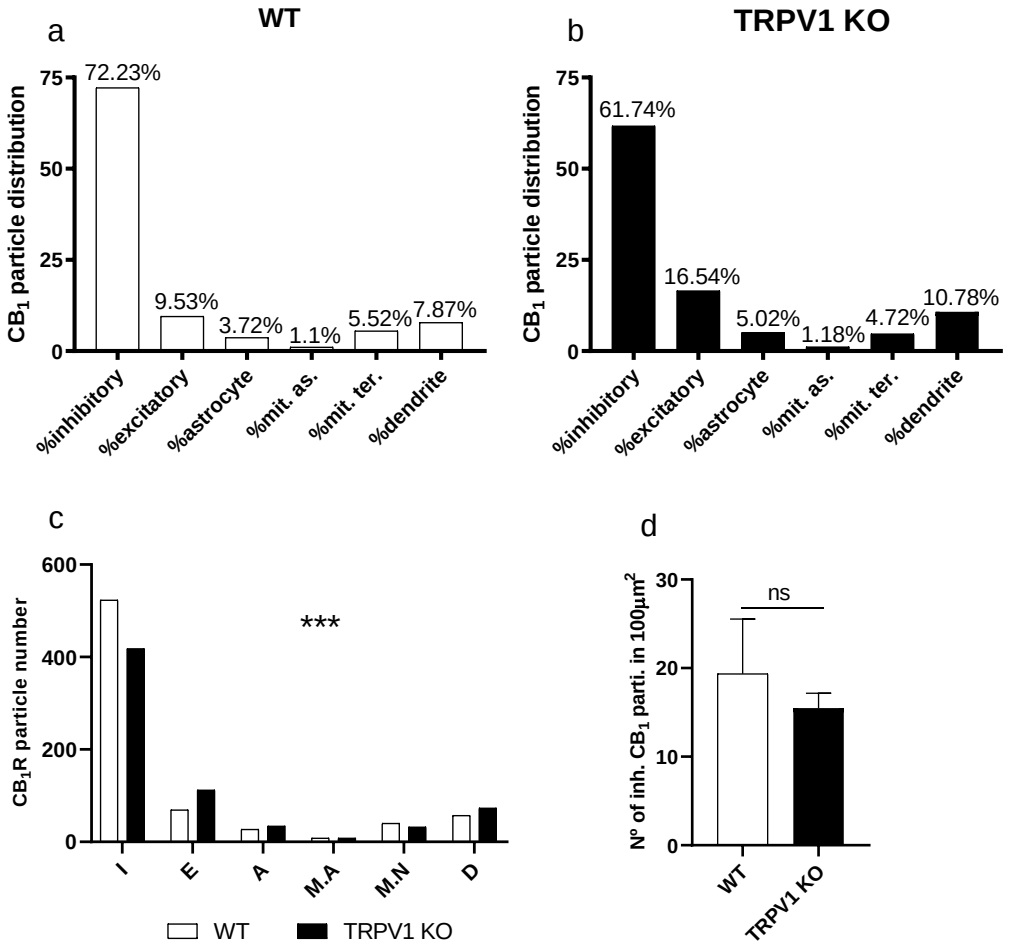

Figure 21: CB_1R distribution in the outer 2/3 of the ML of WT and TRPV1-KO mice. a) Proportion of CB_1R labelling in different compartments normalized to the total CB_1R content in WT. b) Proportion of CB_1R labelling in different compartments normalized to the total CB_1R content in TRPV1-KO. c) Number of CB_1R particles in different membrane compartments in WT and TRPV1-KO. Chi square test. *** $p < 0.001$. d) Number of CB_1R particles in inhibitory terminals in 100 μm^2. Mann Whitney test. $p > 0.05$. All data are represented as mean ± S.E.M.

5.3- Synaptic plasticity in DGML of TRPV1-KO mice.

Synaptic plasticity in the dentate molecular layer was investigated in TRPV1-KO mice by application a low frequency stimulation (LFS) protocol known to reliably induce eCB-eLTD in DG (Peñasco et al., 2019). The DGML was divided into the two zones analysed by electron microscopy: MCFL and outer 2/3 ML. In turn, the outer 2/3 ML was subdivided into the two differentiated zones targeted by the MPP and LPP arising from the entorhinal cortex. CB_1 and

TRPV1 receptors have been described to be localized at different proportions in the ML zones (Puente el al., 2015; Canduela et al., 2015; Gutierrez-Rodriguez et al., 2016; Bonilla-Del Río et al., 2019). Moreover, there have been described several types of synaptic plasticity driven by these receptors in the DGML (Chavéz et al., 2011; 2014; Puente et al., 2011; Wang et al., 2016; 2018; Peñasco et al., 2019).

For the electrophysiological recordings, the minimum intensity needed to obtain the maximal signal was established (figure 22). As a result, around 60% of the maximal value was used for plasticity protocols and synaptic transmission. With respect to the maximum intensity required, there was not found any significant difference between WT (average fEPSP slope: 0.002855 ± 0.0007114) and TRPV1-KO (average fEPSP slope 0.002547 ± 0.000622; p = 0.0977; ns).

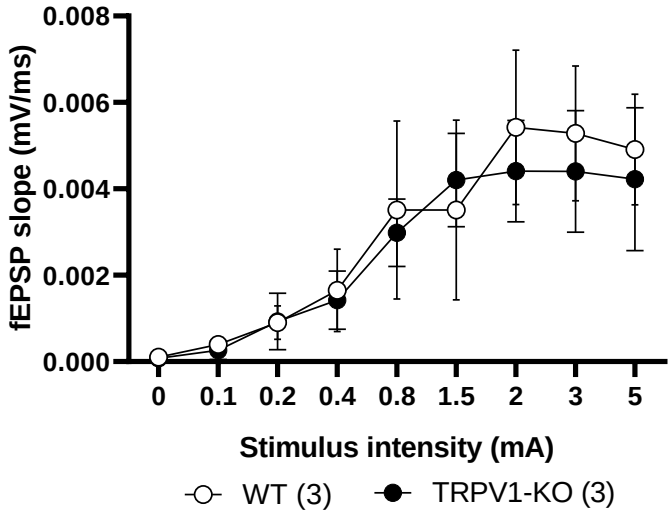

Figure 22: No changes in basal activity frequency after genetic deletion of TRPV1. Input-output curves where mean fEPSP slopes (mv/ms) are plotted against the stimulation intensities in hippocampal slices of WT and TRPV1-KO mice. The area under the curve was calculated to analyse the data. Wilcoxon test. p > 0.05. All data are expressed as mean ± S.E.M.

5.3.1- Synaptic plasticity in the MCFL.

In the MCFL, as shown in our laboratory by Peñasco et al. (2019), there was not an eCB-driven LTD of the fEPSP after LFS stimulation in WT mice. In contrast, a little potentiation of fEPSP was found in WT (111.8 ± 5.111 %; p = 0.0315; *) (figure 23a-b) that was increased in TRPV1-KO (137.2 ± 8.748 %; p = 0.0011; **) (figure 23a-c). This potentiation in the MCFL of TRPV1-KO was not abolished after bath application of the CB_1R inverse agonist AM251 ([4 µm]; 138.7 ± 15.82 %; p = 0.6389; ns) (figure 23d-g) nor by the NMDAR antagonist DL-APV ([50 µm]; 130.1 ± 14.9 %; p = 0.6485; ns) (figure 23e-h). Furthermore, the potentiation obtained after MCFL-LFS stimulation in WT was neither fully reduced by bath application of DL-APV ([50 µm]; 103.1 ± 4.145 %; p = 0.1982; ns) (figure 23f-i).

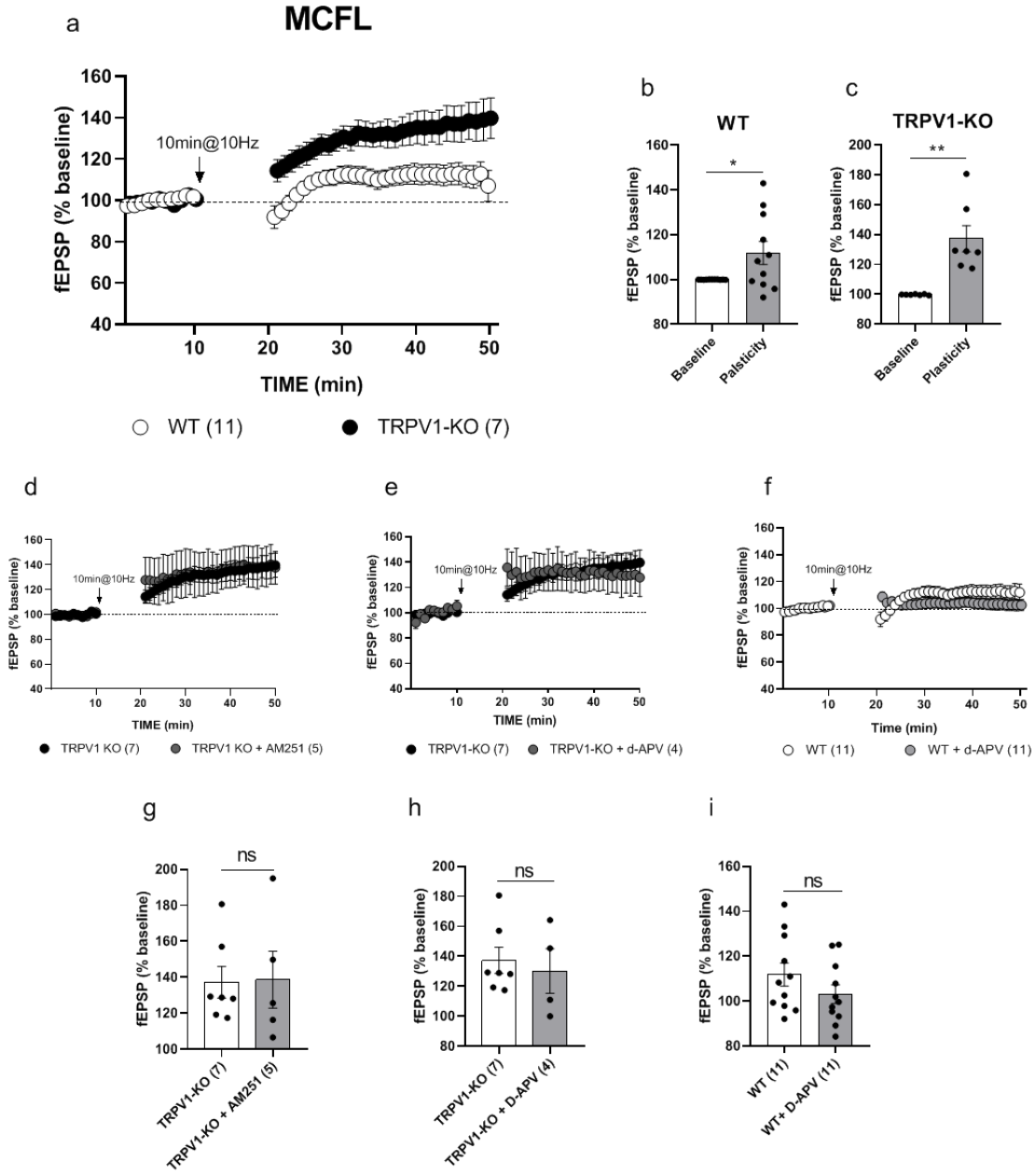

Figure 23: Excitatory long-term potentiation (LTP) at mossy cell fibre layer (MCFL) synapses in WT and TRPV1-KO mice. For representation, each experiment was normalized to its baseline. The average of the fEPSP areas is shown. A black arrow marks low frequency stimulation (LFS) protocol application. a) Low frequency synaptic stimulation (LFS, 10 min, 10 Hz) triggers LTP at MCFL in WT (white circles) and TRPV1-KO (black circles) mice. b) Representative histogram of the last 10 minutes fEPSP after LFS in WT mice. Unpaired t test. *$p < 0.05$. c) Representative histogram of the last 10 minutes fEPSP after LFS in TRPV1-KO mice. Unpaired t test. ** $p < 0.005$. d) AM251 [4 µm] has no effect over the LTP observed after LFS in TRPV1-KO mice (grey circles). e) and f) D-APV [50 µm] has no significant effect over the LTP observed after LFS in TRPV1-KO (grey circles in g) and WT (grey circles in f) mice respectively. g) Representative histogram of the last 10 minutes fEPSP after LFS in the presence of AM251 [4 µm] in TRPV1-KO mice. Mann Whitney test. $p > 0.05$. h) Representative histogram of the last 10 minutes fEPSP after LFS in the presence of D-APV [50 µm] in TRPV1-KO mice. Mann Whitney test. $p > 0.05$. i) Representative histogram of the last 10 minutes fEPSP after LFS in the presence of D-APV [50 µm] in WT mice. Unpaired t test. $p > 0.05$. All data are expressed as mean ± S.E.M.

Taken together, the data showed an effect of the TRPV1 deletion on plasticity in MCL but the shift to LTP was not driven by CB_1R. In contrast, NMDAR seems to participate in the potentiation observed in WT but not in the one observed in TRPV1-KO.

5.3.2- Synaptic plasticity in the PP.

In the MPP, the eCB-eLTD described previously by our laboratory (Peñasco et al., 2019) was confirmed in WT: fEPSP was significantly reduced after LFS (80.21 ± 6.497 %; p = 0.0021; **) (figure 24a-c). In TRPV1-KO, however, a significant fEPSP potentiation was observed after LFS (135 ± 7.119 %; p < 0.0001; ****) (figure 24a-d). In the LPP, the baseline was potentiated in both WT and TRPV1-KO (WT: 142 ± 13.44 %: p = 0.0068; ** (figure 24b-e) // TRPV1-KO: 142.9 ± 8.314 %; p = 0.0022; ** (figure 24b-f)).

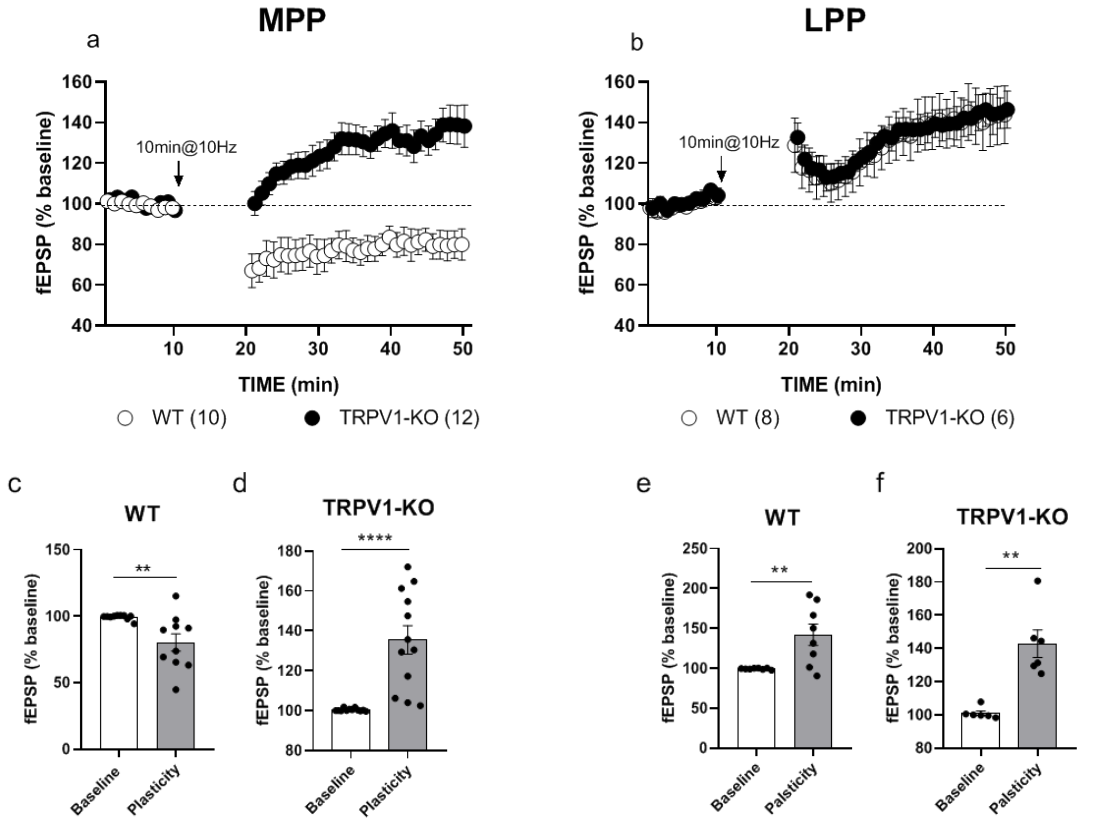

Figure 24: Excitatory long-term potentiation (eLTP) at MPP synapses in TRPV1-KO mice and eLTP at LPP synapses in WT and TRPV1-KO mice. For representation, each experiment was normalized to its baseline. The average of the fEPSP areas is shown. A black arrow marks LFS application. a) LFS (10 min, 10 Hz) triggers LTD at MPP in WT (white circles) and elicits LTP in TRPV1-KO (black circles). b) LFS (10 min, 10 Hz) triggers LTP at LPP in WT (white circles) and TRPV1-KO (black circles). c) Representative histogram of the last 10 minutes fEPSP after LFS at MPP in WT. Mann Whitney test. **p < 0.005. d) Representative histogram of the last 10 minutes fEPSP after LFS at MPP in TRPV1-KO. Mann Whitney test. **** p < 0.0001. e) Representative histogram of the last 10 minutes fEPSP after LFS at LPP in WT. Unpaired t test. **p < 0.005. d) Representative histogram of the last 10 minutes fEPSP after LFS at LPP in TRPV1-KO. Mann Whitney test. ** p < 0.005. All data are expressed as mean ± S.E.M.

Bearing these results in mind, the attention was then focused on the plasticity shift observed in the MPP of TRPV1-KO mice. For a better characterization of it, in addition to investigate the implication of NMDA receptors, the participation of anandamide and 2-AG was also studied by bath application and pre-incubation of drugs affecting synthesis and degradation of both eCBs. Furthermore, to confirm that the changes observed in CB_1R distribution and in endocannabinoid-related protein expression could have a direct impact in the LTP shift observed in the MPP of TRPV1-KO, a pharmacological TRPV1 blockade was tested to mimic the TRPV1 knockout conditions without having compensatory effects and, at the same time, allowing the comparison with the physiological effects seen in TRPV1-KO mice.

To determine whether CB_1R participated in the LTP observed in TRPV1-KO MPP after a LFS application, AM251 was applied. In WT, as previously described by our group (Peñasco et al., 2019) the fEPSP reduction was reverted by blocking of CB_1R ([4 µm]; 98.16 ± 9.553 %; p = 0.1377; ns) (figure 25a-c). In TRPV1-KO, the fEPSP potentiation was significantly reverted after AM251 application ([4 µm]; 95.37 ± 8.263 %; p = 0.0034; **) (figure 25a-d). Moreover, DL-APV did not have any effect on the fEPSP potentiation in TRPV1-KO ([50 µm]; 123 ± 10.17 %; p = 0.3128; ns) (figure 25b-e).

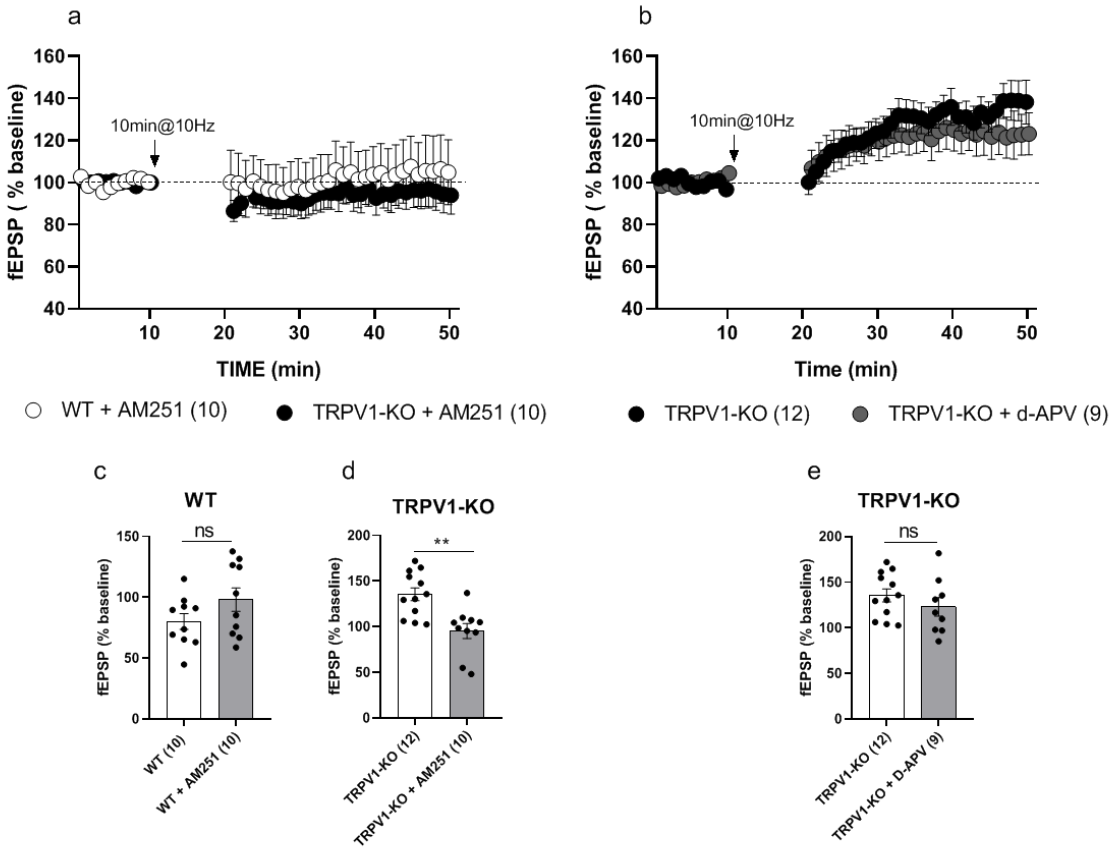

Figure 25: **LTD and LTP at MPP synapses in WT and TRPV1-KO mice respectively are CB_1R dependent but not NMDAR dependent.** For representation, each experiment was normalized to its baseline. The average of the fEPSP areas is shown. A black arrow marks LFS application. a) AM251 [4 µm] has a significant effect over the LTD and LTP observed after LFS in WT (white circles) and TRPV1-KO (black circles) respectively. b) D-APV [50 µm] has no effect over the LTP observed after LFS in TRPV1-KO (grey circles). c) Representative histogram of the last 10 minutes fEPSP after LFS in the presence of AM251 [4 µm] in WT Unpaired t test. $p > 0.05$. d) Representative histogram of the last 10 minutes fEPSP after LFS in the presence of AM251 [4 µm] in TRPV1-KO. Mann Whitney test. $^{**}p < 0.005$. e) Representative histogram of the last 10 minutes fEPSP after LFS in the presence of D-APV [50 µm] in TRPV1-KO. Unpaired t test. $p > 0.05$. All data are expressed as mean ± S.E.M.

In WT, the increase in 2-AG levels by the MAGL inhibitor JZL 184 reverted the fEPSP depression triggered by LFS in MPP ([50 µm]; 98.34 ± 7.11 %; p = 0.0765; ns) (figure 26a-c). Also, the potentiation observed in TRPV1-KO was significantly blocked by JZL 184 ([50 µm]; 104.9 ± 5.317 %; p = 0.0058; **) (figure 26b-d).

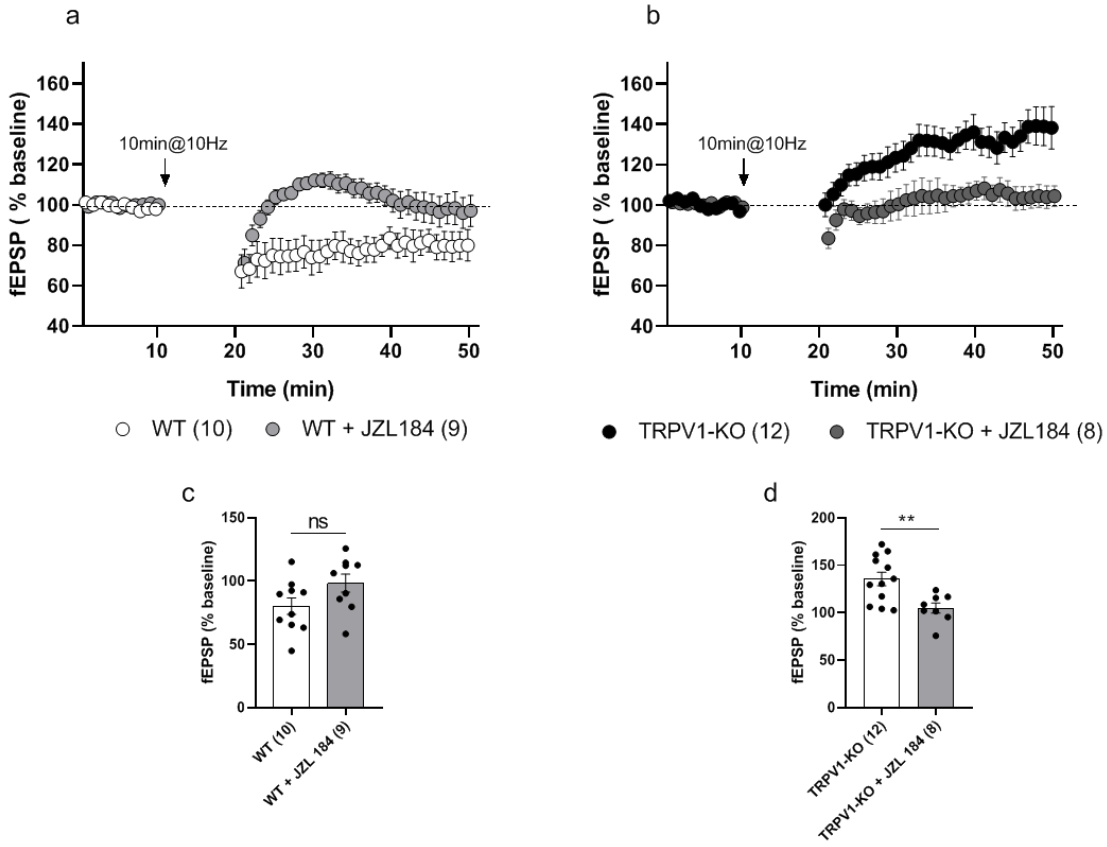

Figure 26: 2-AG increase blocks the LTD and LTP at MPP synapses in WT and TRPV1-KO mice, respectively. For representation, each experiment was normalized to its baseline. The average of the fEPSP areas is shown. A black arrow marks LFS. a) JZL 184 [50 µm] has a significant effect over the LTD observed after LFS in WT (light grey circles). b) JZL 184 [50 µm] significantly affects the LTP observed after LFS in TRPV1-KO (dark grey circles). c) Representative histogram of the last 10 minutes fEPSP after LFS in the presence of JZL 184 [50 µm] in WT. Unpaired t test. $p > 0.05$. d) Representative histogram of the last 10 minutes fEPSP after LFS in the presence of JZL 184 [50 µm] in TRPV1-KO. Unpaired t test. $^{**}p < 0.005$. All data are expressed as mean ± S.E.M.

Then, 2-AG levels were pharmacologically decreased by adding the DAGLα inhibitor THL to the perfusion medium. In WT, THL restored to baseline the depression observed in the fEPSP ([10 µm]; 109.3 ± 7.206 %; p = 0.0077; **) (figure 27a-c). In TRPV1-KO, the fEPSP potentiation was significantly reduced by THL ([10 µm]; 112.9 ± 5.295 %; p = 0.0273; *) (figure 27b-d).

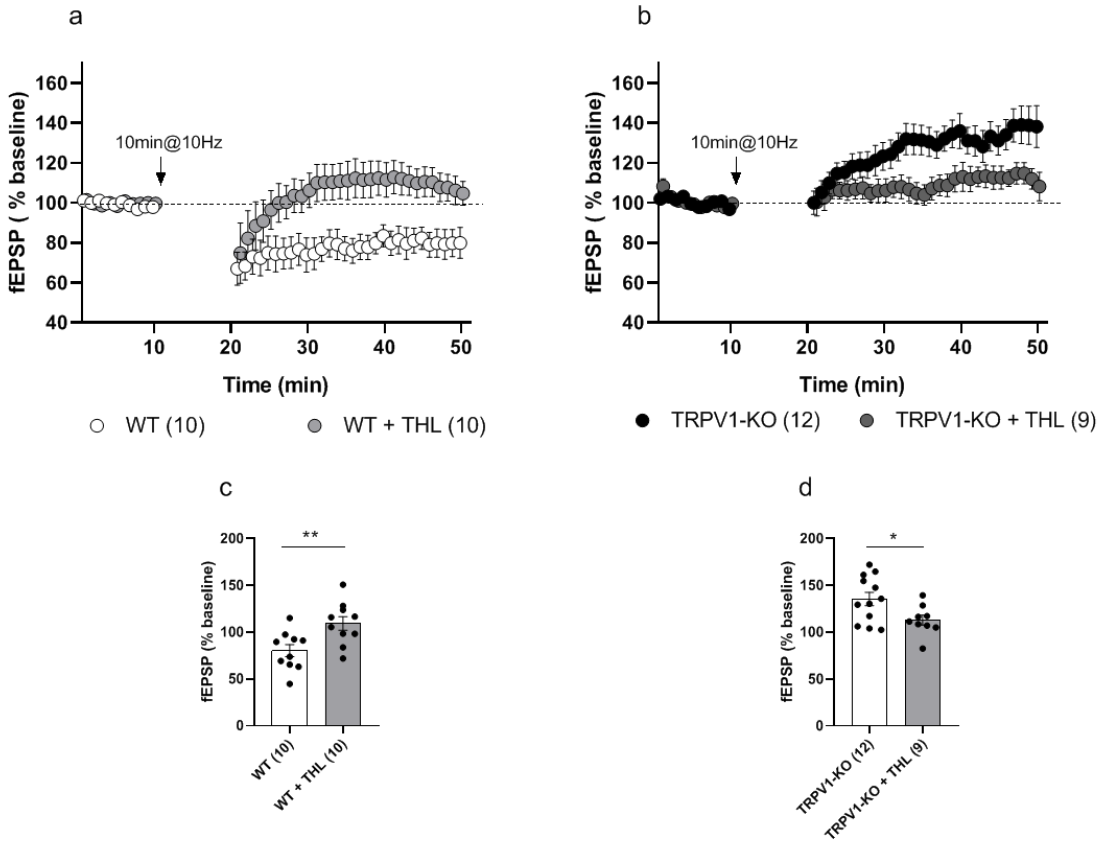

Figure 27: 2-AG decrease blocks LTD and LTP at MPP synapses in WT and TRPV1-KO mice, respectively. For representation, each experiment was normalized to its baseline. The average of the fEPSP areas is shown. A black arrow marks LFS application. a) THL [10 µm] has a significant effect over the LTD observed after LFS in WT (light grey circles). b) THL [10 µm] significantly affects the LTP observed in TRPV1-KO (dark grey circles). c) Representative histogram of the last 10 minutes fEPSP after LFS in the presence of THL [10 µm] in WT. Unpaired t test. **p < 0.005. d) Representative histogram of the last 10 minutes fEPSP after LFS in the presence of THL [10 µm] in TRPV1-KO. Unpaired t test. *p < 0.05. All data are expressed as mean ± S.E.M.

Altogether, these data suggest that a right 2-AG tone is required for normal functioning of the synaptic plasticity driven by CB_1Rs, as increasing or decreasing its levels modifies the plasticity triggered by LFS in the MPP of WT and TRPV1-KO mice.

Finally, the implication of anandamide was also analysed by bath application of the FAAH inhibitor URB597. In WT, URB597 shifted the fEPSP depression to a significant potentiation ([2 µm]; 120.8 ± 5.174 %; p < 0.0001; ****) (figure 28a-c). Paradoxically, the fEPSP potentiation observed in TRPV1-KO after LFS remained unchanged in the presence of URB597 ([2 µm]; 135.5 ± 13.65 %; p = 0.9989; ns) (figure 28b-d).

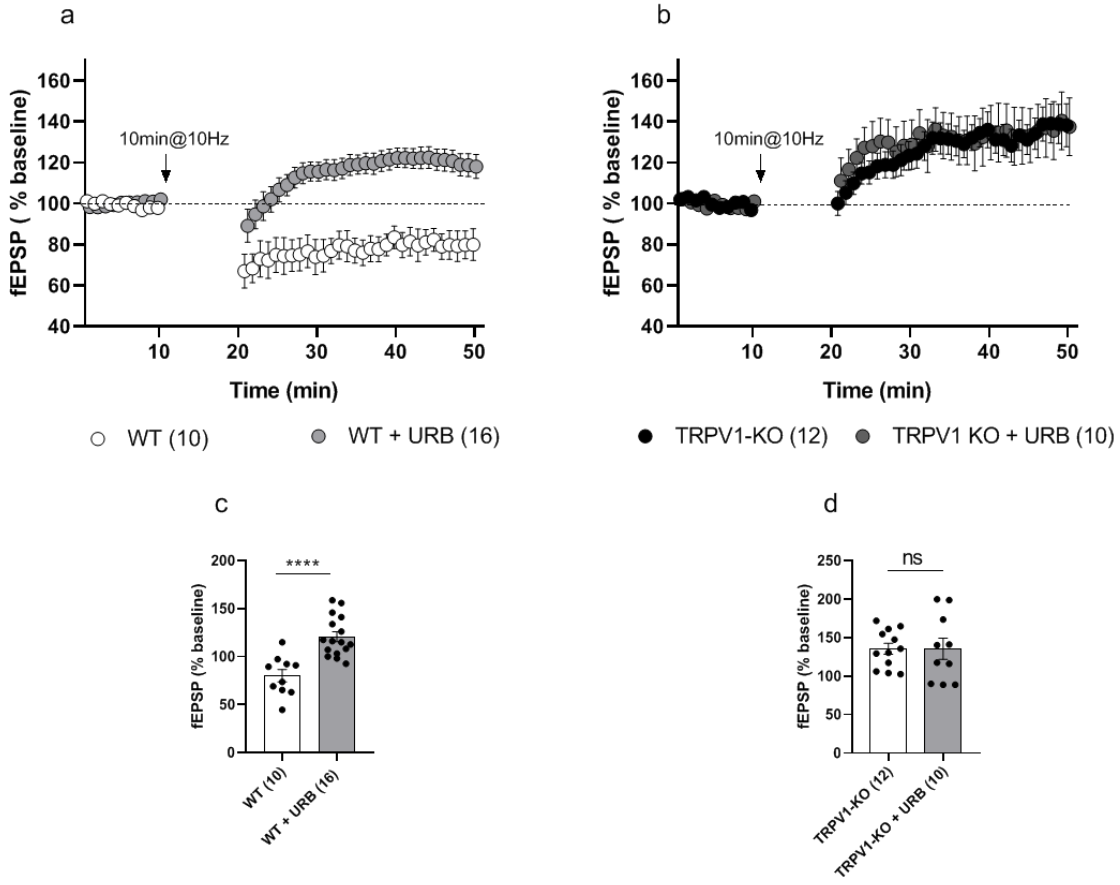

Figure 28: The anandamide increase shifts LTD to LTP at MPP synapses in WT mice. For representation, each experiment was normalized to its baseline. The average of the fEPSP areas is shown. A black arrow marks LFS application. a) URB597 [2 µm] has a significant effect over the LTD observed after LFS in WT (light grey circles). b) URB587 [2 µm] does not affect LTP in TRPV1-KO (dark grey circles). c) Representative histogram of the last 10 minutes fEPSP after LFS in the presence of URB597 [2µm] in WT. Unpaired t test. ****p < 0.0001. d) Representative histogram of the last 10 minutes fEPSP after LFS in the presence of URB597 [2 µm] in TRPV1-KO. Unpaired t test. p > 0.05. All data are expressed as mean ± S.E.M.

Based on these results, we suggest that, unlike 2-AG, anandamide does not participate in the LTP found after LFS at the MPP synapses of TRPV1-KO mice. Although the impact of the lack of anandamide was not assessed, it might be especulated a ceiling effect of anandamide in TRPV1-KO mice. Interestingly, anandamide seems to be triggered a fEPSP potentiation after LFS in WT, which is not driven by TRPV1.

To assess if the ultrastructural changes observed in TRPV1-KO could have an impact in the shift of synaptic plasticity observed in the MPP, the TRPV1 receptor antagonist AMG9810 was applied. Under these conditions, LFS in WT significantly potentiated the fEPSP observed in the MPP ([3 µm]; 116.8 ± 5.957 %; p = 0.0185; *) (figure 29a-b) but this potentiation was not as robust as the one seen in TRPV1-KO (TRPV1-KO: 135.5 ± 7.119 % vs WT: 116.8 ± 5.957 %; p = 0.0638; ns) (figure 29c). Furthermore, AM251 significantly reduced the fEPSP potentiation

elicited by AMG9810 [4 µm]; 100.6 ± 4.653 %; p = 0.0413; *) (figure 29d-e) to a similar extent to the reduction caused by AM251 in TRPV1-KO (TRPV1-KO: 95.37 ± 8.263 % vs WT 100.6 ± 4.653 %; p = 0.8212; ns) (figure 29f).

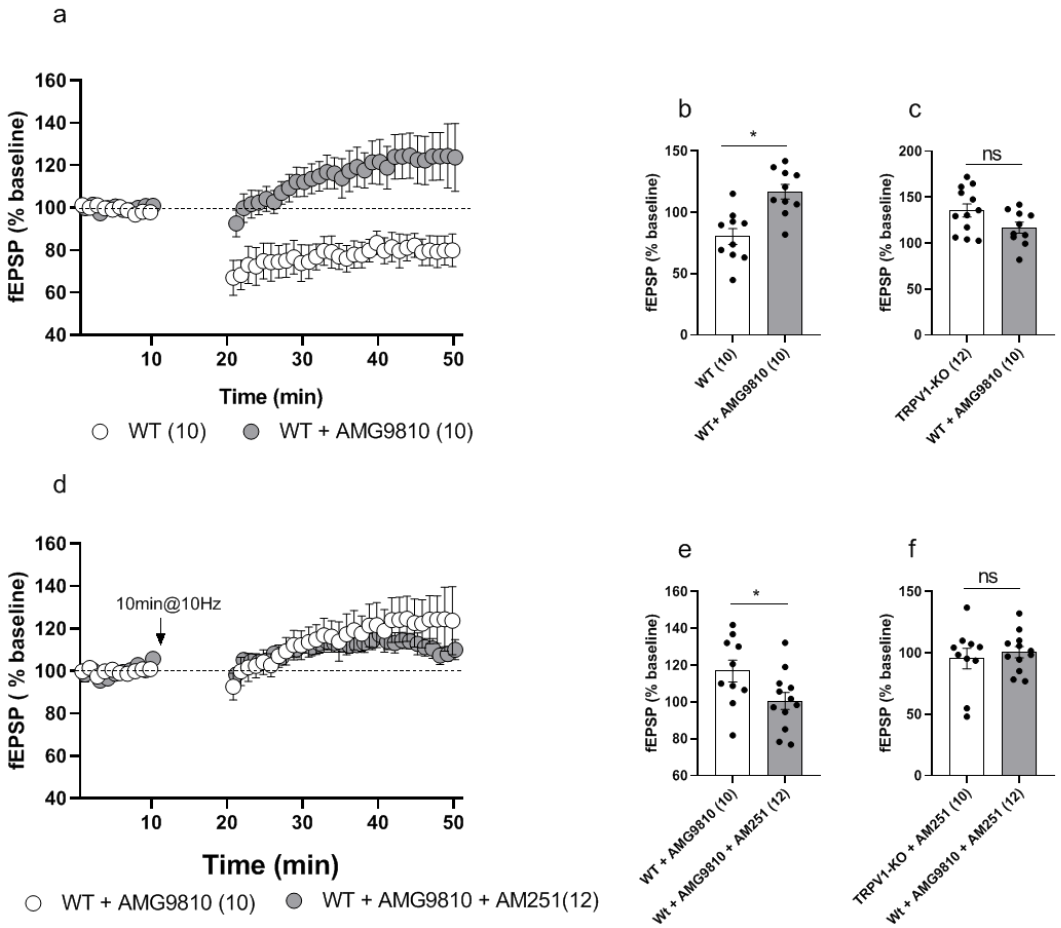

Figure 29: TRPV1 antagonism elicits LTP at MPP synapses in WT mice. For representation, each experiment was normalized to its baseline. The average of the fEPSP areas is shown. A black arrow marks LFS application. a) AMG9810 [3 µm] significantly shifts LTD (white circles) to LTP (grey circles). b) Representative histogram of the last 10 minutes fEPSP after LFS in the presence of AMG9810 [3 µm] in WT. Unpaired t test. *p < 0.05. c) Representative histogram of the last 10 minutes fEPSP after LFS in the presence of AMG9810 [3 µm] in WT compared to the last 10 minutes fEPSP after LFS in in TRPV1-KO. Unpaired t test. p > 0.05. d) AM251 [4 µm] has a significant effect over the LTP observed after LFS in WT + AMG9810 (grey circles). e) Representative histogram of the last 10 minutes fEPSP after LFS in the presence of AM251 [4 µm] in WT + AMG9810. Unpaired t test. *p < 0.05. f) Representative histogram of the last 10 minutes fEPSP after LFS in the presence of AM251 [4 µm] in WT + AMG9810 compared to the last 10 minutes fEPSP after LFS in the presence of AM251 [4 µm] in TRPV1-KO. Mann Whitney test. p > 0.05. All data are expressed as mean ± S.E.M.

These data suggest that the blockade of TRPV1 in the MPP can shift the eCB driven LTD to a LTP elicited by LFS. However, the fEPSP potentiation was not the same when comparing the genetic TRPV1-KO with the TRPV1 antagonism, probably because the biochemical and ultrastructural changes observed in the endocannabinoid system in TRPV1-KO could have a direct impact in this shift in synaptic plasticity, making greater the potentiation in the absence of TRPV1.

To check if this hypothesis could be the mechanism underlying the LTP observed in TRPV1-KO, a the CB_1R agonist WIN 55,212 was applied in the presence of AMG9810 in order to know if a greater CB_1R activation could upregulate the fEPSP potentiation. Actually, WIN 55,212 did not affect the fEPSP potentiation observed with the TRPV1 antagonist ([5 µm]; 116.9 ± 4.291 %; p = 0.9927; ns) (figure 30a-b).

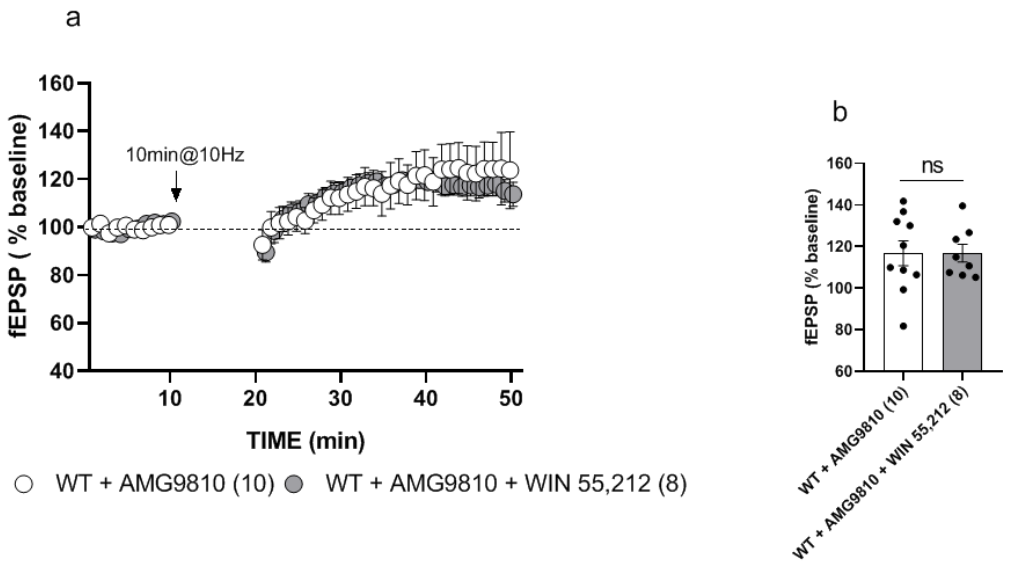

Figure 30: CB_1R activation does not increase the LTP at MPP synapses when TRPV1 is pharmacologically blocked in WT mice. a) WIN 55,212 [5 µm] has not an effect over the LTP observed after LFS in WT + AMG9810 (grey circles). b) Representative histogram of the last 10 minutes fEPSP after LFS in the presence of WIN 55,212 [5 µm] in WT + AMG9810. Unpaired t test. p > 0.05. All data are expressed as mean ± S.E.M.

These data suggest that the fEPSP potentiation observed in TRPV1-KO mice is not due to a greater activation of CB_1R, even though this activation was shown to be necessary. To further figure this issue out, other intracellular mechanisms triggered by CB_1R were explored, for instance, the participation of actin filaments. In the LPP, the phosphorylation of actin filaments was shown to be necessary for the LTP driven by CB_1 receptors (Wang et al., 2018), as it was blocked by the inhibitor of the actin filaments phosphorylation latrunculin-A (LAT-A). Interestingly, LAT-A significantly reduced the LTP observed in TRPV1-KO ([0.5 mM]; 114.6 ± 5.78 %; p = 0.0348; *) (figure 31a-c). LAT-A, in turn, did not modify the fEPSP potentiation elicited by the TRPV1 antagonist AMG9810 in WT (120.9 ± 9.248 %; p = 0.7173; ns) (figure 31b-d).

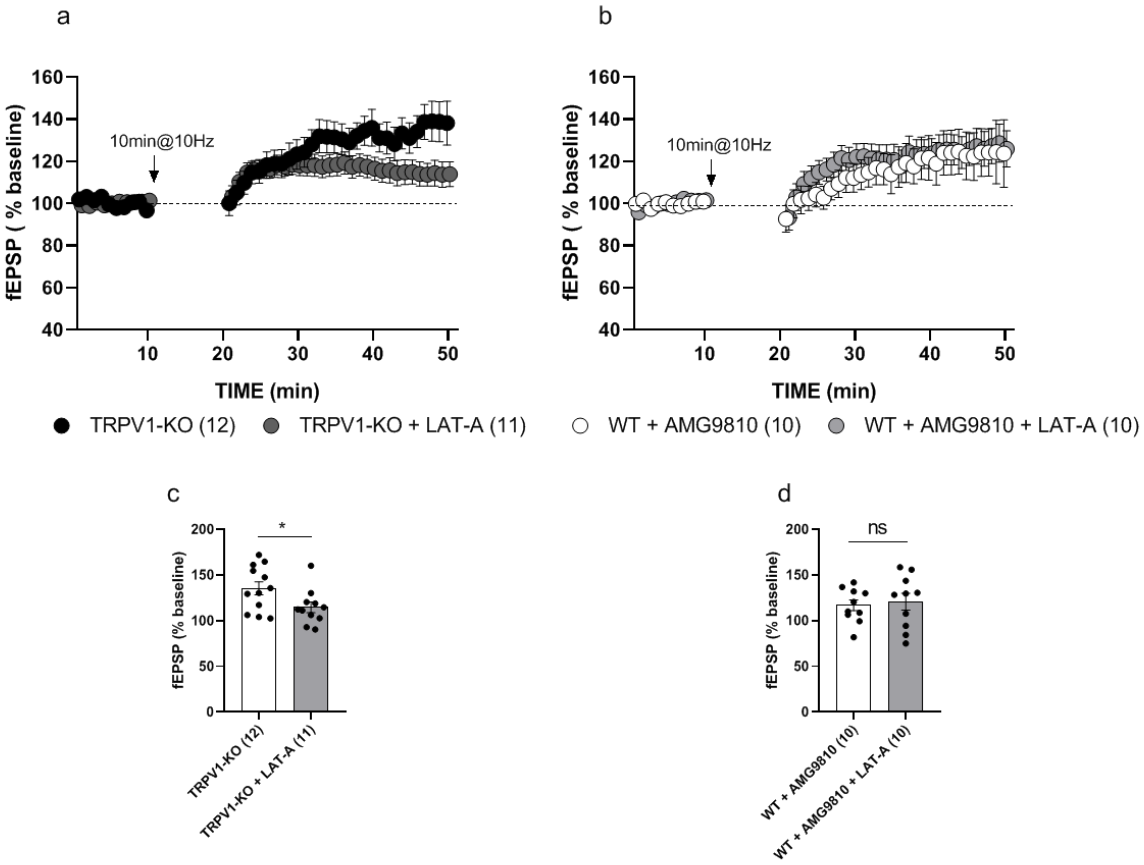

Figure 31: Latrunculin-A reduces LTP at MPP synapses in TRPV1-KO mice but not the LTP elicited by TRPV1 antagonism in WT mice. For representation, each experiment was normalized to its baseline. The average of the fEPSP areas is shown. A black arrow marks LFS application. a) Latrunculin-A [0.5 mM] has a significant effect over the LTP observed after LFS in TRPV1-KO (dark grey circles). b) Latrunculin-A [0.5 mM] has not an effect over the LTP observed after LFS in WT + AMG9810 (light grey circles). c) Representative histogram of the last 10 minutes fEPSP after LFS in the presence of Latrunculin-A [0.5 mM] in TRPV1-KO. Unpaired t test. *$p < 0.05$. d) Representative histogram of the last 10 minutes fEPSP after LFS in the presence of Latrunculin-A [0.5 mM] in WT + AMG9810. Unpaired t test. $p > 0.05$. All data are expressed as mean ± S.E.M.

The analysis of the paired pulse ratio (PPR) revealed a slight difference between WT and TRPV1-KO in the MPP synapses. The PPR was calculated by averaging the ratio of the fEPSP initial slopes (P2/P1) of 30 pairs of pulses (50 msec interpulse interval), where P2 corresponded to fEPSP2 slopes (2nd evoked responses) and P1 to fEPSP1 slopes (1st evoked responses) and these were compared before and after the LFS was applied (Figure 32). In WT, there was a little increase in the PPR after LFS stimulation. In Pre-LFS the ratio was 1.002 ± 0.0493 whereas in Post-LFS the ratio was 1.070 ± 0.0463 ($p = 0.3187$; ns). In TRPV1-KO, in contrast, PPR was reduced after LFS (In Pre-LFS the ratio was 1.146 ± 0.0219 while after LFS (Post-LFS) the ratio was 1.088 ± 0.0337 ($p = 0.1570$; ns).

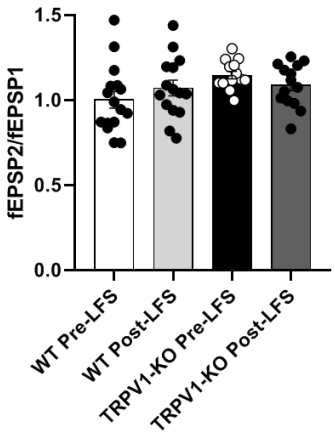

Figure 32: Paired pulse ratio in WT and TRPV1-KO mice. PPR was calculated with slope of 30 sweep i.e. 10 min before and 20 min after stimulation protocol. No significant changes are observed after LFS in TRPV1-KO compared to WT. Unpaired t test. $p > 0.05$. All data are expressed as mean ± S.E.M.

5.3.3- Synaptic transmission in MPP.

The fEPSP response to a CB_1R agonist was assessed in order to corroborate that exogenous activation of the receptor depresses the excitatory synaptic transmission at the MPP-granule cell synapses, as it was shown previously by our laboratory (Peñasco et al., 2019). As expected in WT, the fEPSPs were significantly depressed after applying the CB_1R agonist CP 55,940 ([10 µm]; 75.31 ± 6.496 %; p = 0.0003; ***) (figure 33a-b). In contrast, CP 55,940 elicited the potentiation of fEPSPs in TRPV1-KO ([10 µm]; 118 ± 9.706 %; p = 0.4813; ns) (figure 33a-c).

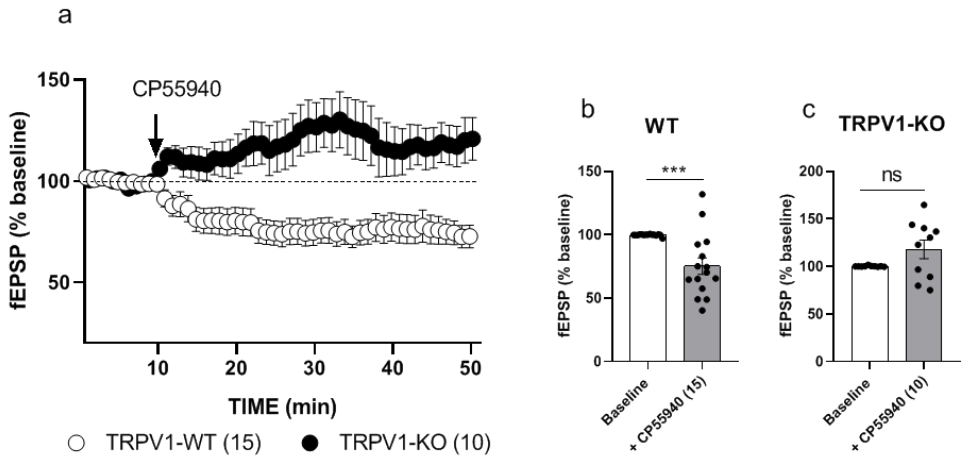

Figure 33: CB_1R-dependent excitatory synaptic transmission at MPP synapses in WT and TRPV1-KO mice. For representation, experiments were normalized to its baseline. Time course plot of average fEPSP areas is represented. Black arrow indicates the time point when the drug was applied. a) CP 55,940 [10 µm] reduces excitatory synaptic transmission in WT (white circles) while causes an increase in TRPV1-KO (black circles). b) Representative histogram of the last 10 minutes fEPSP after CP 55,940 application in WT. Mann Whitney test. ***$p < 0.001$. c) Representative histogram of the last 10 minutes fEPSP after CP 55,940 application in TRPV1-KO. Mann Whitney test. $p > 0.05$. All data are expressed as mean ± S.E.M.

5.4- Hippocampal-related behaviours in TRPV1-KO mice.

5.4.1- Memory assessment.

The changes in hippocampal CB_1R expression caused by the genetic deletion of TRPV1 could also have an impact in hippocampal functions such as memory. As so, the long-term recognition memory and spatial memory of WT and TRPV1-KO mice were evaluated. There was not found any significant difference between WT and TRPV1-KO in the novel object recognition test. Thus, the discrimination index (DI) in WT (0.4055 ± 0.063) and TRPV1-KO (0.4332 ± 0.0666) was similar ($p = 0.7695$) (figure 34a), and the time spent by WT (44 ± 6.105) and TRPV1-KO (39.29 ± 7.946 seconds) to explore the objects ($p = 0.4482$) (figure 34b) were not statistically significant.

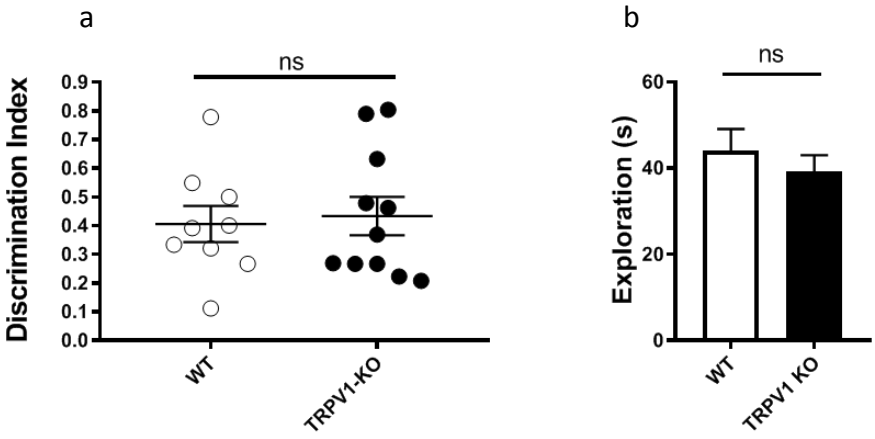

Figure 34: Behavioural evaluation of memory for novel object recognition in WT and TRPV1-KO mice. a) Discrimination index is unaffected in TRPV1-KO realtive to WT. Unpaired t test. $p > 0.05$. b) Object exploration time is not affected in TRPV1-KO. Unpaired t test. $p > 0.05$. All data are expressed as mean ± S.E.M.

Moreover, there were not significant changes in the spatial memory strategy shown by TRPV1-KO versus WT mice in the Barnes Maze test (figure 35a). Hence, the strategies displayed by WT mice the last day of test were: 0 % NS + 20.83 % RA + 4.167 % SE and 75 % SP; while TRPV1-KO displayed: 0 % RA + 25 % RA + 9.091 % SE + 65.91 % SP. Furthermore, TRPV1-KO mice spent similar time to find the escape box to WT (figure 35b) and WT mice took an average of 48.49 ± 13.53 seconds to find the escape box while TRPV1-KO mice spent 48.93 ± 14.39 seconds to complete it. However, a significant difference was found in the number of errors made by TRPV1-KO (6.768 ± 2.427 errors per day) compared to WT (4.8 ± 1.681 errors per day) ($p = 0.0133$) (figure 35c).

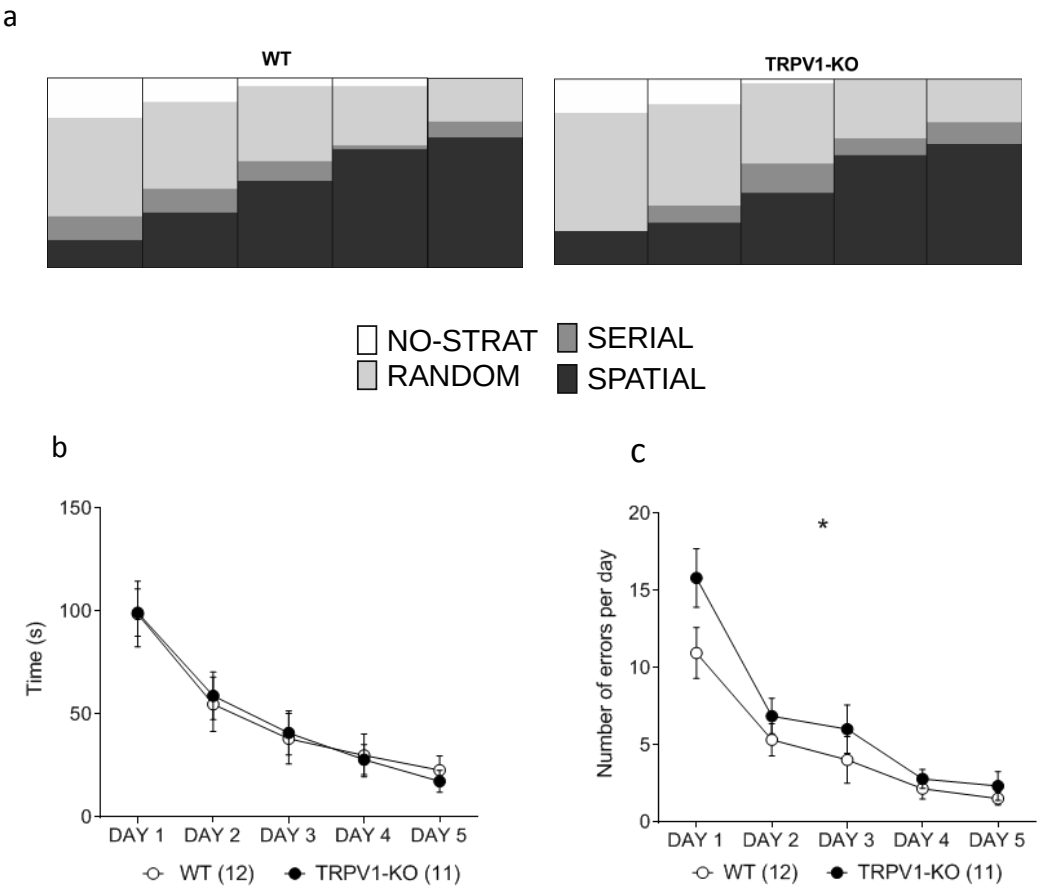

Figure 35: Behavioural assessment of spatial strategies and spatial memory in WT and TRPV1-KO mice. a) Spatial strategies are unaffected in TRPV1-KO compared to WT. b) TRPV1-KO spent the similar time to complete the test each day relative to WT. Two-way ANOVA. $p > 0.05$. c) TRPV1-KO make significantly more errors to find the escape box than WT. Two-way ANOVA. *$p < 0.05$. All data are expressed as mean ± S.E.M.

5.5- Evaluation of pathological conditions in TRPV1-KO mice: kainate seizure model.

Taken into account the relevance of TRPV1 and CB_1 receptors in pathological conditions such as epilepsy, we wanted to investigate the consequences of an epileptogenic insult could have in TRPV1-KO. For this purpose, mice were injected unilaterally with an intrahippocampal kainic acid solution (50 nL 20 mM) in order to evaluate their response to seizures. To assess the seizures a modified Racine's scale was used. We found a significant difference between TRPV1-KO and WT, as mice lacking TRPV1 receptor suffered milder seizures (average score: 3.11 ± 0.0535 points) than the WT (average score: 3.65 ± 0.0223 points) (p = 0.0022; **) (figure 36).

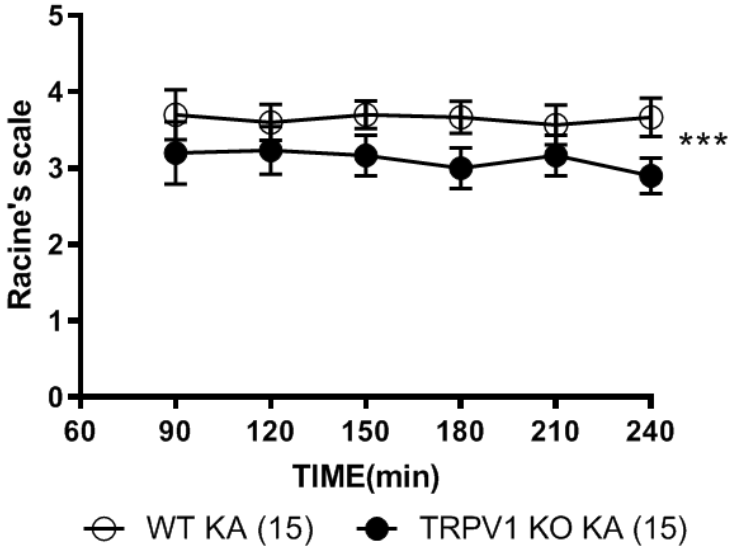

Figure 36: Evaluation of kainate induced-seizures according to a modified Racine's scale in WT and TRPV1-KO mice. Representation of the maximum scores obtained every 30 min based on a modified Racine's scale after intrahippocampal injection of KA. TRPV1-KO suffer milder seizures than WT. Two-way ANOVA. ***p < 0.001. All data are expressed as mean ± S.E.M.

6- Discussion

The aim of my thesis work was to determine the impact of the genetic deletion of TRPV1 on the ECS, in particular, on the expression of some of its components with special attention to the CB_1R localization and its role in hippocampal functions such as synaptic plasticity and memory. The main finding of my dissertation was that the constitutive deletion of the TRPV1 receptor gene has an impact on the endocannabinoid system and some of its interacting proteins. The changes observed were at several levels: protein expression, coupling efficacy of the CB_1R and synaptic plasticity shift from eCB-LTD to robust eCB-LTP at the MPP-granule cell synapses. Furthermore, these alterations did not seem to impair memory and protect against KA-induced epileptiform seizures.

The genetic deletion of compounds of the ECS has been reported to lead to compensatory changes. For instance, mice lacking TRPV1 express higher levels of calcitonin gene-related peptide (CGRP) in dorsal root ganglia primary afferents (Chen et al., 2008). This peptide localized in the same primary afferents as TRPV1 (Guo et al., 1999) is very important in the pathogenesis of arthritis (Schaible et al., 2002). Moreover, a decrease in TRPV1 expression in DG together with an increase in TRPV1 in the cerebellar granule cell layer was reported in CB_1R-KO mice (Cristino et al., 2006). TRPV1 mRNA expression was also seen to increase in FAAH-KO astrocytes which could not be mimicked by FAAH inhibition, suggesting the existence of some compensatory effects (Benito et al., 2012).

6.1- The ECS is altered in the TRPV1-KO hippocampus.

In our hands, immunohistochemistry revealed an increased expression of CB_1R, FAAH, MAGL and NAPE-PLD in TRPV1-KO hippocampus. These results would suggest compensatory effects after genetic deletion of the TRPV1 receptor, thus representing this mouse line a very useful tool for the study of the ECS under circumstances of TRPV1 ablation. At the same time, this allowed us to delve into the versatility of the CB_1R and the importance of the deficiencies derived from the absence of TRPV1.

Western blots of whole hippocampal homogenates showed that the CB_1R increase was not statistically significant and that only FAAH and MAGL significantly rose. Although this is a powerful technique to detect low level proteins (Garro et al., 2001; Kurien and Scofield, 2006; López de Jesús et al., 2006), subtle changes in protein expression are better detected by homogenate fractioning into P2 extracts, and with the cellular and subcellular membranes separated from the cytosolic fraction to obtain raw synaptosomes (Garro et al., 2001). Indeed,

P2 fractions showed that CB_1R expression did not suffer any variation in TRPV1-KO, although it significantly decreased in synaptosomal extracts. However, the limitation of the synaptosomal extracts is that they do not discriminate between presynaptic, postsynaptic, inhibitory or excitatory terminal membranes. Nevertheless, we observed in TRPV1-KO a drastic decrease in the proportion of CB_1R immunoparticles distributed in GABAergic terminals in the MCFL (34.5 % decrease) and in the outer 2/3 of DGML (15.5 % decrease) that was accompanied by an increase in CB_1R labelling in glutamatergic terminals in the MCFL (83.80 % increase) and in the outer 2/3 of DGML (73.50 % increase) (see below). Furthermore, considering the total number of CB_1R particles counted in 100 μm^2, the particles localized in GABA terminals decreased ~ 56 % in the MCFL and ~ 27 % in the outer 2/3 of DGML in TRPV1-KO. Altogether, a decrease in CB_1R expression seems to take place at GABAergic synaptic terminals in TRPV1-KO that should account for the significant decrease in CB_1R expression in synaptosomes.

Also, a significant decrease in MAGL with no changes in FAAH were found in TRPV1-KO synaptosomes which differed from what we observed in whole homogenate extracts. These expression patterns could be due to the different localization of the enzymes. For instance, NAPE-PLD is very high in granule cell axons of the hippocampus (Egertova et al., 2008); FAAH mostly localizes to the membrane surface of intracellular organelles (e.g., mitochondria, smooth endoplasmic reticulum) but it is also present on somatic and dendritic plasma membranes (Gulyas et al., 2004), and MAGL localizes in presynaptic axon terminals (Gulyas et al., 2004; Uchigasima et al., 2011). Our results suggested that MAGL has distinct localizations in TRPV1-KO as it increased in whole hippocampal homogenates but decreased in synaptosomal fractions. This would also reflect that the localization of MAGL in glial cells, as shown at high levels in astrocytes surrounding the mossy cell–granule cell synapses in the DGML (Uchigasima et al., 2011), raises upon the absence of TRPV1. Finally, as DAGLα expression did not change in TRPV1-KO, a dysregulation in the 2-AG metabolism was expected altogether to occur in TRPV1-KO. In addition, the FAAH increase in whole homogenates and the non-significant decrease in NAPE-PLD in synaptosomal extracts from TRPV1-KO suggest that the AEA tone drops in TRPV1-KO. However, NAPE-PLD immunoreactivity was observed to increase in the dentate hilar region and the CA3 stratum lucidum, indicating that AEA might be increased in certain subcellular compartments, e.g., the granule cell axons. Altogether, we argue that the lack of TRPV1 causes changes in the dynamics of synthesis and degradation of the main eCBs, which might affect synaptic activity. Expression experiments in cytosolic and microsomal fractions are currently being carried out to clarify the changes in the main biosynthetic and degrading enzymes for 2-AG and AEA in more detail.

We also investigated the expression of proteins related to CB_1R functionality, such as Gα subunits (o, i1, i2 and i3) and CRIP1a in synaptosomal fractions of TRPV1-KO and WT littermates. Thus, an increase in Gαi1, Gαi2, Gαi3 and CRIP1a expression was found in TRPV1-KO. After having observed these changes, the CB_1R functionality was assessed by [^{35}S] $GTP_\gamma S$ binding assays. In fact, it came to be altered in TRPV1-KO as the receptor showed a lower basal activation while after CP 55.940 stimulation, the maximum efficacy of coupling ratio for G-proteins was significantly higher than in WT. The decrease in the constitutive activation of G-proteins could be at least partly due to the decrease in CB_1R expression observed in synaptosomal fractions. Actually, the CB_1R-induced suppression of the fEPSP by the CB_1R agonist CP 55.940 normally observed at MPP-GC synapses in sham mice (Peñaco et al., 2019) was not observed in TRPV1-KO. In addition, we have very recently observed (Peñasco et al., 2020) that adolescent mice exposed to a four-day-per week drinking in the dark procedure for a total of four weeks had, after two weeks of withdrawal, a significant reduction in CP 55.940 potency for stimulating [^{35}S] GTPγS binding and [^{35}S] GTPγS basal binding in the hippocampus that agreed with the decrease in CB_1R binding (Basavarajappa et al., 1998; Vinod et al., 2006) and G-protein cycling after ethanol intake (Basavarajappa and Hungund, 1999). Furthermore, we also detected in our previous study a specific reduction in the Gαi2 subunit that might be responsible for the observed reduction in [^{35}S] GTPγS basal binding and the impairment in CB_1R signalling in the ethanol-treated mice (Peñasco et al., 2020). Lack of Gαi2 subunit has been shown to lead to abnormalities in learning efficiency, sociability and social recognition (Hamada et al., 2017). However, although CB_1Rs located on glutamatergic synapses are tightly coupled to G protein signalling (Steindel et al., 2013), the basal activation in the hippocampus does not only correspond to CB_1R-linked G-proteins as Gi/o proteins are also coupled to other receptors besides CB_1R (Conn and Pin, 1997).

As already mentioned above, we observed an increase in CRIP1a in TRPV1-KO. This protein is linked to the intracellular internalization, trafficking and translocation of CB_1R as it suppresses the trafficking of *de novo* synthetized CB_1R from perinuclear compartments or endoplasmic reticulum to the plasma membrane, impairs the translocation and renewal of CB_1Rs and decreases CB_1R on the surface of cells overexpressing CRIP1a (Booth et al., 2019). However, CRIP1a overexpression in cells has also been shown to attenuate the internalization caused by CP 55.940 through competing with β-arresting for CB_1R binding (Blume et al., 2016). These observations could explain the changes in CB_1R expression in our synaptosomal fractions from TRPV1-KO, as CB_1Rs might be retained longer intracellularly due to the increased levels of CRIP1a in TRPV1-KO. However, light microscopy immunohistochemistry and whole homogenates

showed the opposite, probably because they might be reflecting the CB_1R localization in synaptic terminals together with the main expression of the receptor in intracellular compartments in TRPV1-KO. Furthermore, our data would also support previous observations indicating that CRIP1a overexpression in N18TG2 cells produces a robust stimulation of [^{35}S] $GTP_\gamma S$ binding to Gαi1 and Gαi2 subunits (Blume et al., 2015). Therefore, taking into account that TRPV1-KO have an increased expression of Gαi proteins in the hippocampus, the potentiation observed in the [^{35}S] $GTP_\gamma S$ binding assay after stimulation with CP 55.940 could be due to a greater coupling of the CB_1R to Gαi subunits and/or an impairment in the agonist-mediated internalization of CB_1Rs caused by the increase in CRIP1a (Blume et al., 2016; Booth et al., 2019).

We also investigated the CB_1R distribution by a preembedding immunogold technique for electron microscopy in order to reveal potential changes in receptor localization at specific subcellular compartments in TRPV1-KO. This study was focused on the inner 1/3 (MCFL) and the outer 2/3 of the DGML (termination zone of the PP). While the MCFL receives the glutamatergic mossy cells commissural/associational axons that travel long distances to innervate multiple dentate granule cells to convey environmental and context information (Amaral and Witter, 1989; Scharfman and Myers, 2013), inputs from the postrhinal cortex transmit 1) spatial information to the medial entorhinal cortex that in turn projects to the dorsal hippocampus through the MPP (Fyhn et al., 2004; Hargreaves et al., 2005) and 2) non-spatial information to the lateral entorhinal cortex which gives rise to the LPP (Burwell, 2000).

Altogether, the glutamatergic PP (Grandes and Streit, 1991), the main input entering into the hippocampal formation, conveys information from the entorhinal cortex layer II to the DGML (Scharfman, 2016). TRPV1 has been shown to be mostly distributed on granule cell dendritic spines receiving the PP synaptic terminals in the outer 2/3 ML, and at much lower rate in dendritic spines receiving the hilar mossy cell axons in the inner 1/3 ML. Hence, of the total TRPV1 immunopositive granule cell dendritic spines and dendrites, about 75 % and 56 %, respectively, were in the outer 2/3, and the rest in the inner 1/3 (Puente et al., 2015). In addition, we found that TRPV1 expression was higher at inhibitory synapses in the inner 1/3 than the outer 2/3 ML (Canduela et al., 2015). Here, about 30 % of the inhibitory synapses in the ML express TRPV1 mostly localized to postsynaptic dendritic membranes in the MCFL (Canduela et al., 2015). TRPV1 is localized in the GC bodies too (Canduela et al., 2015). In the CA1 hippocampus, most CB_1R-positive perisomatic synapses, if not all, contain postsynaptic TRPV1 (Lee et al., 2015), but TRPV1 has also been localized at glutamatergic Schaffer collateral terminals making synapses with CA1 pyramidal cell dendritic spines (Bialecki et al., 2020).

The ultrastructural data on the CB_1R distribution in the DGML of TRPV1-KO confirmed the biochemical results. Thus, similar changes were found in the MCFL and outer 2/3 ML but with slight differences regarding the significance of the changes observed, that might reflect that distinct TRPV1 expression patterns trigger different compensatory effects. For instance, in both DGML sub-layers a significant increase in CB_1R positive excitatory terminals was found but the shift in the MCFL was more pronounced than in the outer 2/3 ML. However, taking into account that the density of CB_1Rs in glutamatergic terminals did not change in both DGML sub-layers of TRPV1-KO, the decrease in the number of excitatory terminals without CB_1Rs would be an explanation for the increase seen in CB_1R positive excitatory terminals. Thus, our data indicate that TRPV1 deletion modifies the total number of excitatory terminals and the proportion of excitatory terminals provided with CB_1R. TRPV1-KO mice have also been shown to have a reduced glutamatergic innervation in other hippocampal regions (Hurtado-Zavala et al., 2017).

Altogether, it seems that, in the absence of TRPV1, CB_1Rs exert a major regulatory effect on the excitatory transmission, which may have important functional consequences in DGML. In this context, we have recently shown that CB_1R immunolabelling decreased by 34 % in excitatory terminals and the proportion of CB_1R immunopositive excitatory buttons decreased by 35 % with no other subcellular compartments affected in the middle 1/3 of DGML of the adult mouse subjected to ethanol intake during adolescence (binge drinking model). These deficits in glutamatergic CB1Rs were associated with the loss of eCB-eLTD at the MPP-GC synapses and recognition memory impairment (Peñasco et al., 2020).

Regarding to the inhibitory terminals, the differences in TRPV1-KO relative to WT were minimal because only a small reduction in CB_1R density was found to be significant in the outer 2/3 ML. This reduction could arise from compensatory effects observed in CRIP1a expression that affects recycling of the highly localized CB_1R in GABAergic terminals (see above) (Kawamura et al., 2006; Ludányi et al., 2008; Marsicano and Kuner, 2008; Katona and Freund, 2012; De-May and Ali, 2013; Steindel et al., 2013; Hu and Mackie, 2015; Lu and Mackie, 2016; Gutiérrez-Rodríguez et al., 2017; Bonilla-Del Río et al., 2019). Bearing in mind that the majority of CB_1R particles are located on GABAergic terminals in the hippocampus (Katona et al., 1999; Marsicano and Lutz, 1999; Hájos et al., 2000; Nyíri et al., 2005; Kano et al., 2009; Katona and Freund, 2012; Lutz et al., 2015; Takács et al., 2015; Gutiérrez-Rodríguez et al., 2017; Bonilla-Del Río et al., 2019), it would be plausible that an impairment in receptor renewal could be more pronounced in inhibitory than excitatory terminals, and therefore easier to be detected. This would also contribute to explain the CB_1R reduction observed in synaptosomal fractions, because if the

overall CB_1R expression at excitatory synaptic terminals remained unchanged, the decrease in CB_1R density at inhibitory synaptic terminals could indeed be responsible for the drop in CB_1Rs.

With respect to mitochondria, our laboratory discovered the localization of CB_1Rs in mitochondria and their participation in cellular respiration in hippocampal neurons (Benard et al. 2012; Hebert-Chatelain et al. 2014a, b). We could not find any change in the proportion of mitochondrial CB_1Rs in TRPV1-KO despite the fact that TRPV1 has also been found to be expressed in mitochondrial membranes (Luo et al., 2012; Miyake et al., 2015). However, the number of mitochondrial sections was increased in terminals and decreased in dendrites in the MCFL; and a significant reduction in the number of mitochondrial sections was found in terminals and dendrites in the outer 2/3 ML, suggesting that TRPV1 could have a direct implication in the mitochondrial dynamics in ML. The differences observed between both sub-layers may be due to differences in their neuronal composition and the distinct effect of the lack of TRPV1. Thus, strong mitochondrial calcium-influx mediated by TRPV1 has been shown to cause cytotoxicity and cell death in HEK 293 cells and DRG neurons (Stueber et al., 2017). In contrast, TRPV1 knockdown improved mitochondrial function and inhibited apoptosis in primary cardiomiocyte cells, whereas TRPV1 knockout improved cardiac functions (Sun et al., 2014). The functional consequences of the decrease in mitochondrial sections observed in the DG of TRPV1-KO in this thesis work, needs a detailed investigation.

As mentioned before, CB_1Rs are also expressed in astrocytes (Rodríguez et al., 2001; Navarrete and Araque, 2008, 2010; Stella, 2010; Han et al., 2012; Bosier et al., 2013; Metna-Laurent and Marsicano, 2015; Viader et al., 2015; Oliveira Da Cruz et al., 2016; Kovács et al., 2017; Gutiérrez-Rodríguez et al., 2017). Calcium rise linked to TRPV1 activation has been shown to drive cytoskeletal rearrangement, disassembly of microtubules and reorganization of f-actin filaments that lead to astrocyte migration (Goswami et al., 2007; Han et al., 2007; Martin et al., 2012; Morales-Lázaro et al., 2013), while TRPV1 antagonism reduces astrocyte migration through a decrease in calcium influx and cytoskeletal remodelling (Ho et al., 2014). However, we did not observe any difference in the astrocytic parameters measured in the TRPV1-KO. We have recently studied in a model of binge drinking during the adolescence (4–8-week-old male mice exposed to 20 % ethanol over a period of 4 weeks) the effects of ethanol in the adult CA1 stratum radiatum (Bonilla-Del Río et al., 2019). Interestingly, astrocytes held a swollen morphology under these conditions as shown by the measurements taken (perimeter, area) in the adult CA1 stratum radiatum four weeks after cessation of ethanol intake. Astrocytic swelling seems to be a phenomenon associated with ethanol consumption that leads to astroglial dysfunction

(Adermark and Bowers, 2016) and disruption of GFAP found in the astrocyte intermediate filaments (Renau-Piqueras et al., 1989). Altogether, astrocytic disturbance does not seem to happen in the absence of TRPV1. This might partly be explained by the fact that the genetic deletion of TRPV1 could have triggered compensatory mechanisms in other receptors/channels that could supply its function and therefore sustain a normal development. We still need to know the ethanol effects on astrocytes in TRPV1-KO mice. Furthermore, we have not observed changes in the proportion of CB_1R positive astrocytic processes in TRPV1-KO dentate ML. However, the ultrastructural analysis revealed a significant reduction in CB_1R density in astrocytes in the outer 2/3 ML of TRPV1-KO that mimicks the results obtained in our recent work showing a decrease in CB_1R density in astrocytes (in addition to the reduction in CB_1R immunopositive astrocytic processes) in the model of binge drinking mentioned above (Bonilla-Del Río et al., 2019). Astrocytes participate in inflammatory responses through the release of pro-inflammatory molecules (Farina et al., 2007) that can be alleviated by eCBs-mediated anti-inflammatory responses acting on astroglial CB_1Rs (Metna-Laurent and Marsicano, 2015). Hence, because of the reduction in CB_1R density in TRPV1-KO astrocytes, it is reasonable to expect an impairment of the anti-inflammatory response signalled by astrocytes in TRPV1-KO. The decrease in CB_1R density in astrocytes of TRPV1-KO could also have functional consequences in synaptic transmission and plasticity, as astrocytes may not be effective in sensing the endocannabinoids produced on demand by neural activity, compromising gliotransmitter availability elicited by cannabinoids at the synapses (Han et al., 2012; Araque et al., 2014).

6.2- Changes in synaptic plasticity in TRPV1-KO mice.

TRPV1 has been shown to participate in synaptic plasticity (Marsch et al., 2007; Gibson et al., 2008; Kauer and Gibson, 2009; Maione et al., 2009; Chávez et al., 2010, 2014; Grueter et al., 2010; Puente et al., 2011), learning and memory (Marsch et al., 2007; Li et al., 2008), fear and anxiety (Marsch et al., 2007; Micale et al., 2009), and to modulate cortical excitability in humans (Mori et al., 2012). TRPV1 and its endogenous agonist AEA participate in synaptic LTD in several brain areas (Di Marzo et al., 2001; 2002; 2008; Ross, 2003; Gibson et al., 2008; Kauer and Gibson, 2009; Maione et al., 2009; Grueter et al., 2010; Chávez et al., 2011). For instance, TRPV1 mediates a presynaptic LTD at glutamatergic synapses onto CA1 hippocampal interneurons through calcium-activated signalling cascades (Gibson et al., 2008). Also, calcineurin produced in a TRPV1-dependent manner reduces voltage-gated calcium channel activity in dorsal root ganglion neurons (Wu et al., 2005; 2006) and presynaptic calcium is required for TRPV1-driven LTD at striatal synapses (Singla et al., 2007). TRPV1 has been shown to participate in NMDA

receptor-dependent LTP in CA1 hippocampus that increased after TRPV1 activation (Marsch et al. 2007; Li et al. 2008). In addition, we have demonstrated very recently the presynaptic localization of TRPV1 at the Schaffer collateral terminals in CA1 hippocampus where facilitates glutamate release (Bialecki et al., 2020). Postsynaptic pannexin-1 channels that modulate metabotropic NMDAR and suppress presynaptic glutamate release by regulating AEA levels (Bialecki et al., 2020) controlled this facilitation. However, the notion of a wide distribution of TRPV1 in the brain was challenged because TRPV1 reporter mice displayed a restricted TRPV1 brain expression that it is conserved from rodents to humans (Cavanaugh et al. 2011). Thus, TRPV1 in these mice was only found in the hippocampus in Cajal–Retzius cells (Cavanaugh et al. 2011).

However, the confined TRPV1 expression to these particular hippocampal neurons is difficult to conciliate with the functional role of the channel in the CA1 hippocampus (see below) (Marsch et al., 2007; Gibson et al., 2008; Li et al., 2008; Bialecki et al., 2020) and with the AEA-activating TRPV1 that triggers a CB_1R-independent LTD at MPP-GC synapses in the DGML (Chávez et al., 2010). Therefore, it was assumable that TRPV1 should be localized at the excitatory PP-DGML synapses to mediate such a long-term form of synaptic plasticity. In fact, we unveiled the localization of TRPV1 mostly at postsynaptic dendritic spines and small dendrites receiving asymmetric synapses in the DGML (see above) (Puente et al., 2015). Furthermore, the dendritic spines targeted by the PP contain the highest TRPV1 density, followed by the spines distributed in the inner 1/3. However, the TRPV1 background in synaptic terminals makes unlikely that TRPV1 has a presynaptic functional role in the DGML. Altogether, TRPV1 is mostly distributed postsynaptically in the glutamatergic perforant path synaptic terminals and to smaller extent in postsynaptic profiles to the hilar mossy cell axon terminals in the MCFL (see above) (Puente et al., 2015).

In other brain regions, the TRPV1-LTD induced by stimulation at 10 Hz for 10 min in the bed nucleus of the stria terminalis (BNST) was 1) mediated by postsynaptic mGluR5-dependent production of AEA acting on postsynaptic TRPV1 mostly located at perisynaptic positions distributed on membranes of dendrites and postsynaptic spines receiving asymmetrical synapses, and 2) strongly inhibited by depletion of intracellular calcium stores (Puente et al., 2011). In addition, TRPV1 activation by capsaicin or AEA depresses somatic inhibitory transmission in the DG (Chávez et al., 2014). In fact, we localized TRPV1 immunoparticles in thick postsynaptic dendrites receiving symmetric synapses in the DGML (Canduela et al., 2015). In this case, about 30 % of the total counted inhibitory synapses were TRPV1 immunopositive. So far,

TRPV1-positive axon buttons with ultrastructural features of inhibitory synaptic terminals (pleomorphic vesicles and forming symmetric synapses) were not observed (Canduela et al., 2015). Of the 30 % TRPV1 immunolabeled synapses, about 80 % of them were distributed in the inner 1/3 and the rest in the outer 2/3 of the ML. Furthermore, the immunoparticle density in dendrites receiving symmetric synapses was significantly higher in the MCFL than in the outer 2/3 of the DGML. TRPV1 was also localized in the granule cell bodies (Canduela et al., 2015).

After having observed that the expression of CB_1Rs and ECS-related enzymes was changed and that there was an increase in the maximum coupling efficacy of the CB_1R in TRPV1-KO hippocampus, we next evaluated the effects of the TRPV1 deletion on synaptic plasticity in the DGML.

We first analysed the MCFL because the effects observed on the ECS in TRPV1-KO might have determined local functional modifications, though there has not been shown long-term synaptic plasticity driven by eCBs but just CB_1R-mediated depolarization induced suppression of excitation (DSE) and inhibition (DSI) (Chiu and Castillo, 2008; Hashimotodani et al., 2017). Hence, we found in TRPV1-KO after applying LFS (10min @ 10 Hz) at MCFL synapses in the presence of PTX, an increase in the potentiation as previously observed in WT (Chiu and Castillo, 2008; Peñasco et al., 2019). We hypothesized that this LTP might be due to the lack of TRPV1 itself, or the changes given in the ECS and excitatory terminals in TRPV1-KO, or both. The CB_1R inverse agonist AM251 did not have any effect on the potentiation neither in WT as shown previously (Chiu and Castillo, 2008) nor in the TRPV1-KO, ruling out that the modification in CB_1R positive excitatory terminals in TRPV1-KO might be playing a role. Furthermore, as NMDARs participate in LTP (Bliss et al., 2007), the NMDAR antagonist D-APV was applied though the potentiation triggered in the MCFL was shown to be NMDAR-independent (Hashimotodani et al., 2017). Indeed, D-APV did not significantly affect the potentiation in TRPV1-KO nor in WT littermates, even though the fEPSP values went down to baseline in WT. Altogether, our results further support that NMDARs have no role in LTP in MCFL even in the absence of TRPV1. TRPV1 activation has been reported to depress inhibitory synaptic transmission onto dentate granule cell bodies (but not dendritic inhibitory transmission) in a CB_1R-independent manner, through the rise in postsynaptic calcium, calcineurin activation and GABA-A receptors internalization (Chávez et al., 2014). So then, it is plausible that the lack of TRPV1 entails an increase in excitability because of the loss of the inhibitory control exerted onto the dentate granule cells. In addition to this TRPV1 effect, we have noticed a significant decrease in the CB_1R-positive inhibitory terminals in MCFL, as we have already discussed before. So, these changes would also

account for the LTP observed in MCFL of TRPV1-KO. Future investigations in our laboratory will be intended to clarify the mechanisms of this LTP.

6.2.1- CB_1R is involved in LTP at MPP-GC synapses in TRPV1-KO.

Based on our newly described CB_1R-eLTD mediated by 2-AG, mGluR1, mGluR5 and intracellular calcium at the MPP-GC synapses of WT mice (Peñasco et al., 2019), we aimed in my doctoral thesis to determine if the compensatory changes in the ECS observed after genetic deletion of TRPV1 in the PP termination zone would have a direct impact on synaptic plasticity. The results showed a shift from CB_1R-eLTD to LTP in TRPV1-KO after applying the same LFS paradigm as before (Peñasco et al., 2019). This LTP was completely blocked by AM251, confirming the participation of CB_1R in this potentiation. However, there was not found any change after applying D-APV, suggesting that the CB_1R-LTP was NMDAR-independent. We observed previously that the magnitude of eCB-eLTD elicited by LFS at the MPP-GC synapses was unaffected by D-APV (Peñasco et al., 2019), indicating that NMDA receptors were neither involved in the eCB-eLTD despite the fact that eCB-eLTD may require NMDA receptor activity at other synapses (Bender et al., 2006; Sjöström et al., 2003, Lutzu and Castillo, 2020).

Furthermore, the CB_1R-LTP in TRPV1-KO was also 2-AG dependent as the 10 Hz stimuli applied in the presence of the DAGL inhibitor THL (10 µM) completely abolished it. Furthermore, the MAGL inhibitor JZL184 (50 µM) also blocked the CB_1R-LTP suggesting that 2-AG regulation may be a limiting factor for the CB_1R-LTP in TRPV1-KO. Consequently, CB_1R-desensitization caused by high 2-AG concentration and the JZL 184 incubation time before recordings could be responsible for the CB_1R-LTP blockade, as we had seen to happen the JZL 184 blockade of the eCB-eLTD elicited by LFS of the MPP-GC synapses (Peñasco et al., 2019). Furthermore, this is in line with previous studies showing that long-term increase in 2-AG elicits CB_1R desensitization (Chanda et al., 2010; Schlosburg et al., 2010). As proposed by Cui and colleagues (2018), eCBs could underlie bidirectional plasticity depending on their levels and timing of the eCB release. In this sense, we found that inhibition of the synthesis or degradation of 2-AG had the same blocking effect on synaptic plasticity, suggesting that 2-AG acting on CB_1Rs is participating in LTD and LTP at the MPP synapses in WT and TRPV1-KO.

By contrast, CB_1R-LTP in TRPV1-KO was unaffected by the potent and selective FAAH inhibitor URB597 (2 µM), suggesting that AEA could not be involved in CB1R-LTP at the MPP-GC synapses in TRPV1-KO. However in WT, URB597 at the same concentration (2 µM) triggered fEPSP

potentiation after LFS. This was a puzzling finding as the eCB-eLTD elicited by similar LFS at the same MPP-GC synapses was unaffected by URB597 in WT (Peñasco et al., 2019). Although we still have to characterize this effect better, the discrepancy may be because our previous experiments were performed in the dark phase of the circadian cycle (Peñasco et al., 2019) during which mice are known to drink alcohol (Peñasco et al., 2020), while the experiments of my doctoral thesis were done in the light phase. Moreover, the daily fluctuations in the CB_1R expression and eCB levels in the hippocampus (Martinez-Vargas et al., 2003; 2013; Valenti et al., 2004; Murillo-Rodriguez et al., 2006; Glaser and Kaczocha, 2009; Martinez-Vargas et al., 2013) could also account for.

Moreover as we have already mentioned, the TRPV1-LTD induced in the BNST in our previous work by the same LFS stimulation (10 Hz for 10 min) mediated by postsynaptic mGluR5-dependent production of AEA acting on postsynaptic TRPV1 receptors, was strongly inhibited by depletion of the intracellular calcium stores (Puente et al., 2011). The CB_1R-eLTD at the MPP-GC synapses upon MPP stimulation (10 Hz for 10 min) was also group I mGluR-dependent and required intracellular calcium influx (Peñasco et al., 2019). We could then guess that the LFS (10 Hz for 10 min) applied to the MPP-GC synapses of the 6–8 week-old male mice littermates with the rise in AEA by URB597, desensitised TRPV1 by the further increase in intracellular calcium (De Petrocellis et al. 2011; Szymaszkiewicz et al., 2020) leading to the depletion of the intracellular calcium stores needed to maintain the LTD under normal conditions (Peñasco et al., 2019). In line with this, it would be the potentiation effect caused by the TRPV1 antagonist AMG9810 after LFS in WT (see below).

The CB_1R-LTP at the MPP-GC synapses in TRPV1-KO might stand on the ability of LFS (1Hz) of the MPP-GC synapses to induce CB_1R-independent LTD that relies on AEA, postsynaptic TRPV1 activation and internalization of AMPA receptors (Chávez et al., 2010). Actually, the high TRPV1 expression in granule cell dendritic spines postsynaptic to the perforant path synaptic terminals in the outer 2/3 of the DGML (Puente et al., 2015) supports anatomically the TRPV1-mediated synaptic plasticity at the MPP-GC synapses, as already discussed. The differences observed between eCB-eLTD at presynaptic (Peñasco et al., 2019) or postsynaptic sites of the MPP-GC synapses (Chávez et al., 2010) could be due, in addition to the stimulation paradigm, to several critical factors, like age (PND 74–80) and/or temperature of the *in vitro* experiments (32–35 °C). We speculate that both LTDs might be regarded as the synergistic effect of CB_1R reducing glutamate release (Peñasco et al., 2019) and TRPV1 depressing excitatory currents by promoting AMPAR internalization at the MPP-GC synapses (Chávez et al., 2010). Then, in the absence of

TRPV1, LFS would not longer endorse LTD (Chávez et al., 2010) and there only under HFS conditions could be revealed the shift from CB_1R-LTD (Peñasco et al., 2019) to CB_1R-LTP (this doctoral work) based on the CB_1R changes elicited by the lack of TRPV1 (see above). In fact, HFS of the LPP-GC synapses triggered LTP that was mediated by CB_1Rs, postsynaptic NMDARs and production of mGluR5-dependent 2-AG (Wang et al., 2016). Furthermore, the CB_1R activation at LPP synaptic terminals was seen to cause the assembly of latrunculin-sensitive actin filaments, the reorganization of the actin cytoskeleton by an integrin-associated kinase (FAK) and its downstream effector ROCK, resulting in the enhancement of glutamate release (Wang et al., 2018). Interestingly, LTP significantly decreased in TRPV1-KO after latrunculin A application in our experiments; however, it did not have any effect in WT in the presence of the TRPV1 antagonist AMG9810. Altogether, it is plausible that CB_1Rs activation at the MPP-GC synapses in TRPV1-KO increases actin phosphorylation and intracellular signalling cascades endorsing greater glutamate release that leads to CB_1R-LTP.

To further test the hypothesis that the CB_1R changes were underlying the shift to CB_1R-LTP at the MPP-GC synapses upon LFS, the TRPV1 antagonist AMG9810 was applied in WT. In these conditions, LTP was significantly reduced by AM251 but was unaffected by latrunculin A, indicating that the induced LTP upon pharmacological blockade of TRPV1 shares the participation of CB_1R but not the intracellular signalling cascades turned on in the absence of TRPV1 at the MPP-GC synapses. Interestingly, WIN had not any effect on the AMG9810-induced LTP in WT after LFS. WIN at the concentration used (5 μm) might be stabilizing the CB_1R in a conformation state that would lead to its coupling shift from Gi/o to Gq/11, therefore enhancing PLC activity with the consequent calcium release from intracellular stores (Lauckner et al., 2005), eventually increasing glutamate release and NMDA receptor activation (Errington et al., 1987; Lutzu and Castillo, 2020). As the slight potentiation observed in CB_1R-KO after LFS disappeared with D-APV (Peñasco et al., 2019), it remains to be known the effect of D-APV on the LTP seen in the presence of AMG9810 and WIN at the MPP-GC synapses. Furthermore, our LFS protocol triggered LTP at the LPP-GC synapses in WT as shown previously (Wang et al., 2016; 2018) and in TRPV1-KO. It remains to be assessed the participation of CB_1Rs in the LTP observed in LPP of TRPV1-KO. As a final consideration, we should keep in mind that CB_1R agonism has been shown to increase glutamate release in the hippocampus (Funada and Takebayashi-Ohsawa, 2018) and that the activation CB_1Rs localized in astrocytes promotes glutamate release locally inducing LTD mediated by AMPAR endocytosis (Han et al., 2012), and also remotely potentiating synaptic transmission (Araque et al., 2017).

Together, our findings further suggest that the precise subcellular localization of the ECS components in specific cell types and synapses are key players for the induction of diverse forms of synaptic plasticity through distinct signalling mechanisms (Castillo et al., 2012; Puente et al., 2011). Furthermore, the shift in synaptic plasticity observed at the MPP-GC synapses in TRPV1-KO could be due to both the lack of TRPV1 and the compensatory effects triggered by the genetic deletion of TRPV1. Measurements of endocannabinoids in TRPV1-KO will be carried out in the coming future.

6.3- Memory in TRPV1-KO mice.

Different studies have shown that TRPV1-KO mice have impaired nociception and reduced sensitivity to painful heat (Caterina et al., 2000), deficits in learning and conditioned fear, attenuated fever responses (Iida et al., 2005) and anxiolytic behaviours in the light–dark box and in the elevated plus maze, with no differences in locomotion (Marsch et al., 2007). Therefore, we wanted to explore in this thesis work whether recognition memory was affected by the absence of TRPV1-KO, attributable to its potential effect on the developing hippocampus, parahippocampus and neocortex (Tanimizu et al., 2017).

CB_1Rs have been shown to participate in working memory through astroglial CB_1Rs (Han et al., 2012) and to regulate memory processes via mitochondrial CB_1Rs (Bénard et al., 2012; Hebert-Chatelain et al., 2016). Moreover, CB_1Rs have a crucial role in the perturbed consolidation of non-emotional memory induced by acute stress (Busquets-Garcia et al., 2016) and are involved in appetitive retrieval, but not aversive olfactory memory (Terral et al., 2019). Thus, the changes in synaptic plasticity observed in our study could have an impact on the behaviour of TRPV1-KO mice. However, there were not found significant changes in the discrimination index or exploration time in the NOR test, as the TRPV1-KO mice did similarly to their WT littermates. This could be due to the mice age used in this test (8 weeks) as memory deficits were detected in 10-14-week-old mice (Marsch et al., 2007) and older (Iida et al., 2005).

As the hippocampus is also involved in spatial memory, the Barnes maze test was also used to assess the capacity to learn the relationship between distal cues in the surrounding environment and a fixed escape location (Pitts, 2018). Again, TRPV1-KO mice did not show significant differences neither in the time spent to complete the task nor in the strategy displayed to look for the escape box, with respect to WT littermates. However, they made more errors in comparison to their WT littermates. The number of errors could be due to the reduced anxiety

of these mice, though this factor could also cause the opposite action. Thus, WT littermates were placed in a more stressful situation trying to achieve the goal faster, so they could not afford to be wrong. The difference in the number of errors was more pronounced in the first days and was reduced in the last days of trial, confirming that learning was not affected in 8 week-old TRPV1-KO mice.

Therefore, the biochemical, anatomical and functional changes taking place in the ECS of TRPV1-KO mice, i.e., decrease of CB_1Rs in GABAergic terminals and increase in glutamatergic terminals, decrease in MAGL with no changes in DAGLα and FAAH, increase in Gαi1, Gαi2, Gαi3 and CRIP1a expression, low basal CB_1R activation, high CB_1R coupling efficacy to G-proteins and shift from CB_1R-eLTD to CB_1R-LTP, seem to not endure any impairment in the hippocampal behaviours tested in my thesis. However, we have recently observed in a mouse model of binge drinking during the adolescence, a significant reduction in CP 55.940 potency for stimulating [^{35}S] GTPγS binding as well as in [^{35}S] GTPγS basal binding and a reduction in the Gαi2 subunit in the adult hippocampus, which may be related to the absence of eCB-eLTD and deficits in the NOR test (Peñasco et al., 2020). Also, there was an increase in MAGL in our EtOH model, as shown by others (Subbanna et al., 2015) but no changes in in DAGLα. Lack of Gαi2 subunit was shown to cause deficits in learning efficiency, sociability and social recognition (Hamada et al., 2017). Interestingly, MAGL inhibition was able to overcome the functional and behavioural disturbances induced by EtOH, most likely due to the increase in 2-AG (Peñasco et al., 2020). Actually, pharmacological or genetic ablation of MAGL have been shown to enhance long-term synaptic plasticity, improve cognitive performance through CB_1 receptor-mediated mechanisms (Long et al., 2009; Chen et al., 2012).

Altogether, we guess that the changes in the ECS of TRPV1-KO mice were not pronounced enough to cause obvious hippocampus-based memory deficits. Nonetheless, more behavioural tests (novel object location test -for spatial recognition memory-; object-in-place test -for associative recognition memory-; open field -for anxiety-; rotarod -for motor coordination-; beam walking balance test -for balance-; tail suspension test -for depressive-like behaviour-; light–dark box -for unconditioned anxious behaviour-) as we did for studying the effects of an enriched environment on the cognitive deficits in the adult associated with the EtOH binge drinking during the adolescence (Rico-Barrio et al., 2019), should be performed in order to detect changes in these paradigms.

6.4- TRPV1-KO mice suffer milder seizures.

Finally, because TRPV1 has been shown to be involved in epileptiform activity (Bhaskaran and Smith, 2010; Sun et al., 2012; Iannotti et al., 2014; Naderi et al., 2015; Cho et al., 2018), we investigated the effect of the intrahippocampal injection of KA (50 nl of 20 mM) in WT and TRPV1-KO mice, a model of medial temporal lobe epilepsy (MTLE). Interestingly, epileptiform seizures were milder in TRPV1-KO than in WT littermates as they held lower score in the modified Racine's scale during the KA-induced status epilepticus. Furthermore, KA yielded after 30 days, in addition to the well-known granule cell dispersion, a decrease in CB_1R, DAGLα and NAPE-PLD immunoreactivity as well as a decrease in the proportion of CB_1R-immunopositive synaptic terminals in TRPV1-KO hippocampus (Grandes et al., 2014; Egaña et al., 2017, unpublished).

The ECS has been shown to play a protective role in epileptiform seizures through the modulation of overexcited brain circuits (Marsicano et al., 2003; Monory et al., 2006; Naidoo et al., 2011; Fezza et al., 2014; Katona, 2015; Soltesz et al., 2015; Cristino et al., 2020). Thus, the ECS promotes neuronal survival against KA- and glutamate-induced neurotoxicity (Marsicano et al., 2003; Marsicano and Lutz, 2006; Zani et al., 2007; Wolf et al., 2010) CB_1Rs increase selectively at inhibitory but not excitatory synapses in a model of febrile seizures (Chen et al., 2003; 2007) and protect against acute pentylenetetrazol (PTZ)-induced seizures (Naderi et al., 2015), and an increase in 2-AG levels suppresses spontaneous seizures (Sugaya et al., 2016). On the other hand, the TRPV1 absence by itself would also favour protection against the acute excitotoxic insult elicited by KA, as the TRPV1 up-regulates during epileptiform activity (Sun et al., 2012); and capsazepine inhibits the increase in action potential-dependent and -independent firing of DG cells elicited by capsaicin after a single pilocarpine injection (Bhaskaran and Smith, 2010), protects against PTZ-induced seizures (Naderi et al., 2015) and reduces seizure severity in a genetic rat model of epilepsy (Cho et al., 2018).

Signal integration by granule cells is under control of the hilar mossy cells, which are critically involved in learning of information sequences (Lisman et al., 2005) and epileptiform activity (Ratzliff et al., 2002). The mossy cells receive glutamatergic mossy fibre collaterals of the granule cells, and in turn send commissural/associational fibres that innervate GABAergic interneurons and multiple dentate granule cells forming mossy-granule cell synapses in the dentate MCFL (Amaral and Witter, 1989; Ratzliff et al., 2002; Johnston and Amaral, 2004; Scharfman and Myers, 2013). This layer also receives glutamatergic inputs from CA3 pyramidal neurons (Li et

al., 1994). The glutamatergic synapses of the three excitatory pathways targeting the dentate granule cells (MPP, LPP, MCF) contain CB_1Rs (Marsicano and Lutz, 1999; Katona et al., 2006; Kawamura et al., 2006; Monory et al., 2006; Uchigashima et al., 2011; Katona and Freund, 2012; Wang et al., 2016; Gutiérrez-Rodríguez et al., 2017).

So, we could argue that since CB_1Rs at glutamatergic synaptic terminals in the hippocampus protect against acute KA-induced seizures (Monory et al., 2006) and the TRPV1 favours epileptiform activity, the changes in the CB_1R distribution taking place at specific subcellular compartments of the MCFL and outer 2/3 of the DGML in TRPV1-KO (CB_1Rs decrease in inhibitory terminals, and increase in excitatory terminals and astrocytes) as well as the global changes in the hippocampus (decrease in MAGL with no changes in DAGLα and FAAH, increase in Gαi1, Gαi2, Gαi3 and CRIP1a, low basal CB_1R activation, high CB_1R coupling efficacy to G-proteins) should be rendering higher protection to TRPV1-KO mice against the epileptiform seizures caused by acute KA in the hippocampus (Egaña et al., 2017, unpublished).

Altogether, these findings suggest that the absence of TRPV1 triggers some adaptative changes in the ECS in the dentate gyrus that may be beneficial in the control of seizures.

7- Conclusions

The conclusions drawn from the characterization in this doctoral thesis of the structure and function of the endocannabinoid system in the TRPV1-KO mouse hippocampus are:

1. There is an impact on the expression of components of the endocannabinod system in mouse dentate gyrus.
2. The changes in protein expression vary depending on which fraction the proteins are localized: CB_1R and MAGL enzyme increase in whole homogenates and decrease in synaptosomal fractions.
3. It alters the expression of the CRIP1a protein.
4. There is an increase in the maximum efficacy of CB_1R to couple to G-proteins in the hippocampus.
5. There are more CB_1R-positive excitatory terminals but less excitatory terminals, less mitochondria, lower CB_1R density in inhibitory terminals and astrocytes, and not changes in the number of inhibitory terminals as well as in the area of astrocytic processes in the outer 2/3 of the dentate molecular layer.
6. It affects synaptic plasticity in the mossy cell fibre layer of the dentate molecular layer.
7. There is a shift from eCB-LTD to eCB-LTP at the medial perforant path synapses with no changes in synaptic plasticity at the lateral perforant path synapses.
8. 2-AG and the phosphorylation of actin filaments are involved in the eCB-LTP at the medial perforant path synapses.
9. Recognition and spatial memories are not impaired in young adult mice.
10. Kainate-induced excitotoxic seizures are milder.

8- Bibliography

1- Adermark L. and Bowers M.S. (2016): Disentangling the role of astrocytes in alcohol use disorder. Alcohol. Clin. Exp. Res. 40: 1802-1816.
2- Ahn K., McKinney M.K., Cravatt B.F. (2008): Enzymatic pathways that regulate endocannabinoid signalling in the nervous system. Chem. Rev. 108: 1687-1707.
3- Akopian A.N., Ruparel N.B., Patwardhan A., Hargreaves K.M. (2008): Cannabinoids desensitize capsaicin and mustard oil responses in sensory neurons via TRPA1 activation. J Neuroscience. 28: 1064-1075.
4- Akopian A.N., Ruparel N.B., Jeske N.A., Patwardhan A., Hargreaves K.M. (2009): Role of ionotropic cannabinoid receptors in peripheral antipain and antihyperalgesia. Trends. Pharmacol. Sci. 30: 79-84.
5- Alger B.E. (2006): Not too excited? Thank your endocannabinoids. Neuron. 51(4): 393-5.
6- Al-Hayani A., Wease K.N., Ross R.A., Pertwee R.G., Davies S.N. (2001): The endogenous cannabinoid anandamide activates vanilloid receptors in the rat hippocampal slice. Neuropharmacology. 41: 1000-1005.
7- Amaral D.G. and Witter M.P. (1989): The three-dimensional organization of the hippocampal formation: A review of anatomical data. Neuroscience. 31: 571-591.
8- Amaral D.G., Scharfman H.E., Lavenex P. (2007): The dentate gyrus: fundamental neuroanatomical organization (dentate gyrus for dummies). Prog. Brain Res. 163: 3-22.
9- Andersen P., Morris R., Amaral D.G., Bliss T., O'Keefe J. (2006): The hippocampus book. Oxford, UK: Oxford University Press.
10- Araque A., Castillo P.E., Manzoni O.J., Tonini R. (2017): Synaptic functions of endocannabinoid signalling in health and disease. Neuropharmacology. 124: 13-24.
11- Athanasiou A., Smith P.A., Vakilpour S., Kumaran N.M., Turner A.E., Bagiokou D., Layfield R., Ray D.E., Westwell A.D., Alexander S.P., et al. (2007): Vanilloid receptor agonists and antagonists are mitochondrial inhibitors: How vanilloids cause non-vanilloid receptor mediated cell death. Biochem. Biophys. Res. Commun. 354: 50-55.
12- Atwood B.K., Mackie K. (2010): CB2: A cannabinoid receptor with an identity crisis. Br. J. Pharmacol. 160: 467-479.
13- Bach M.E., Hawkins R.D., Osman M., Kandel E.R., Mayford M. (1995): Impairment of spatial but not contextual memory in CaMKII mutant mice with a selective loss of hippocampal ltp in the range of the θ frequency. Cell. 81: 905-915.
14- Badawy R.A., Harvey A.S., Macdonell R.A. (2009a): Cortical hyperexcitability and epileptogenesis: understanding the mechanisms of epilepsy—part 1. J. Clin. Neurosci. 16.
15- Badawy R.A., Harvey A.S., Macdonell R.A. (2009b): Cortical hyperexcitability and epileptogenesis: understanding the mechanisms of epilepsy—part 2. J. Clin. Neurosci. 16.

16- Barabasi A.L., Oltvai Z.N. (2004): Network biology: understanding the cell's functional organization. Nat. Rev. Genet. 5(2): 101-13.

17- Barrondo S., Sallés J. (2009): Allosteric modulation of 5-HT1A receptors by zinc: binding studies. Neuropharmacology. 56: 455-462.

18- Basavarajappa B.S., Cooper T.B., Hungund B.L. (1998): Chronicethanol administration down-regulates cannabinoid receptors in mousebrain synaptic plasma membrane. Brain Research. 793: 212-218.

19- Basavarajappa B.S. and Hungund B.L. (1999): Down-regulation of canna-binoid receptor agonist-stimulated [$_{35}$S] GTP$_{\gamma}$S binding in synaptic plasma membrane from chronic ethanol exposed mouse. Brain Research. 815: 89-97.

20- Basu J., Srinivas K.V., Cheung S.K., Taniguchi H., Huang Z.J., Siegelbaum S.A. (2013): A cortico-hippocampal learning rule shapes inhibitory microcircuit activity to enhance hippocampal information flow. Neuron 79, 1208-1221.

21- Baude A., Nusser Z., Roberts J.D.B., Mulvihill E., Mcllhinney R.A.J., Somogyi P. (1993): The metabotropic glutamate receptor (mGluRlα) is concentrated at perisynaptic membrane of neuronal subpopulations as detected by immunogold reaction. Neuron. 11: 771-787

22- Benard G., Massa F., Puente N., Lourenco J., Bellocchio L., Soria- Gómez E., Matias I., Delamarre A., Metna-Laurent M., Cannich A., Hebert-Chatelain E., Mulle C., Ortega-Gutiérrez S., Martín-Fontecha M., Klugmann M., Guggenhuber S., Lutz B., Gertsch J., Chaouloff F., López-Rodríguez M.L., Grandes P., Rossignol R., Marsicano G. (2012): Mitochondrial CB1 receptors regulate neuronal energy metabolism. Nat. Neurosci. 15: 558-564.

23- Bender V.A., Bender K.J., Brasier D.J., Feldman D.E. (2006): Two coincidence detectors for spike timing-dependent plasticity in somatosensory cortex. J. Neurosci. 26: 4166-4177.

24- Benito C., Tolón R.M., Castillo A.I., Ruiz-Valdepeñas L., Martínez-Orgado J.A., Fernández-Sánchez F.J., Vázquez C., Cravatt B.F., Romero J. (2012): β-Amyloid exacerbates inflammation in astrocytes lacking fatty acid amide hydrolase through a mechanism involving PPAR-α, PPAR-γ and TRPV1, but not CB_1 or CB_2 receptors. British Journal of Pharmacology. 166: 1474-1489.

25- Bhaskaran M.D. and Smith B.N. (2010): Effects of TRPV1 activation on synaptic excitation in the dentate gyrus of a mouse model of temporal lobe epilepsy. Exp. Neurol. 223: 529-536.

26- Bialecki J., Werner A., Weilinger N.L., Tucker C.M., Vecchiarelli H.A., Egaña J., Mendizabal-Zubiaga J., Grandes P., Hill M.N., Thompson R.J. (2020): Suppression of Presynaptic Glutamate Release by Postsynaptic Metabotropic NMDA Receptor Signalling to Pannexin-1. Journal of Neuroscience. 257-19.

27- Birder L.A., Nakamura Y., Kiss S., Nealen M.L., Barrick S., Kanai A.J., et al. (2002): Altered urinary bladder function in mice lacking the vanilloid receptor TRPV1. Nature Neuroscience. 5(9): 856-860.

28- Blair R.E., Deshpande L.S., Delorenzo R.J. (2015): Endocannabinoids and epilepsy. Cannabinoids in neurologic and mental disease. 1st. Waltham, MA, USA: Academic Press: 125-172.

29- Blankman J.L., Simon G.M., Cravatt B.F. (2007): A comprehensive profile of brain enzymes that hydrolyze the endocannabinoid 2-arachidonoylglycerol. Chem. Biol. 14: 1347-1356.

30- Bliss T.V. and Lomo T. (1973): Long-lasting potentiation of synaptic transmission in the dentate area of the anaesthetized rabbit following stimulation of the perforant path. J. Physiol. 232: 331-356.

31- Bliss T.V., Collingridge G.L., Morris R.G. (2007): Synaptic plasticity in the hippocampus. The Hippocampus Book. Oxford University Press: 343-474.

32- Blume L.C., Eldeeb K., Bass C.E., Selley D.E., Howlett A.C. (2015): Cannabinoid receptor interacting protein (CRIP1a) attenuates CB1R signalling in neuronal cells. Cell Signal. 27 (3): 716-26.

33- Blume L.C., Leone-Kabler S., Luessen D.J., Marrs G.S., Lyons E., Bass C.E., Chen R., Selley D.E., Howlett A.C. (2016): Cannabinoid receptor interacting protein suppresses agonist-driven CB1 receptor internalization and regulates receptor replenishment in an agonist-biased manner. J. Neurochem. 139: 396-407.

34- Bonilla-Del Rio I., Puente N., Penasco S., Rico I., Gutierrez-Rodriotaguez A., Elezgarai I., Ramos A., Reguero L., Gerrikagoitia I., Christie B.R., Nahirney P., Grandes P. (2019): Adolescent ethanol intake alters cannabinoid type-1 receptor localization in astrocytes of the adult mouse hippocampus. Addict Biol. November 23.

35- Booth W.T., Walker N.B., Lowther W.T., Howlett A.C. (2019): Cannabinoid receptor interacting protein 1a (CRIP1a): Function and structure. Molecules. 24 (20): 1-9.

36- Bosier B., Bellocchio L., Metna-Laurent M., Soria-Gómez E., Matias I., Hebert-Chatelain E., Cannich A., Maitre M., Leste-Lasserre T., Cardinal P., Mendizabal-Zubiaga J., Canduela M.J., Reguero L., Hermans E., Grandes P., Cota D., Marsicano G. (2013): Astroglial CB1 cannabinoid receptors regulate leptin signaling in mouse brain astrocytes. Mol. Metab. 2: 393-404.

37- Brailoiu G.C., Oprea T.I., Zhao P., Abood M.E., Brailoiu E. (2011): Intracellular cannabinoid type 1 (CB1) receptors are activated by anandamide. J. Biol. Chem. 286: 29166-29174.

38- Buckmaster P.S., Wenzel H.J., Kunkel D.D., Schwartzkroin P. A. (1996): Axon arbors and synaptic connections of hippocampal mossy cells in the rat in vivo. J. Comp. Neurol. 366: 271-292.

39- Burwell RD. (2000): The parahippocampal region: corticocortical connectivity. Ann N Y Acad Sci. 911: 25-42.

40- Busquets-Garcia A., Gomis-Gonzalez M., Srivastava R.K., Cutando L., Ortega-Alvaro A., Ruehle S., Remmers F., Bindila L., Bellocchio L., Marsicano G., Lutz B., Maldonado R., Ozaita A. (2016): Peripheral and central CB1 cannabinoid receptors control stress-induced impairment of memory consolidation. Proc. Natl. Acad. Sci. USA. 113: 9904-9909.

41- Cadigan K.M., Grossniklaus U., Gehring W.J. (2004): Functional redundancy: the respective roles of the two sloppy paired genes in Drosophila segmentation. Proceedings of the National Academy of Sciences of the United States of America. 91 (14): 6324-8.

42- Cajal S.R.Y. (1955): Histologie du systeme nerveux de l'homme & des vertebres. Consejo Superior de Investigaciones Cientificas, Instituto Ramon y Cajal.

43- Calabrese E.J., Rubio-Casillas A. (2018): Biphasic effects of THC in memory and cognition. Eur. J. Clin. Investig. 48: 12920.

44- Caporale N. and Dan Y., (2008): Spike timing-dependent plasticity: a Hebbian learning rule. Annu. Rev. Neurosci. 31: 25-46.

45- Canduela M.J., Mendizabal-Zubiaga J., Puente N., Reguero L., Elezgarai I., Ramos-Uriarte A., Gerrikagoitia I., Grandes P. (2015): Visualization by high resolution immunoelectron microscopy of the transient receptor potential vanilloid-1 at inhibitory synapses of the mouse dentate gyrus. PLoS One.10 (3).

46- Carlson G., Wang Y., Alger B.E. (2002): Endocannabinoids facilitate the induction of LTP in the hippocampus. Nat. Neurosci. 5: 723-724.

47- Casado V., Barrondo S., Spasic M., Callado L.F., Mallol J., Canela E., et al. (2010): Gi protein coupling to adenosine A_1-A_{2A} receptor heteromers in human brain caudate nucleus. J. Neurochem. 114 (4): 972-80.

48- Castillo P.E., Younts T.J., Chávez A.E., Hashimotodani Y. (2012): Endocannabinoid signaling and synaptic function. Neuron. 76: 70-81.

49- Caterina M.J., Schumacher M.A., Tominaga M., Rosen T.A., Levine J.D., Julius D. (1997): The capsaicin receptor: a heat-activated ion channel in the pain pathway. Nature. 389 (6653): 816-824.

50- Caterina M.J., Leffler A., Malmberg A.B., Martin W.J., Trafton J., Petersen-Zeitz K.R., Koltzenburg M., Basbaum A.I., Julius D. (2000): Impaired nociception and pain sensation in mice lacking the capsaicin receptor. Science. 288: 306-313.

51- Caterina M. J. (2014): TRP channel cannabinoid receptors in skin sensation, homeostasis, and inflammation. ACS Chem. Neurosci. 5: 1107-1116.

52- Cavanaugh D.J., Chesler A.T., Bráz J.M., Shah N.M., Julius D., Basbaum AI. (2011): Restriction of transient receptor potential vanilloid-1 to the peptidergic subset of primary afferent neurons follows its developmental downregulation in nonpeptidergic neurons. J Neurosci. 31 (28): 10119-27.

53- Chanda P.K., Gao Y., Mark L., Btesh J., Strassle B. W., Lu P., et al. (2010): Monoacylglycerol lipase activity is a critical modulator of the tone and integrity of the endocannabinoid system. Mol. Pharmacol. 78: 996-1003.

54- Chávez A.E., Chiu C.Q., Castillo P.E. (2010): TRPV1 activation by endogenous anandamide triggers postsynaptic long-term depression in dentate gyrus. Nat. Neurosci. 13: 1511-1518.

55- Chávez A.E., Hernández V.M., Rodenas-Ruano A., Savio-Chan C., Castillo P.E. (2014): Compartment-specificmodulation of GABAergic synaptic transmission by TRPV1 channels in the dentate gyrus. The Journal of Neuroscience. 34 (50): 16621-16629.

56- Chen, K., Ratzliff, A., Hilgenberg, L., Gulyas, A., Freund, T.F., Smith, M., Dinh, T.P., Piomelli, D., Mackie, K., Soltesz, I. (2003): Long-term plasticity of endocannabinoid signaling induced by developmental febrile seizures. Neuron. 39: 599-611.

57- Chen K., Neu A., Howard A.L., Foldy C., Echegoyen J., Hilgenberg L., et al. (2007): Prevention of plasticity of endocannabinoid signaling inhibits persistent limbic hyperexcitability caused by developmental seizures. J. Neurosci. 27: 46-58.

58- Chen Y., Willcockson H.H., Valtschanoff J.G. (2008): Increased expression of CGRP in sensory afferents of arthritic mice–effect of genetic deletion of the vanilloid receptor TRPV1. Neuropeptides. 42: 551-6.

59- Chen Y., Willcockson H.H., Valtschanoff J.G. (2009): Influence of the vanilloid receptor TRPV1 on the activation of spinal cord glia in mouse models of pain. Exp. Neurol. 220: 383-390.

60- Chen R., Zhang J., Wu Y., Wang D., Feng G., Tang Y.P., Teng Z., Chen C. (2012): Monoacylglycerol lipase is a therapeutic target for Alzheimer's disease. Cell Rep. 2: 1329.

61- Chevaleyre V. and Castillo P.E. (2003): Heterosynaptic LTD of hippocampal GABAergic synapses: a novel role of endocannabinoids in regulating excitability. Neuron. 38: 461-472.

62- Chevaleyre V. and Castillo P.E. (2004): Endocannabinoid-mediated metaplasticity in the hippocampus. Neuron. 43: 871-881.

63- Chiarlone A., Bellocchio L., Blazquez C., Resel E., Soria-Gómez, E., Cannich A., Ferrero J.J., Sagredo O., Benito C., Romero J. et al. (2014): A restricted population of CB1 cannabinoid receptors with neuroprotectiveactivity. Proc. Natl. Acad Sci. USA. 111: 8257-8262.

64- Chiu C.Q. and Castillo P.E. (2008): Input-specific plasticity at excitatory synapses mediated by endocannabinoids in the dentate gyrus. Neuropharmacology. 54: 68-78.

65- Cho S.J., Vaca M.A., Miranda C.J., N'Gouemo P. (2018): Inhibition of transient potential receptor vanilloid type 1 suppresses seizure susceptibility in the genetically epilepsy-prone rat. *CNS Neuroscience & Therapeutics*. 24 (1): 18-28.

66- Clement A.B., Hawkins E.G., Lichtman A.H., Cravatt B.F. (2003): Increased seizure susceptibility and proconvulsant activity of anandamide in mice lacking fatty acid amide hydrolase. J. Neurosci. 23: 3916-3923.

67- Cohen R., Yokoi T., Holland J.P., Pepper A.E., Holland M.J. (1987): Transcription of the constitutively expressed yeast enolase gene ENO1 is mediated by positive and negative cis-acting regulatory sequences. Molecular and cellular biology. 7 (8): 2753-61.

68- Conn P.J. and Pin J.P. (1997): Pharmacology and functions of metabotropic glutamate receptors. Annu. Rev. Pharmacol. Toxicol. 37: 205-237.

69- Cortright D.N., Crandall M., Sanchez J.F., Zou T., Krause J.E., White G. (2001): The tissue distribution and functional characterization of human VR1. Biochem. Biophys. Res. Commun. 281: 1183–1189.

70- Cristino L., De Petrocellis L., Pryce G., Baker D., Guglielmotti V., Di Marzo V. (2006): Immunohistochemical localization of cannabinoid type 1 and vanilloid transient receptor potential vanilloid type 1 receptors in the mouse brain. Neuroscience. 139: 1405-1415.

71- Cristino L., Strarowicz K., De Petrocellis L., Morishita J., Ueda N., Guglielmotti V. et al. (2008): Immunohistochemical localization of anabolic and catabolic enzymes for anandamide and other putative endovanilloids in the hippocampus and cerebellar cortex of the mouse brain. Neuroscience. 151: 955-968.

72- Cristino L., Bisogno T., Di Marzo V. (2020): Cannabinoids and the expanded endocannabinoid system in neurological disorders. Nat. Rev. Neurol. 16 (1): 9-29.

73- Cui Y., Perez S., Venance L. (2018): Endocannabinoid-LTP mediated by CB1 and TRPV1 receptors encodes for limited occurrences of coincident activity in neocortex. Frontiers in Cellular Neuroscience. 12: 182.

74- Daude N., Wohlgemuth S., Brown R., Pitstick R., Gapeshina H., Yang J., et al. (2012): Knockout of the prion protein (PrP)-like Sprn gene does not produce embryonic lethality in combination with PrP(C)-deficiency. Proceedings of the National Academy of Sciences of the United States of America. 109 (23): 9035-40.

75- Davidson E. and Levin M. (2005): Gene regulatory networks. Proceedings of the National Academy of Sciences of the United States of America. 102(14): 4935.

76- De Lago E., De Miguel R., Lastres-Becker I., Ramos J.A., Fernandez-Ruiz J. (2004): Involvement of vanilloid-like receptors in the effects of anandamide on motor behavior and nigrostriatal dopaminergic activity: in vivo and in vitro evidence. Brain Res. 1007: 152-159.

77- De May C.L. and Ali A.B. (2013): Cell type-specific regulation of inhibition via cannabinoid type 1 receptors in rat neocortex. J. Neurophysiol. 109: 216-224.

78- De Petrocellis L., Starowicz K., Moriello A.S., Vivese M., Orlando P., Di Marzo V. (2007): Regulation of transient receptor potential channels of melastatin type 8 (TRPM8): effect of cAMP, cannabinoid CB1 receptors and endovanilloids. Exp. Cell Res. 313: 1911-1920.

79- De Petrocellis L., Ligresti A., Moriello A.S., Allarà M., Bisogno T., Petrosino S., et al. (2011): Effects of cannabinoids and cannabinoid-enriched Cannabis extracts on TRP channels and endocannabinoid metabolic enzymes. Br. J. Pharmacol. 163: 1479-1494.

80- De Petrocellis L., Nabissi M., Santoni G., Ligresti A. (2017): Actions and regulation of ionotropic cannabinoid receptors. Adv. Pharmacol. 80: 249-289.

81- De Souza A.T., Dai X., Spencer A.G., Reppen T., Menzie A., Roesch P.L., et al. (2006): Transcriptional and phenotypic comparisons of Ppara knockout and siRNA knockdown mice. Nucleic acids research. 34 (16): 4486-94.

82- Demuth D.G. and Molleman A. (2006): Cannabinoid signalling. Life Sci. 78 (6): 549-563.

83- Den Boon F.S., Chameau P., Schaafsma-Zhao Q., van Aken W., Bar, M., Oddi S., Kruse C.G., Maccarrone M., Wadman W.J., Werkman T.R. (2012): Excitability of prefrontal cortical pyramidal neurons is modulated by activation of intracellular type-2 cannabinoid receptors. Proc. Natl. Acad. Sci. USA. 109: 3534-3539.

84- Devane W.A., Dysarz F.A. 3rd, Johnson M.R., Melvin L.S., Howlett A.C. (1988): Determination and characterization of a cannabinoid receptor in rat brain. Mol. Pharmacol. 34: 605-613.

85- Devane W.A., Hanus L., Breuer A., Pertwee R.G., Stevenson L.A., Griffin G., Gibson D., Mandelbaum A., Etinger A., Mechoulam R. (1992): Isolation and structure of a brain constituent that binds to the cannabinoid receptor. Science. 258: 1946-1949.

86- Dhopeshwarkar A. and Mackie K. (2014): CB2 cannabinoid receptors as a therapeutic target-what does the future hold? Mol. Pharmacol. 86: 430-437.

87- Di Marzo V., Melck D., Bisogno T., De Petrocellis L. (1998): Endocannabinoids: endogenous cannabinoid receptor ligands with neuromodulatory action. Trends Neurosci. 21 (12).

88- Di Marzo V., De Petrocellis L., Bisogno T. (2001): Endocannabinoids Part I: molecular basis of endocannabinoid formation, action and inactivation and development of selective inhibitors. Expert Opin. Ther. Targets. 5 (2): 241-265.

89- Di Marzo V., Lastres-Becker I., Bisogno T., De Petrocellis L., Milone A., Davis J.B., Fernandez-Ruiz J.J. (2001): Hypolocomotor effects in rats of capsaicin and two long chain capsaicin homologues. Eur. J. Pharmacol. 420: 123-131.

90- Di Marzo V., Blumberg P.M., Szallasi A. (2002): Endovanilloid signalling in pain. Curr. Opin. Neurobiol. 12: 372-379.

91- Di Marzo V., Gobbi G., Szallasi A. (2008): Brain TRPV1: a depressing TRP down memory lane? Trends Pharmacol Sci. 29 (12): 594-600.

92- Di Marzo V. (2009): The endocannabinoid system: its general strategy of action, tools for its pharmacological manipulation and potential therapeutic exploitation. Pharmacol. Res. Official J. Italian Pharmacol. Soc. 60: 77-84.

93- Di Marzo V. and De Petrocellis L. (2012): Why do cannabinoid receptors have more than one endogenous ligand? Philos. Trans. R. Soc. B. 367: 3216-3228.

94- Di Marzo V., Stella N., Zimmer A. (2015): Endocannabinoid signalling and the deteriorating brain. Nat. Rev. Neurosci. 16: 30-42.

95- Dinh T.P., Carpenter D., Leslie F.M., Freund T.F., Katona I., Sensi S.L., Kathuria S., Piomelli D. (2002): Brain monoglyceride lipase participating in endocannabinoid inactivation. Proc. Natl. Acad. Sci. U. S. A. 99: 10819-10824.

96- Dodd P.R., Hardy J.A., Oakley A.E., Edwardson J.A., Perry E.K., Delaunoy J.-P. (1981): A rapid method for preparing synaptosomes: comparison, with alternative procedures. Brain Res. 226: 107-118.

97- Doly S., Fischer J., Salio C., Conrath M. (2004): The vanilloid receptor-1 is expressed in rat spinal dorsal horn astrocytes. *Neurosci Lett*. 357: 123-126.

98- Drebot I.I., Storozhuk M.V., Kostyuk P. G. (2006): An unexpected effect of capsaicin on spontaneous GABAergic IPSCs in hippocampal cell cultures. Neurophysiology. 38 (4): 308-311.

99- Dudman J.T., Tsay D., Siegelbaum S.A. (2007): A role for synaptic inputs at distal dendrites: instructive signals for hippocampal long-term plasticity. Neuron. 56: 866-879.

100- Egaña-Huguet J., Rico-Barrio I., Terradillos I., Mendizabal-Zubiaga J.L., Puente N., Gerrikagoitia I., Elezgarai I., Grandes P. (2017): TRPV1-KO saguek epilepsia krisi arinagoak jasatearen zergatiak bilatzen. II. IkerGazte nazioarte kongresua. Osasun zientziak (I): 80-87

101- Egertova M. and Elphick M.R. (2000): Localization of cannabinoid receptors in the rat brain using antibodies to the intracellular C-terminal tail of CB. J. Comp. Neurol. 422: 159-171.

102- Egertova M., Simon G.M., Cravatt B.F., Elphick M.R. (2008): Localization of N-acyl phosphatidylethanolamine phospholipase D (NAPE-PLD) expression in mouse brain: A new

perspective on N-acylethanolamines as neural signaling molecules. J. Comp. Neurol. 506: 604-615.

103- El-Brolosy M.A. and Stainier D.Y.R. (2017): Genetic compensation: A phenomenon in search of mechanisms. PLoS Genet. 13 (7): 1006780.

104- Elezgarai I., Diez J., Puente N., Azkue J.J., Benitez R., Bilbao A., Knöpfel T., Doñate-Oliver F., Grandes P. (2003): Subcellular localization of the voltage-dependent potassium channel K_v3.1b in postnatal and adult rat medial nucleus of the trapezoid body. Neuroscience. 118: 889-898.

105- Errington M.L., Lynch M.A., Bliss T.V. (1987): Long-term potentiation in the dentate gyrus: Induction and increased glutamate release are blocked by D (-) aminophosphonovalerate. Neuroscience. 20: 279-284.

106- Evers B., Jastrzebski K., Heijmans J.P., Grernrum W., Beijersbergen R.L., Bernards R. (2016): CRISPR knockout screening outperforms shRNA and CRISPRi in identifying essential genes. Nature biotechnology. 34 (6): 631-3.

107- Farina C., Aloisi F., Meinl E. (2007): Astrocytes are active players in cerebral innate immunity. Trends Immunol. 28: 138-145.

108- Fegley D., Kathuria S., Mercier R., Li C., Goutopoulos A., Makriyannis A., et al. (2004): Anandamide transport is independent of fatty-acid amide hydrolase activity and is blocked by the hydrolysis-resistant inhibitor AM1172. Proc. Natl. Acad. Sci. USA. 101: 8756-8761.

109- Fezza F., Marrone M.C., Avvisati R., Di Tommaso M., Lanuti M., Rapino C., et al. (2014): Distinct modulation of the endocannabinoid system upon kainic acid-induced in vivo seizures and in vitro epileptiform bursting. Mol. Cell Neurosci. 62: 1-9.

110- Fimiani C., Mattocks D., Cavani F., Salzet M., Deutsch D.G., Pryor S., et al. (1999): Morphine and anandamide stimulate intracellular calcium transients in human arterial endothelial cells: coupling to nitric oxide release. Cell. Signal. 11 (3): 189-193.

111- Flores Á., Maldonado R. and Berrendero F. (2013): Cannabinoid-hypocretin cross-talk in the central nervous system: what we know so far. Frontiers Neuroscience. 7

112- Fredens K. (1981): Genetic variation in the histoarchitecture of the hippocampal region in mice. Anat. Embryol. 161: 265-281.

113- Freund T.F., Katona I., Piomelli D. (2003): Role of endogenous cannabinoids in synaptic signaling. Physiol. Rev. 83: 1017-1066.

114- Fu M., Xie Z., Zuo H. (2009): TRPV1: a potential target for antiepileptogenesis. Med. Hypotheses. 73: 100-102.

115- Funada M. and Takebayashi-Ohsawa M. (2018): Synthetic cannabinoid AM2201 induces seizures: involvement of cannabinoid CB1 receptors and glutamatergic transmission Toxicol. Appl. Pharmacol. 338: 1-8.

116- Fyhn M., Molden S., Witter M.P., Moser E.I., Moser M.-B. (2004): Spatial representation in the entorhinal cortex. Science. 305: 1258-1264.

117- Gaoni Y. and Mechoulam R. (1964): Isolation, structure, and partial synthesis of an active constituent of hashish. J. Am.Chem. Soc. 86. 1646-1647.

118- Gardner-Medwin A.R. (1976): The recall of events through the learning of associations between their parts. Proc. R. Soc. Lond. B. 194: 375-402.

119- Garro M.A., Lopez de Jesus M., Ruiz de Azua I., et al. (2001): Regulation of phospholipase Cβ activity by muscarinic acetylcholine and 5-HT_2 receptors in crude and synaptosomal membranes from human cerebral cortex. Neuropharmacology. 40 (5): 686-695.

120- Gerdeman G., Lovinger D.M. (2001): CB1 cannabinoid receptor inhibits synaptic release of glutamate in rat dorsolateral striatum. J. Neurophysiol. 85: 468-471.

121- Gerdeman G.L., Ronesi J., Lovinger D.M. (2002): Postsynaptic endocannabinoid release is critical to long-term depression in the striatum. Nature Neuroscience. 5: 446-451.

122- Gibson H.E., Edwards J.G., Page R.S., Van Hook M.J., Kauer J.A. (2008): TRPV1 channels mediate long-term depression at synapses on hippocampal inter-neurons. Neuron. 57: 746-759.

123- Glaser S.T. and Kaczocha M. (2009): Temporal changes in mouse brain fatty acid amide hydrolase activity. Neuroscience. 163: 594-600.

124- Gomez-Gonzalo M., Navarrete M., Perea G., Covelo A., Martin-Fernandez M., Shigemoto R., Lujan R., Araque A. (2015): Endocannabinoids induce lateral long term potentiation of transmitter release by stimulation of gliotransmission. Cereb. Cortex. 25: 3699-3712.

125- Gong J.P., Onaivi E.S., Ishiguro H., Liu Q.R., Tagliaferro P.A., Brusco A., Uhl G.R. (2006): Cannabinoid CB2 receptors: Immunohistochemical localization in rat brain. Brain Res. 1071: 10-23.

126- González-Gaitán M., Rothe M., Wimmer E.A., Taubert H., Jäckle H. (1994): Redundant functions of the genes knirps and knirps-related for the establishment of anterior Drosophila head structures. Proceedings of the National Academy of Sciences of the United States of America. 91 (18): 8567-71.

127- Gonzalez-Reyes L.E., Ladas T.P., Chiang C.-C., Durand D.M. (2013): TRPV1 antagonist capsazepine suppresses 4-AP-induced epileptiform activity *in vitro* and electrographic seizures *in vivo*. Exp. Neurol. 250: 321-332.

128- Goswami C., Schmidt H., Hucho F. (2007): TRPV1 at nerve endings regulates growth cone morphology and movement through cytoskeleton reorganization. FEBS J. 274 (3): 760-772.

129- Grandes P. and Streit P. (1991): Effect of perforant path lesion on pattern of glutamate-like immunoreactivity in rat dentate gyrus. Neuroscience. 41 (2-3): 391-400.

130- Grandes, P. (2014): Anatomy and functional role of the transient receptor potential vanilloid type 1 in the dentate gyrus of a kainate-induced seizures mouse model. 24th Annual ICRS Symposium. NIDA Symposium "TRP Channels: The only TR(i)P you can have on cannabinoids?" Chair: Vincenzo di Marzo. Baveno.

131- Grimsey N.L., Graham E.S., Dragunow M., Glass M. (2010): Cannabinoid receptor 1 trafficking and the role of the intracellular pool: Implications for therapeutics. Biochem. Pharmacol. 80: 1050-1062.

132- Grueter B.A., Brasnjo G., Malenka R.C. (2010): Postsynaptic TRPV1 triggers cell type-specific long-term depression in the nucleus accumbens. Nat. Neurosci. 13: 1519-1525.

133- Guggenhuber S., Monory K., Lutz B., Klugmann M. (2010): AAV vector-mediated overexpression of CB1 cannabinoid receptor in pyramidal neurons of the hippocampus protects against seizure-induced excitoxicity. PLoS One. 5: 15707.

134- Gulyas A.I., Cravatt B.F., Bracey M.H., Dinh T.P., Piomelli D., Boscia F., Freund T.F. (2004): Segregation of two endocannabinoid-hydrolyzing enzymes into pre- and postsynaptic compartments in the rat hippocampus, cerebellum and amygdala. Eur. J. Neurosci. 20: 441-458.

135- Guo A., Vulchanova L., Wang J., Li X., Elde R. (1999): Immunocytochemical localization of the vanilloid receptor1 (VR1): relationship to neuropeptides, the P2X3 purinoceptor and IB4 binding sites.Eur J Neurosci. 11: 946-958.

136- Gutiérrez-Rodríguez A., Puente N., Elezgarai I., Ruehle S., Lutz B., Reguero L., Gerrikagoitia I., Marsicano G., Grandes P., (2017): Anatomical characterization of the cannabinoid CB1 receptor in cell-type-specific mutant mouse rescue models. J. Comp. Neurol. 525: 302-318.

137- Gutierrez-Rodriguez A., Bonilla-Del Rio I., Puente N., Gomez-Urquijo S.M., Fontaine C.J., Egana-Huguet J., Elezgarai I., Ruehle S., et al. (2018): Localization of the cannabinoid type-1 receptor in subcellular astrocyte compartments of mutant mouse hippocampus. Glia. 66 (7): 1417-1431.

138- Hajos N., Katona I., Naiem S.S., MacKie K., Ledent C., Mody I., et al. (2000): Cannabinoids inhibit hippocampal GABAergic transmission and network oscillations. Eur. J. Neurosci. 12: 3239-3249.

139- Hamada N., Negishi Y., Mizuno M., Miya F., Hattori A., Okamoto N. et al. (2017): Role of a heterotrimeric G-protein, Gi2, in the corticogenesis: possible involvement in periventricular nodular heterotopia and intellectual disability. J Neurochem. 140: 82-95.

140- Han J., Kesner P., Metna-Laurent M., Duan T., Xu L., Georges F., et al. (2012): Acute cannabinoids impair working memory through astroglial CB1 receptor modulation of hippocampal LTD. Cell. 148 (5): 1039-50.

141- Han P., McDonald H.A., Bianchi B.R., Kouhen R.E., Vos M.H., Jarvis M.F., Faltynek C.R., Moreland R.B. (2007): Capsaicin causes protein synthesis inhibition and microtubule disassembly through TRPV1 activities both on the plasma membrane and intracellular membranes. Biochem. Pharmacol. 73 (10): 1635-1645.

142- Hargreaves E.L., Rao G., Lee I., Knierim J.J. (2005): Major dissociation between medial and lateral entorhinal input to dorsal hippocampus. Science. 308: 1792-1794.

143- Hartley T., Lever C., Burgess N., O'Keefe J. (2014): Space in the brain: how the hippocampal formation supports spatial cognition. Phil. Trans. R. Soc. B. 369: 20120510.

144- Hashimotodani Y., Nasrallah K., Jensen K.R., Chávez A.E., Carrera D., Castillo P.E. (2017): LTP at hilar mossy cell-dentate granule cell synapses modulates dentate gyrus output by increasing excitation/inhibition balance. Neuron. 95: 928-943.

145- Hauser A., Hesdorffer D. (1990): Prognosis. In W.A. Hauser, D.C. Hesdorffer (Eds) Epilepsy: frequency, causes and consequences. Demos. NY. 197-243.

146- Hebert-Chatelain E., Reguero L., Puente N., Lutz B., Chaouloff F., Rossignol R., Piazza P.V., Benard G., Grandes P., Marsicano G. (2014a): Cannabinoid control of brain bioenergetics: exploring the subcellular localization of the CB1 receptor. Mol. Metab. 3: 495-504.

147- Hebert-Chatelain E., Reguero L., Puente N., Lutz B., Chaouloff F., Rossignol R., Piazza P.V., Benard G., Grandes P., Marsicano G. (2014b): Studying mitochondrial CB1 receptors: yes we can. Mol. Metab. 3: 339.

148- Hebert-Chatelain E., Desprez T., Serrat R., Bellocchio L., Soria-Gomez E., Busquets-Garcia A., Pagano Zottola A.C., Delamarre A., Cannich A., Vincent P., Varilh M., Robin L.M., Terral G., García-Fernández M.D., Colavita M., Mazier W., Drago F., Puente N., Reguero L., Elezgarai I., Dupuy J.W., Cota D., Lopez-Rodriguez M.L., Barreda-Gómez G., Massa F., Grandes P., Bénard G., Marsicano G. (2016): A cannabinoid link between mitochondria and memory. Nature. 539: 555-559.

149- Heifets B.D. and Castillo P.E. (2009): Endocannabinoid signaling and long-term synaptic plasticity. Annu. Rev. Physiol. 71: 283-306.

150- Helliwell R.J., McLatchie L.M., Clarke M., Winter J., Bevan S., McIntyre P. (1998): Capsaicin sensitivity is associated with the expression of the vanilloid (capsaicin) receptor (VR1) mRNA in adult rat sensory ganglia. Neurosci. Lett. 250 (3): 177-180.

151- Herkenham M., Lynn A.B., Little M.D., Johnson M.R., Melvin L.S., De Costa B.R., Rice K.C. (1990): Cannabinoid receptor localization in brain. Proc. Natl. Acad. Sci. USA. 87: 1932-1936.

152- Herkenham M., Lynn A.B., Johnson M.R., Melvin L.S., De Costa B.R., Rice K.C. (1991): Characterization and localization of cannabinoid receptors in rat brain: a quantitative in vitro autoradiographic study. J. Neurosci. 11.

153- Hjorth-Simonsen A. (1972): Projection of the lateral part of the entorhinal area to the hippocampus and fascia dentata. J. Comp. Neurol. 146: 219-232.

154- Hillard C.J., Weinlander K.M., Stuhr K.L. (2012): Contributions of endocannabinoid signaling to psychiatric disorders in humans: genetic and biochemical evidence. Neuroscience. 204: 207-229.

155- Hironaka K., Ozaki N., Hattori H., Nagamine K., Nakashima H., Ueda M., Sugiura Y. (2014): Involvement of glial activation in trigeminal ganglion in a rat model of lower gingival cancer pain. Nagoya J. Med. Sci. 76: 323-332.

156- Ho K.W., Ward N.J., Calkins D.J. (2012): TRPV1: A stress response protein in the central nervous system. Am. J. Neurodegener. Dis. 1: 1-14.

157- Ho K.W., Lambert W.S., Calkins D.J. (2014): Activation of the TRPV1 cation channel contributes to stress-induced astrocyte migration. Glia. 62 (9): 1435-51.

158- Hoffmann F.M. (1991): Drosophila abl and genetic redundancy in signal transduction. Trends in genetics: TIG. 7 (11-12): 351-5.

159- Hofmann M.E., Nahir B., Frazier C.J. (2006): Endocannabinoid-mediated depolarizationinduced suppression of inhibition in hilar mossy cells of the rat dentate gyrus. J. Neurophysiol. 96: 2501-2512.

160- Howlett A.C. and Mukhopadhyay S. (2000): Cellular signal transduction by anandamide and 2-arachidonoylglycerol. Chem. Phys. Lipids. 108: 53-70.

161- Howlett A.C., Barth F., Bonner T.I., Cabral G., Casellas P., Devane W.A., Felder C.C., Herkenham M., Mackie K., Martin B.R., et al. (2002). International union of pharmacology. XXVII. Classification of cannabinoidreceptors. Pharmacol. Rev. 54. 161-202.

162- Hu S.S.J. and Mackie K. (2015): Distribution of the endocannabinoid system in the central nervous system. In: Pertwee R.G. editor. Handbook of Experimnental Pharmacology, Endocannabinoids. Berlin: Springer. 59-93.

163- Huang C., Hu Z.L., Wu W.N., Yu D.F., Xiong Q.J., Song J.R., Shu Q., Fu H., Wang F., Chen J.G. (2010): Existence and distinction of acid-evoked currents in rat astrocytes. Glia 58: 1415-1424.

164- Huang H., McIntosh A.L., Martin G.G., Landrock D., Chung S., Landrock K.K., Dangott L.J., Li S.R., Kier A.B., Schroeder F. (2016): Fabp1: A novel hepatic endocannabinoid and cannabinoid binding protein. Biochemistry. 55: 5243-5255.

165- Huang W.X., Min J.W., Liu Y.Q., He X.H., Peng B.W. (2014): Expression of TRPV1 in the C57BL/6 mice brain hippocampus and cortex during development NeuroReport. 25: 379-385.

166- Huang W.X., Yu F., Sanchez R.M., Liu Y.Q., Min J.W., Hu J.J., Bsoul N.B., Han S., Yin J., Liu W.H., He X.H., Peng B.W. (2015): TRPV1 promotes repetitive febrile seizures by pro-inflammatory cytokines in immature brain Brain Behav. Immun. 48: 68-77.

167- Hurtado-Zavala J.I., Ramachandran B., Ahmed S. et al. (2017): "TRPV1 regulates excitatory innervation of OLM neurons in the hippocampus" Nature Communications. 8: 15878.

168- Iannotti F. A., Hill C. L., Leo A., Alhusaini A., Soubrane C., Mazzarella E. et al. (2014): Nonpsychotropic plant cannabinoids, cannabidivarin (CBDV) and cannabidiol (CBD), activate and desensitize transient receptor potential vanilloid 1 (TRPV1) channels in vitro: potential for the treatment of neuronal hyperexcitability. ACS Chem. Neurosci. 5: 1131-1141.

169- Iida T., Shimizu I., Nealen M.L., Campbell A., Caterina M. (2005): Attenuated fever response in mice lacking TRPV1. Neurosci. Lett. 378: 28-33.

170- Iversen L. (2003): Cannabis and the brain. Brain. 126: 1252-1270.

171- Isokawa M. and Alger B.E. (2005): Retrograde endocannabinoid regulation of GABAergic inhibition in the rat dentate gyrus granule cell. J. Physiol. 567: 1001-1010.

172- Jancso-Gabor A., Szolcsanyi J., Jancso N. (1970): Stimulation and desensitization of the hypothalamic heat-sensitive structures by capsaicin in rats. J. Physiol. 208 (2): 449-459.

173- Jimenez-Blasco et al., Nature submitted.

174- Johnston D. and Amaral D.G. (2004): Hippocampus. In: Shepherd GM, editor. The synaptic organization of the brain. ed. Oxford: Oxford University Press. 455-498.

175- Jung M., Calassi R., Rinaldi-Carmona M., Chardenot P., Le Fur G., Soubrie P., Oury-Donat F. (1997): Characterization of CB1 receptors on rat neuronal cell cultures: binding and functional studies using the selective receptor antagonist SR 141716A. J. Neurochem. 68 (1): 402-409.

176- Kano M., Ohno-Shosaku T., Hashimotodani Y., Uchigashima M., Watanabe M. (2009): Endocannabinoid-mediated control of synaptic transmission. Physiol. Rev. 89: 309-380.

177- Karakas B., Weeraratna A.T., Abukhdeir A.M., Konishi H., Gustin J.P., Vitolo M.I. et al. (2007): P21 gene knock down does not identify genetic effectors seen with gene knock out. Cancer biology & therapy. 6 (7): 1025-30.

178- Katona I., Sperlagh B., Sik A., Kafalvi A., Vizi E.S., Mackie K., Freund T.F. (1999): Presynaptically located CB1 cannabinoid receptors regulate GABA release from axon terminals of specific hippocampal interneurons. J. Neurosci. 19: 4544-4558.

179- Katona I., Urban G.M., Wallace M., Ledent C., Jung K.M., Piomelli D., Mackie K., Freund T.F. (2006): Molecular composition of the endocannabinoid system at glutamatergic synapses. J. Neurosci. 26: 5628-5637.

180- Katona I., Freund T.F. (2008): Endocannabinoid signaling as a synaptic circuit breaker in neurological disease. Nat. Med. 14: 923-930.

181- Katona I., Freund T.F. (2012): Multiple functions of endocannabinoid signaling in the brain. Annu. Rev. Neurosci. 35: 529-558.

182- Katona I. (2015): Cannabis and endocannabinoid signaling in epilepsy. 231: 285-316.

183- Kauer J.A. and Gibson H.E. (2009): Hot flash: TRPV channels in the brain. Trends Neurosci. 32: 215-224.

184- Kawahara H., Drew G.M., Christie M.J., Vaughan C.W. (2011): Inhibition of fatty acid amide hydrolase unmasks CB_1 receptor and TRPV1 channel-mediated modulation of glutamatergic synaptic transmission in midbrain periaqueductal grey. Br. J. Pharmacol. 163: 1214-1222.

185- Kawamura Y., Fukaya M., Maejima T., Yoshida T., Miura E., Watanabe M., Ohno-Shosaku T., Kano M. (2006): The CB1 cannabinoid receptor is the major cannabinoid receptor at excitatory presynaptic sites in the hippocampus and cerebellum. J. Neurosci. 26: 2991-3001.

186- Kofalvi A., Oliveira C.R., Cunha R.A. (2006): Lack of evidence for functional TRPV1 vanilloid receptors in rat hippocampal nerve terminals. Neurosci. Lett. 403: 151-156.

187- Kong W.-L., Min J.-W., Liu Y.-L., Li J.-X., He X.-H., Peng B.-W. (2014): Role of TRPV1 in susceptibility to PTZ-induced seizure following repeated hyperthermia challenges in neonatal mice. Epilepsy Behav. 31: 276-280.

188- Kovacs G.G., Robinson J.L., Xie S.X., Lee E.B., Grossman M., Wolk D.A., Irwin D.J., Weintraub D., Kim C.F., Schuck T., Yousef A., Wagner S.T., Suh E., Van Deerlin V.M., Lee V.M., Trojanowski J.Q. (2017): Evaluating the patterns of aging-related tau astrogliopathy unravels novel insights into brain aging and neurodegenerative diseases. J. Neuropathol. Exp. Neurol. 76: 270-288.

189- Kunos G., Osei-Hyiaman D., Bátkai S., Gao B. (2006): Cannabinoids hurt, heal in cirrhosis. Nat. Med. 12: 608-610.

190- Law S.H. and Sargent T.D. (2014): The serine-threonine protein kinase PAK4 is dispensable in zebrafish: identification of a morpholino-generated pseudophenotype. PLoS ONE. 9 (6): 100268.

191- Lafourcade M., Elezgarai I., Mato S., Bakiri Y., Grandes P., Manzoni O.J. (2007): Molecular components and functions of the endocannabinoid system in mouse prefrontal cortex. PLoS One. 2: 1-11.

192- Lauckner J.E., Hille B., Mackie K. (2005): The cannabinoid agonist WIN55,212-2 increases intracellular calcium via CB1 receptor coupling to Gq/11 G proteins. Proc. Natl. Acad. Sci. USA. 102 (52): 19144-19149.

193- Lee L. Y., Ni D., Hayes D., Lin R. L. (2011): TRPV1 as a cough sensor and its temperature-sensitive properties. Pulmonary Pharmacology & Therapeutics. 24 (3): 280-285.

194- Lee S.H., Ledri M., Tóth B., Marchionni I., Henstridge C.M., Dudok B., et al. (2015): Multiple Forms of Endocannabinoid and Endovanilloid Signaling Regulate the Tonic Control of GABA Release. J. Neurosci. 35 (27): 10039-57.

195- Leterrier C., Bonnard D., Carrel D., Rossier J., Lenkei Z. (2004): Constitutive endocytic cycle of the CB1 cannabinoid receptor. J. Biol. Chem. 279: 36013-36021.

196- Letzkus J.J., Wolff S.B., Luthi A. (2015): Disinhibition, a circuit mechanism for associative learning and memory. Neuron. 88: 264-276.

197- Lévesque M. and Avoli M. (2013): The kainic acid model of temporal lobe epilepsy. Neurosci. Biobehav. Rev. 37: 2887-99.

198- Li X.G., Somogyi P., Ylien A., Buszáki G. (1994): The hippocampal CA3 network: an in vivo intracellular labeling study. J. Comp. Neurol. 339: 181-208.

199- Li H.-B., Mao R.-R., Zhang J.-C., Yang Y., Cao J., Xu L. (2008): Antistress effect of TRPV1 channel on synaptic plasticity and spatial memory. Biol. Psychiatry. 64 (4): 286-292.

200- Lisman J.E., Talamini L.M., Raffone A. (2005): Recall of memory sequences by interaction of the dentate and CA3: a revised model of the phase precession. Neural networks: the official journal of the International Neural Network Society. 18: 1191-1201.

201- Long J.Z., Li W., Booker L., Burston J.J., Kinsey S.G., Schlosburg J.E., Pavón F.J., Serrano A.M., Selley D.E., Parsons L.H., Lichtman A.H., Cravatt B.F. (2009): Selective blockade of 2-arachidonoylglycerol hydrolysis produces cannabinoid behavioral effects. Nat Chem Biol 5: 37-44.

202- Lopez De Jesus M., Stope M.B., Oude Weernink P.A., Mahlke Y., Borgermann C., Ananaba V.N., Rimmbach C., Rosskopf D., Michel M.C., Jakobs K.H., Schmidt M. (2006): Cyclic AMP-dependent and Epac-mediated activation of R-Ras by G protein-coupled receptors leads to phospholipase D stimulation. J. Biol. Chem. 281: 21837-21847.

203- Lothman E.W., Bertram E.H., Stringer J.L. (1991): Functional anatomy of hippocampal seizures. Prog. Neurobiol. 37 (1).

204- Lu H.C. and Mackie K. (2016): An introduction to the endogenous cannabinoid system. Biol. Psychiatry. 79: 516-525.

205- Ludanyi A., Eross L., Czirjak S., Vajda J., Halasz P., Watanabe M., Palkovits M., Magloczky Z., Freund T.F., Katona I. (2008): Downregulation of the CB1 cannabinoid receptor and related molecular elements of the endocannabinoid system in epileptic human hippocampus. J. Neurosci. 28: 2976-2990.

206- Ludanyi A., Hu S.S., Yamazaki M., Tanimura A., Piomelli D., Watanabe M., Kano M., Sakimura K., Magloczky Z., Mackie K., Freund T.F., Katona I (2011): Complementary synaptic distribution of enzymes responsible for synthesis and inactivation of the endocannabinoid 2-arachidonoylglycerol in the human hippocampus. Neuroscience. 174: 50-63.

207- Luján R., Roberts J.D., Shigemoto R., Ohishi H., Somogyi P. (1997): Differential plasma membrane distribution of metabotropic glutamate receptors mGluR1 alpha, mGluR2 and mGluR5, relative to neurotransmitter release sites. J. Chem. Neuroanat. 13: 219-241.

208- Luo Z., Ma L., Zhao Z., He H., Yang D., Feng X., Ma S., Chen X., Zhu T., Cao T., Liu D., Nilius B., Huang Y., Yan Z., Zhu Z. (2012): TRPV1 activation improves exercise endurance and energy metabolism through PGC-1 alpha upregulation in mice. Cell. Res. 22: 551-564.

209- Lüttjohann A., Fabene P.F., van Luijtelaar G. (2009): A revised Racine's scale for PTZ-induced seizures in rats. Physiology & Behavior. 98 (5): 579-586.

210- Lutz B., Marsicano G., Maldonado R., Hillard C.J. (2015): The endocannabinoid system in guarding against fear, anxiety and stress. Nature Reviews Neuroscience. 16: 705-718.

211- Lutzu S. and Castillo P.E. (2020): Modulation of NMDA Receptors by G-protein-coupled receptors: Role in Synaptic Transmission, Plasticity and Beyond. Neuroscience.

212- Maccarrone M., Bab R., Biro T., Cabral G.A., Dey S.K., di Marzo V., Konje J.C., Kunos G., Mechoulam R., Pacher P., et al. (2015): Endocannabinoid signaling at the periphery: 50 years after thc. Trends Pharmacol. Sci. 36: 277-296.

213- Mackie K. (2005): Distribution of cannabinoid receptors in the central and peripheral nervous system. Handb. Exp. Pharmacol. 299-325.

214- Mackie K. and Stella N. (2006): Cannabinoid receptors and endocannabinoids: evidence for new players. AAPS J. 8.

215- Mailleux P. and Vanderhaeghen J-J. (1992): Distribution of neuronal cannabinoid receptor in the adult rat brain: a comparative receptor binding radioautography and in situ hybridization histochemistry. Neuroscience. 48: 655-668.

216- Maione S., Cristino L., Migliozzi A.L., Georgiou A.L., Starowicz K., Salt T.E., et al. (2009): TRPV1 channels control synaptic plasticity in the developing superior colliculus. J. Physiol. 587: 2521-2535.

217- Manna S.S.S. and Umathe S.N. (2012): Involvement of transient receptor potential vanilloid type 1 channels in the pro-convulsant effect of anandamide in pentylenetetrazole-induced seizures. Epilepsy Res. 100: 113-124.

218- Mannari T., Morita S., Furube E., Tominaga M., Miyata S. (2013): Astrocytic TRPV1 ion channels detect blood-borne signals in the sensory circumventricular organs of adult mouse brains. Glia. 61: 957-971.

219- Marinelli S., Vaughan C.W., Christie M.J., and Connor M. (2002): Capsaicin activation of glutamatergic synaptic transmission in the rat locus coeruleus in vitro. The Journal of Physiology. 543 (2): 531-540.

220- Marinelli S., Di Marzo V., Berretta N., Matias I., Maccarrone M., Bernardi G., Mercuri N.B. (2003): Presynaptic facilitation of glutamatergic synapses to dopaminergic neurons of the rat substantia nigra by endogenous stimulation of vanilloid receptors. J Neurosci. 23: 3136-3144.

221- Marinelli S., Pacioni S., Bisogno T., di Marzo V., Prince D.A., Huguenard J.R., Bacci, A. (2008): The endocannabinoid 2-arachidonoylglycerol is responsible for the slow self-inhibition in neocortical linterneurons. J. Neurosci. 28: 13532-13541.

222- Marinelli S., Pacioni S., Cannich A., Marsicano G., Bacci A. (2009): Self-modulation of neocortical pyramidal neurons by endocannabinoids. Nat. Neurosci. 12: 1488-1490.

223- Marr D. (1971): Simple memory: a theory for archicortex. Phil. Trans. R. Soc. Lond. B 262, 23-81.

224- Marrone M.C., Morabito A., Giustizieri M., Chiurchiu V., Leuti A., Mattioli M., et al. . (2017): TRPV1 channels are critical brain inflammation detectors and neuropathic pain biomarkers in mice. Nat. Commun. 8: 15292.

225- Marrs W.R., Blankman J.L., Horne E.A., Thomazeau A., Lin Y.H., Coy J., Bodor A.L., Muccioli G.G., Hu S.S., Woodruff G., Fung S., Lafourcade M., Alexander J.P., Long J.Z., Li W., Xu C., Moller T., Mackie K., Manzoni O.J., Cravatt B.F., Stella N. (2010): The serine hydrolase ABHD6 controls the accumulation and efficacy of 2-AG at cannabinoid receptors. Nat. Neurosci. 13: 951-957.

226- Marsch R., Foeller E., Rammes G., Bunck M., Kössl M., Holsboer F., et al. (2007): Reduced anxiety, conditioned fear, and hippocampal long-term potentiation in transient receptor potential vanilloid type 1 receptor-deficient mice. J. Neurosci. 27 (4): 832-9.

227- Marsicano G. and Lutz B. (1999): Expression of the cannabinoid receptor CB1 in distinct neuronal subpopulations in the adult mouse forebrain. Eur. J. Neurosci. 11: 4213-4225.

228- Marsicano G., Goodenough S., Monory K., Hermann H., Eder M., Cannich A., Azad S.C., Cascio M.G., Gutierrez S.O., van der Stelt M., et al. (2003): CB1 cannabinoid receptors and on-demand defense against excitotoxicity. Science. 302: 84-88.

229- Marsicano G. and Lutz B. (2006): Neuromodulatory functions of the endocannabinoid system. J. Endocrinol. Invest. 29: 27-46.

230- Marsicano G. and Kuner R. (2008): Anatomical distribution of receptors, ligands and enzymes in the brain and in the spinal cord: circuitries and neurochemistry. Cannabinoids and the brain. New York: Springer. 161-201.

231- Martin E., Dahan D., Cardouat G., Gillibert-Duplantier J., Marthan R., Savineau J.P., Ducret T. (2012): Involvement of TRPV1 and TRPV4 channels in migration of rat pulmonary arterial smooth muscle cells. Pflugers Arch. 464 (3): 261-272.

232- Martínez-Vargas M., Murillo-Rodriguez E., González-Rivera R., Landa A., Méndez-Diaz M., Prospero-Garcia O., Navarro L. (2003): Sleep modulates cannabinoid receptor 1 expression in the pons of rats. Neuroscience. 117: 197-201.

233- Mateos J.M., Elezgarai I., Benitez R., Osorio A., Bilbao A., Azkue J.J., et al. (1999): Clustering of the group III metabotropic glutamate receptor 4a at parallel fiber synaptic terminals in the rat cerebellar molecular layer. *Neurosci. Res.* 35: 71-74.

234- Mather K. (1953): Genetical control of stability in development. Heredity. 7 (3): 297-336.

235- Matsuda L.A., Lolait S.J., Brownstein M.J., Young A.C., Bonner T.I. (1990): Structure of a cannabinoid receptor and functional expression of the cloned cdna. Nature. 346: 561-564.

236- Matsuda L.A., Bonner T.I., Lolait S.J. (1993): Localization of cannabinoid receptor mRNA in rat brain. J. Comp. Neurol. 327: 535-550.

237- Matsuda L.A. (1997): Molecular aspects of cannabinoid receptors. Crit. Rev. Neurobiol 11: 143-166.

238- McAllister S.D. and Glass M. (2002): CB(1) and CB(2) receptor-mediated signalling: a focus on endocannabinoids. Prostaglandins Leukot. Essent. Fatty Acids. 66 (2-3): 161-171.

239- McJunkin K., Mazurek A., Premsrirut P.K., Zuber J., Dow L.E., Simon J., et al. (2011): Reversible suppression of an essential gene in adult mice using transgenic RNA interference. Proceedings of the National Academy of Sciences of the United States of America. 108 (17): 7113-8.

240- Mechoulam R. (1986): The Pharmacohistory of Cannabis sativa, in Cannabis as Therapeutic Agent; CRC Press: Boca Raton, FL, USA.

241- Mechoulam R., Benshabat S., Hanus L., Ligumsky M., Kaminski N.E., Schatz A.R., Gopher A., Almog S., Martin B.R., Compton D.R. et al. (1995): Identification of an endogenous 2-monoglyceride, present in canine gut, that binds to cannabinoid receptors. Biochem. Pharmacol. 50: 83-90.

242- Mechoulam R. and Parker L.A. (2013): The endocannabinoid system and the brain. Annu. Rev. Psychol. 64: 21-47.

243- Metna-Laurent M. and Marsicano G. (2015): Rising stars: modulation of brain functions by astroglial type-1 cannabinoid receptors. Glia. 63: 353-364.

244- Mezey E., Toth Z.E., Cortright D.N., Arzubi M.K., Krause J.E., Elde R. et al. (2000): Distribution of mRNA for vanilloid receptor subtype 1 (VR1), and VR1-like immunoreactivity, in the central nervous system of the rat and human. Proc. Natl. Acad. Sci. USA. 97 (7): 3655-3660.

245- Micale V., Cristino L., Tamburella A., Petrosino S., Leggio G.M., Drago F., et al. (2009): Anxiolytic effects in mice of a dual blocker of fatty acid amide hydrolase and transient receptor potential vanilloid type-1 channels. Neuropsychopharmacology. 34: 593-606.

246- Mitchell J.A., Williams F.M., Williams T.J., Larkin S.W. (1997): Role of nitric oxide in the dilator actions of capsaicin-sensitive nerves in the rabbit coronary circulation. Neuropeptides. 31(4): 333-338.

247- Miyake T., Shirakawa H., Nakagawa T., Kaneko S. (2015): Activation of mitochondrial transient receptor potential vanilloid 1 channel contributes to microglial migration. Glia. 63: 1870-1882

248- Miyake T., Shirakawa H., Nakagawa T., Kaneko S. (2015): Activation of mitochondrial transient receptor potential vanilloid 1 channel contributes to microglial migration. Glia. 63: 1870-1882.

249- Monory K., Massa F., Egertova M., Eder M., Blaudzun H., Westenbroek R., et al. (2006): The endocannabinoid system controls key epileptogenic circuits in the hippocampus. Neuron. 51: 455-466.

250- Montell C. (2005): The TRP superfamily of cation channels. Science. STKE (3): 272.

251- Morales P., Hurst D.P., Reggio P.H. (2017a): Molecular targets of the phytocannabinoids: a complex picture. Prog. Chem. Org. Nat. Prod. 103: 103-131.

252- Morales P. and Reggio P.H. (2017b): An update on non-CB1, non-CB2 cannabinoid related G-protein-coupled receptors. Cannabis Cannabinoid Res. 2: 265-273.

253- Morales P., Isawi I., Reggio P.H. (2018): Towards a better understanding of the cannabinoid-related orphan receptors GPR3, GPR6, and GPR12. Drug Metab. Rev. 50: 74-93.

254- Morales-Lázaro S.L., Simon S.A., Rosenbaum T. (2013): The role of endogenous molecules in modulating pain through transient receptor potential vanilloid 1 (TRPV1). J. Physiol. 591: 3109-3121.

255- Morgens D.W., Deans R.M., Li A., Bassik M.C. (2016): Systematic comparison of CRISPR/Cas9 and RNAi screens for essential genes. Nature biotechnology. 34 (6): 634-6.

256- Mori F., Ribolsi M., Kusayanagi H., Monteleone F., Mantovani V., Buttari F., Marasco E., Bernardi G., Maccarrone M., Centonze D. (2012): TRPV1 channels regulate cortical excitability in humans. J. Neurosci. 32: 873-879.

257- Muller C., Morales P., Reggio P.H. (2019): Cannabinoid Ligands Targeting TRP Channels. Front. Mol. Neurosci. 11: 487.

258- Munro S., Thomas K.L., Abu-Shaar M. (1993): Molecular characterization of a peripheral receptor for cannabinoids. Nature. 365: 61-65.

259- Murataeva N., Straiker A., Mackie K. (2014): Parsing the players: 2-arachidonoylglycerol synthesis and degradation in the CNS. Br. J. Pharmacol. 171: 1379-1391.

260- Murillo-Rodriguez E., Désarnaud F., Prospéro-Garcia O. (2006): Diurnal variation of arachidonoylethanolamine, palmitoylethanolamide and oleoylethanolamide in the brain of the rat. Life Sci. 79: 30-37.

261- Musella A., De Chiara V., Rossi S. et al. (2009): "TRPV1 channels facilitate glutamate transmission in the striatum. Molecular and Cellular Neuroscience. 40 (1): 89-97.

262- Naderi N., Shafieirad E., Lakpoor D., Rahimi A., Mousavi Z. (2015): Interaction between Cannabinoid Compounds and Capsazepine in Protection against Acute Pentylenetetrazole-induced Seizure in Mice. Iran. J. Pharm. Res. 14: 115-20.

263- Naidoo V., Nikas S., Karanian D., Hwang J., Zhao J., Wood J., Alapafuja S., Vadivel S., Butler D., Makriyannis A., Bahr B. (2011): A New Generation Fatty Acid Amide Hydrolase Inhibitor Protects Against Kainate-Induced Excitotoxicity. Journal of Molecular Neuroscience. 43: 493-502.

264- Navarrete M. and Araque A. (2008): Endocannabinoids mediate neuron-astrocyte communication. Neuron. 57: 883-893.

265- Navarrete M. and Araque A. (2010). Endocannabinoids potentiate synaptic transmission through stimulation of astrocytes. Neuron. 68: 113-126.

266- Navarrete M., Diez A., Araque A. (2014): Astrocytes in endocannabinoid signaling. Philos. Trans. R. Soc. Lond. B. Biol. Sci. 369: 20130599.

267- Nedvetzki S., Gonen E., Assayag N., Reich R., Williams R.O., Thurmond R.L., et al. (2004): RHAMM, a receptor for hyaluronan-mediated motility, compensates for CD44 in inflamed

CD44-knockout mice: a different interpretation of redundancy. Proceedings of the National Academy of Sciences of the United States of America. 101 (52):18081-6

268- Nicolussi S., Gertsch J. (2015): Endocannabinoid transport revisited. Vitam. Horm. 98: 441-485.

269- Nie J. and Lewis D.L. (2001a): The proximal and distal C-terminal tail domains of the CB1 cannabinoid receptor mediate G protein coupling. Neuroscience. 107: 161-167.

270- Nie J. and Lewis D.L. (2001b): Structural domains of the CB1 cannabinoid receptor that contribute to constitutive activity and G-protein sequestration. J. Neurosci. 21: 8758-8764.

271- Niehaus J.L., Liu Y., Wallis K.T., Egertova M., Bhartur S.G., Mukhopadhyay S., et al. (2007): CB_1 Cannabinoid Receptor Activity Is Modulated by the Cannabinoid Receptor Interacting Protein CRIP1a. Mol. Pharmacol. 72 (6): 1557-66.

272- Nilius B. and Szallasi A. (2014): Transient receptor potential channels as drug targets: from the science of basic research to the art of medicine. Pharmacol. Rev. 66: 676-814.

273- Nyiri G., Cserep C., Szabadits E., Mackie K., Freund T.F. (2005): CB1 cannabinoid receptors are enriched in the perisynaptic annulus and on preterminal segments of hippocampal GABAergic axons. Neuroscience. 136: 811-822.

274- Oliveira da Cruz J.F., Robin L.M., Drago F., Marsicano G., Metna-Laurent M. (2016): Astroglial type-1 cannabinoid receptor (CB1): a new player in the tripartite synapse. Neuroscience. 323: 35-42.

275- Pacher P., Batkai S., Kunos, G. (2006): The endocannabinoid system as an emerging target of pharmacotherapy. Pharmacol. Rev. 58: 389-462.

276- Parsons L.H. and Hurd Y.L. (2015): Endocannabinoid signalling in reward and addiction. Nat. Rev. Neurosci. 16: 579-594.

277- Patel S., Hill M.N., Cheer J.F., Wotjak C.T., Holmes A. (2017): The endocannabinoid system as a target for novel anxiolytic drugs. Neurosci. Biobehav. Rev. 76: 56-66.

278- Pegorini S., Zani A., Braida D., Guerini-Rocco C., Sala M. (2006): Vanilloid VR1 receptor is involved in rimonabant-induced neuroprotection. British Journal of Pharmacology. 147 (5): 552-559.

279- Peñasco S., Rico-Barrio I., Puente N., Gómez-Urquijo S.M, Fontaine C.J., Egaña-Huguet J., Achicallende S., Ramos A., Reguero L., Elezgarai I., Nahirney P.C., Christie B.R., Grandes P. (2019): Endocannabinoid long-term depression revealed at medial perforant path excitatory synapses in the dentate gyrus. Neuropharmacology. 153: 32-40.

280- Peñasco S., Rico-Barrio I., Puente N., Fontaine C.J., Ramos A., Reguero L., Gerrikagoitia I., Rodríguez de Fonseca F., Suarez J., Barrondo S., Aretxabala X., García del Caño G., Sallés J., Elezgarai I., Nahirney P.C., Christie B.R., Grandes P. (2020): Intermittent ethanol exposure

during adolescence impairs cannabinoid type 1 receptor-dependent long-term depression and recognition memory in adult mice. Neuropsychopharmacology. 45: 309-318

281- Pertwee R.G. (2006): Cannabinoid pharmacology: The first 66 years. Br. J. Pharmacol. 147: 163-171.

282- Pertwee R.G., Howlett A.C., Abood M.E., Alexander S.P., di Marzo V., Elphick M.R., Greasley P.J., Hansen H.S., Kunos G., Mackie K. et al. (2010): International union of basic and clinical pharmacology. LXXIX. Cannabinoid receptors and their ligands: Beyond CB1 and CB2. Pharmacol. Rev. 62: 588-631.

283- Pinar C., Fontaine C.J., Triviño-Paredes J., Lottenberg C.P., Gil-Mohapel J., Christie B.R. (2017): Revisiting the flip side: long-term depression of synaptic efficacy in the hippocampus. Neurosci. Biobehav. Rev. 80: 394-413.

284- Pitts M.W. (2018): Barnes maze procedure for spatial learning and memory in mice. Bio Protocols. 8

285- Puente N., Elezgarai I., Lafourcade M., Reguero L., Marsicano G., Georges F., et al. (2010a): Localization and function of the cannabinoid CB1 receptor in the anterolateral bed nucleus of the stria terminalis. PLoS One. 5: 8869.

286- Puente N., Mendizabal-Zubiaga J., Elezgarai I., Reguero L., Buceta I., Grandes P. (2010b): Precise localization of the voltage-gated potassium channel subunits Kv3.1b and Kv3.3 revealed in the molecular layer of the rat cerebellar cortex by a pre-embedding immunogold method. Histochem. Cell Biol. 403-409.

287- Puente N., Cui Y., Lassalle O., Lafourcade M., Georges F., Venance L., Grandes P., Manzoni O.J. (2011): Polymodal activation of the endocannabinoid system in the extended amygdala. Nat. Neurosci. 14: 1542-1547.

288- Puente N., Reguero L., Elezgarai I., Canduela M.J., Mendizabal-Zubiaga J., Ramos-Uriarte A., Fernández-Espejo E., Grandes P. (2015): The transient receptor potential vanilloid-1 is localized at excitatory synapses in the mouse dentate gyrus. Brain Struct. Funct. 220: 1187-1194.

289- Puente N., Bonilla-Del Río I., Achicallende S., Nahirney P.C. and Grandes, P. (2019): High resolution immunoelectron microscopy techniques for revealing distinct subcellular type 1 cannabinoid receptor domains in brain. Bio-protocol. 9 (2): e3145.

290- Puighermanal E., Marsicano G., Busquets-Garcia A., Lutz B., Maldonado R., Ozaita A. (2009): Cannabinoid modulation of hippocampal long-term memory is mediated by mTOR signaling. Nature Neuroscience. 12: 1152-1158.

291- Racine R. (1972): Modification of seizure activity by electrical stimulation: II. Motor seizure. Electroencephalography and Clinical Neurophysiology. 32 (3): 281-294.

292- Ratzliff A.D., Santhakumar V., Howard A., Soltesz I. (2002): Mossy cells in epilepsy: rigor mortis or vigor mortis? Trends Neurosci. 25: 140-144.

293- Renau-Piqueras J., Zaragoza R., De Paz P., Baguena-Cervellera R., Megias L., Guerri C. (1989): Effects of prolonged ethanol exposure on the glial fibrillary acidic protein-containing intermediate filaments of astrocytes in primary culture: a quantitative immunofluorescence and immunogold electron microscopic study. J. Histochem. Cytochem. 37: 229-240.

294- Reguero L., Puente N., Elezgarai I., Mendizabal-Zubiaga J., Canduela M.J., Buceta I., et al. (2011): GABAergic and cortical and subcortical glutamatergic axon terminals contain CB1 cannabinoid receptors in the ventromedial nucleus of the hypothalamus. PLoS One. 6: e26167.

295- Reguero L., Puente N., Elezgarai I., Ramos-Uriarte A., Gerrikagoitia I., Bueno-López J.L., et al. (2014): Subcellular localization of NAPE-PLD and DAGL-α in the ventromedial nucleus of the hypothalamus by a preembedding immunogold method. Histochemistry and Cell Biology. 141 (5): 543-550.

296- Ribak C.E., Seress L., Amaral D.G. (1985): The development, ultrastructure and synaptic connections of the mossy cells of the dentate gyrus. J. Neurocytol. 14: 835-857.

297- Rico-Barrio I., Peñasco S., Puente N., Ramos A., Fontaine C.J., Reguero L., Giordano M.E., Buceta I., Terradillos I., Lekunberri L., , Mendizabal-Zubiaga J., Rodríguez de Fonseca F., Gerrikagoitia I., Elezgarai I., Grandes P. (2018): Cognitive and neurobehavioral benefits of an enriched environment on young adult mice after chronic ethanol consumption during adolescence. Addict. Biol. 24(5):969-980.

298- Robbe D., Kopf M., Remaury A., Bockaert J., Manzoni O.J. (2002): Endogenous cannabinoids mediate long-term synaptic depression in the nucleus accumbens. Proc. Natl. Acad. Sci. USA. 99: 8384-8388.

299- Roberts J.C., Davis J.B., Benham C.D. (2004): [H3]Resiniferatoxin auto- radiography in the CNS of wild-type and TRPV1 null mice defines TRPV1 (VR-1) protein distribution. Brain Res. 995: 176-183.

300- Rodriguez M., Abdala P., Barroso-Chinea P., Gonzalez-Hernandez T. (2001): The deep mesencephalic nucleus as an output center of basal ganglia: morphological and electrophysiological similarities with the substantia nigra. J. Comp. Neurol. 438: 12-31.

301- Rosenberg E.C., Tsien R.W., Whalley B.J., et al. (2015): Cannabinoids and epilepsy. Neurotherapeutics. 12: 747-68.

302- Ross R.A. (2003). Anandamide and vanilloid TRPV1 receptors. Br. J. Pharmacol. 140: 790-801.

303- Rouzer C.A. and Marnett L.J. (2011): Endocannabinoid oxygenation by cyclooxygenases, lipoxygenases, and cytochromes p450: Cross-talk between the eicosanoid and endocannabinoid signaling pathways. Chem. Rev. 111: 5899-5921.

304- Rozenfeld R. and Devi L.A. (2008): Regulation of CB1 cannabinoid receptor trafficking by the adaptor protein ap-3. FASEB J. 22: 2311-2322.

305- Rozenfeld R. (2011): Type I cannabinoid receptor trafficking: All roads lead to lysosome. Traffic. 12: 12-18.

306- Rueda-Orozco P.E., Soria-Gomez E., Montes-Rodriguez C.J., Martínez-Vargas M., Galicia O., Navarro L., Prospero-García O. (2008): A potential function of endocannabinoids in the selection of a navigation strategy by rats. Psychopharmacology. 198: 565-576.

307- Ruparel N.B., Patwardhan A.M., Akopian A.N., Hargreaves K.M. (2011): Desensitization of transient receptor potential ankyrin 1 (TRPA1) by the TRP vanilloid 1-selective cannabinoid arachidonoyl-2 chloroethanolamine. Mol. Pharmacol. 80: 117-123.

308- Ryberg E., Larsson N., Sjogren S., Hjorth S., Hermansson N.O., Leonova J., Elebring T., Nilsson K., Drmota T., Greasley P.J. (2007): The orphan receptor GPR55 is a novel cannabinoid receptor. Br. J. Pharm. 152: 1092-1101.

309- Sanchez J.F., Krause J.E., Cortright D.N. (2001): The distribution and regulation of vanilloid receptor VR1 and VR1 5 = splice variant RNA expression in rat. Neuroscience. 107: 373-381.

310- Santamaria D., Barriere C., Cerqueira A., Hunt S., Tardy C., Newton K., et al. (2007): Cdk1 is sufficient to drive the mammalian cell cycle. Nature. 448 (7155): 811-5.

311- Schaible H.G., Ebersberger A., Von Banchet G.S. (2002): Mechanisms of pain in arthritis. Ann. N. Y. Acad. Sci. 966: 343-354.

312- Scharfman H.E. (2007): The neurobiology of epilepsy. Curr. Neurol. Neurosci. Rep. 7.

313- Scharfman H.E. and Myers C.E. (2013): Hilar mossy cells of the dentate gyrus: a historical perspective. Front. Neural Circuits. 6: 106.

314- Scharfman H.E. (2016): The enigmatic mossy cell of the dentate gyrus. Nat. Rev. Neurosci. 17: 562-575.

315- Schlosburg J.E., Blankman J.L., Long J.Z. (2010): Chronic monoacylglycerol lipase blockade causes functional antagonism of the endocannabinoid system. Nat Neurosci. 13 (9): 1113-1119.

316- Schmidt D. and Sillanpaa M. (2012): Evidence-based review on the natural history of the epilepsies. Curr. Opin. Neurol. 25.

317- Sharkey K.A., Cristino L., Oland L.D., Van Sickle M.D., Starowicz K., Pittman Q.J., Guglielmotti V., Davison J.S., Di Marzo V. (2007): Arvanil, anandamide and N-arachidonoyl-

dopamine (NADA) inhibit emesis through cannabinoid CB1 and vanilloid TRPV1 receptors in the ferret. Eur. J. Neurosci. 25: 2773-2782.

318- Sierra A., Martin-Suarez S., Valcarcel-Martin R., Pascual-Brazo J., Aelvoet S.A., Abiega O., et al. (2015): Neuronal hyperactivity accelerates depletion of neural stem cells and impairs hippocampal neurogenesis. Cell Stem Cell. 16: 488-503.

319- Silvin A. and Ginhoux F. (2018): Microglia heterogeneity along a spatio-temporal axis: more questions than answers. Glia. 66: 2045-2057.

320- Singla S., Kreitzer A.C., Malenka R.C. (2007): Mechanisms for synapse specificity during striatal long-term depression. J. Neurosci. 27: 5260-5264.

321- Sjöström P.J., Turrigiano G.G., Nelson S.B. (2003): Neocortical LTD via coincident activation of presynaptic NMDA and cannabinoid receptors. Neuron. 39: 641-654.

322- Smith T.H., Sim-Selley L.J., Selley D.E. (2010): Cannabinoid CB1 receptor-interacting proteins: novel targets for central nervous system drug discovery? Br. J. Pharmacol. 160 (3): 454-466.

323- Soltesz I., Alger B.E., Kano M., Lee S.-H., Lovinger D.M., Ohno-Shosaku T., Watanabe M. (2015): Weeding out bad waves: Towards selective cannabinoid circuit control in epilepsy. Nat. Rev. Neurosci. 16: 264.

324- Steindel F., Lerner R., Haring M., Ruehle S., Marsicano G., Lutz B., Monory K. (2013): Neuron-type specific cannabinoid mediated G protein signalling in mouse hippocampus. J. Neurochem. 124: 1-13.

325- Stella N. (2009): Endocannabinoid signalling in microglial cells. Neuropharmacology. 56: 244-253.

326- Stella N. (2010): Cannabinoid and cannabinoid-like receptors in microglia, astrocytes, and astrocytomas. Glia. 58: 1017-1030

327- Steward O. and Scoville S. A. (1976): Cells of origin of entorhinal cortical afferents to the hippocampus and fascia dentata of the rat. J. Comp. Neurol. 169: 347-370.

328- Stueber T., Eberhardt M.J., Caspi Y., Lev S., Binshtok A., Leffler A. (2017): Differential cytotoxicity and intracellular calcium-signalling following activation of the calcium-permeable ion channels TRPV1 and TRPA1. Cell Calcium. 68: 34-44.

329- Subbanna S., Psychoyos D., Xie S., Basavarajappa B.S. (2015): Postnatal ethanol exposure alters levels of 2-arachidonylglycerol-metabolizing enzymes and pharmacological inhibition of monoacylglycerol lipase does not cause neurodegeneration in neonatal mice. J. Neurochem. 134: 276-287.

330- Sugaya Y., Yamazaki M., Uchigashima M., Kobayashi K., Watanabe M., Sakimura K., Kano M. (2016): Crucial roles of the endocannabinoid 2-arachidonoylglycerol in the suppression of epileptic seizures. Cell Rep. 16: 1405-1415.

331- Sugiura T., Kondo S., Sukagawa A., Nakane S., Shinoda A., Itoh K., Yamashita A., Waku K. (1995): 2-arachidonoylgylcerol - A possible endogenous cannabinoid receptor-ligand in brain. Biochem. Biophys. Res. Commun. 215: 89-97.

332- Sun Y. and Bennett A. (2007): Cannabinoids: a new group of agonists of PPARs. PPAR Res. 23513.

333- Sun F.J., Guo W., Zheng D.H., Zhang C.Q., Li S., Liu S.Y., et al. (2013): Increased expression of TRPV1 in the cortex and hippocampus from patients with mesial temporal lobe epilepsy. J. Mol. Neurosci. 49: 182-193.

334- Sun Z., Han J., Zhao W., Zhang Y., Wang S., Ye L., Liu T. (2014): TRPV1 activation exacerbates hypoxia /reoxygenation-induced apoptosis in H9C2 cells via calcium overload and mitochondrial dysfunction. Int. J. Mol. Sci. 15: 18362-18380.

335- Sun F.J., Guo W., Zheng D.H., Zhang C.Q., Li S., Liu S.Y., et al. (2013): Increased expression of TRPV1 in the cortex and hippocampus from patients with mesial temporal lobe epilepsy. J. Mol. Neurosci. 49: 182-193.

336- Szabo T., Biro T., Gonzalez A.F., Palkovits M., Blumberg P.M. (2002): Pharmacological characterization of vanilloid receptor located in the brain. Brain Res. Mol. Brain Res. 98: 51-57.

337- Szallasi A. and Blumberg P.M. (1999): Vanilloid (Capsaicin) receptors and mechanisms. Pharmacol. Rev. 51 (2): 159-212.

338- Szallasi A. and Di Marzo V. (2000): New prospective on enigmatic vanilloid receptors. Trends Neurosci. 23: 491-497.

339- Szolcsanyi J., Joo F., Jancso-Gabor A. (1971): Mitochondrial changes in preoptic neurons after capsaicin desensitization of the hypothalamic thermo detectors in rats. Nature. 229 (5280): 116-117.

340- Szymaszkiewicz A., Włodarczyk J., Wasilewski A., Di Marzo V., Storr M., Fichna J., Zielińska M. (2020): Desensitization of transient receptor potential vanilloid type-1 (TRPV1) channel as promising therapy of irritable bowel syndrome: characterization of the action of palvanil in the mouse gastrointestinal tract. Naunyn Schmiedebergs Arch. Pharmacol.

341- Tahmasebi L., Komaki A., Karamian R., Shahidi S., Sarihi A., Salehi I., Nikkhah A. (2015): The interactive role of cannabinoid and vanilloid systems in hippocampal synaptic plasticity in rats Eur. J. Pharmacol. 757: 68-73.

342- Takács V.T., Szőnyi A., Freund T.F., Nyiri G., Gulyás A.I. (2015): Quantitative ultrastructural analysis of basket and axo-axonic cell terminals in the mouse hippocampus. Brain Struct. Funct. 220: 919-940.

343- Tanimizu T., Kono K., Kida S. (2018): Brain networks activated to form object recognition memory. Brain Res. Bull. 141: 27-34.

344- Tautz D. (1992): Redundancies, development and the flow of information. BioEssays: news and reviews in molecular, cellular and developmental biology. 14 (4): 263-6.

345- Terral G., Busquets-Garcia A., Varilh M., Achicallende S., Cannich A., Bellocchio L., Bonilla-Del Río I., Massa F., Puente N., Soria-Gomez E., Grandes P., Ferreira G., Marsicano G. (2019): CB1 Receptors in the Anterior Piriform Cortex Control Odor Preference Memory. Current Biology. 29 (15): 2455-2464.

346- Tominaga M., Caterina M.J., Malmberg A.B., Rosen T.A., Gilbert H., Skinner K. et al. (1998): The cloned capsaicin receptor integrates multiple pain-producing stimuli. Neuron. 21 (3): 531-543.

347- Tóth A., Boczan J., Kedei N., Lizanecz E., Bagi Z., Papp Z., Edes I., Csiba L., Blumberg P.M. (2005): Expression and distribution of vanilloid receptor 1 (TRPV1) in the adult rat brain. Brain Res. Mol. Brain Res 135:162-168.

348- Touretzky D.S. (2015): Anatomy of the Hippocampus. Compu. Mod. Of Neu. Syst. 3 (2).

349- Tsou K., Brown S., Sanudo-Pena M.C., Mackie K., Walker J.M. (1998): Immunohistochemical distribution of cannabinoid CB1 receptors in the rat central nervous system. Neuroscience. 83: 393-411.

350- Valenti M., Vigano D., Cascico M.G., Rubino T., Steardo L., Parolaro D., di Marzo V. (2004): Differential diurnal variations of anandamide and 2-arachidonoyl-glycerol levels in rat brain. Cell Mol. Life Sci. 61: 945-950.

351- Vay L., Gu C., McNaughton P. A. (2012): The thermo-TRP ion channel family: properties and therapeutic implications. Br. J. Pharmacol. 165: 787-801.

352- Viader A., Blankman J.L., Zhong P., Liu X., Schlosburg J.E., Joslyn C.M., et al. (2015): Metabolic interplay between astrocytes and neurons regulates endocannabinoid action. Cell Rep. 12: 798-808.

353- Vinod K.Y., Yalamanchili R., Xie S., Cooper T.B., Hungund B.L. (2006): Effect of chronic ethanol exposure and its withdrawal on theendocannabinoid system. Neurochemistry International. 49 (6): 619-625.

354- Vinogradova L.V. and van Rijn C.M. (2008): Anticonvulsive and antiepileptogenic effects of levetiracetam in the audiogenic-kindling model. Epilepsia. 49: 1160-8.

355- Volkow N.D., Hampson A.J., Baler R.D. (2017): Don't worry, Be happy: endocannabinoids and cannabis at the intersection of stress and reward. Annu. Rev. Pharmacol. Toxicol. 57: 285-308.

356- Von Koch C.S., Zheng H., Chen H., Trumbauer M., Thinakaran G., van der Ploeg L.H. et al. (1997): Generation of APLP2 KO mice and early postnatal lethality in APLP2/APP double KO mice. Neurobiology of aging. 18 (6): 661-9.

357- Waddington C.H. (1959): Canalization of Development and Genetic Assimilation of Acquired Characters. Nature. 183 (4676): 1654-5.

358- Wang Y., Schnegelsberg P.N., Dausman J., Jaenisch R. (1996): Functional redundancy of the muscle specific transcription factors Myf5 and myogenin. Nature. 379 (6568): 823-5.

359- Wang W., Trieu B.H., Palmer L.C., Jia Y., Pham D.T., Jung K.-M., Karsten C.A., Merrill C.B., Mackie K., Gall C.M., Piomelli D., Lynch G. (2016): A primary cortical input to Hippocampus expresses a pathway-specific and endocannabinoid-dependent form of long-term potentiation. eNeuro 3.

360- Wang W., Jia Y., Pham D.T., Palmer L.C., Jung K.M., Cox C.D., et al. (2018): Atypical endocannabinoid signalling initiates a new form of memory-related plasticity at a cortical input to hippocampus. Cereb. Cortex. 28: 2253-66.

361- West M.J. and Andersen A.H. (1980): An allometric study of the area dentata in the rat and mouse. Brain Res. Rev. 2: 317-348.

362- Wilcox K.S., Dixon-Salazar T., Sills G.J., Ben-Menachem E., White H.S., Porter R.J., et al. (2013): Issues related to development of new antiseizure treatments. Epilepsia. 54.

363- Wilson R.I. and Nicoll R.A. (2001): Endogenous cannabinoids mediate retrograde signalling at hippocampal synapses. Nature. 410: 588-592.

364- Winter Z., Buhala A., Ötvös F., Jósvay K., Vizler C., Dombi G., et al. (2013): Functionally important amino acid residues in the transient receptor potential vanilloid 1 (TRPV1) ion channel - an overview of the current mutational data. Mol. Pain. 9: 30.

365- Witter M.P., Groenewegen H.J., Lopes da Silva F.H., Lohman A.H.M. (1989): Functional organization of the extrinsic and intrinsic circuitry of the parahippocampal region. Prog Neurobiol. 33: 161-253.

366- Witter M.P. (2007): The perforant path: projections from the entorhinal cortex to the dentate gyrus. Prog. Brain Res. 163: 43-61.

367- Wolf E., Seppi K., Katzenschlager R., Hochschorner G., Ransmayr G., Schwingenschuh P., Ott E., Kloiber I., Haubenberger D., Auff E., et al. (2010): Long-Term Antidyskinetic Efficacy of Amantadine in Parkinson’s Disease. Mov. Disord. 25: 1357-1363.

368- Wortley M.A., Birrell M.A., Belvisi M.G. (2016): Drugs affecting TRP channels. Handbook of Experimental Pharmacology. 237: 213-241.

369- Wu Z.Z., Chen S.R., Pan H.L. (2005): Transient receptor potential vanilloid type 1 activation down-regulates voltage-gated calcium channels through calcium-dependent calcineurin in sensory neurons. J. Biol. Chem. 280: 18142-18151.

370- Wu Z.Z., Chen S.R., Pan H.L. (2006): Signalling mechanisms of down- regulation of voltage-activated Ca2+ channels by transient receptor potential vanilloid type 1 stimulation with olvanil in primary sensory neurons. Neuroscience. 141: 407-419.

371- Xu J.Y., Zhang J., Chen C. (2012): Long-lasting potentiation of hippocampal synaptic transmission by direct cortical input is mediated via endocannabinoids. J. Physiol. 590 (10): 2305-2315.

372- Yamamoto S., Jaiswal M., Charng W.L., Gambin T., Karaca E., Mirzaa G., et al. (2014): A drosophila genetic resource of mutants to study mechanisms underlying human genetic diseases. Cell. 159 (1): 200-14.

373- Young R., Passet B., Vilotte M., Cribiu E.P., Beringue V., Le Provost F., et al. (2009): The prion or the related Shadoo protein is required for early mouse embryogenesis. FEBS letters. 583 (19): 3296-300.

374- Zador F. and Wollemann M. (2015): Receptome: Interactions between three pain-related receptors or the “triumvirate” of cannabinoid, opioid and TRPV1 receptors. Pharmacological Research. 102: 254-263.

375- Zani A., Braida D., Capurro V., Sala M. (2007): Delta9-tetrahydrocannabinol (THC) and AM 404 protect against cerebral ischaemia in gerbils through a mechanism involving cannabinoid and opioid receptors. Br. J. Pharmacol. 152 (8): 1301-1311.

376- Zimmer A., Zimmer A.M., Hohmann A.G., Herkenham M., Bonner T.I. (1999): Increased mortality, hypoactivity, and hypoalgesia in cannabinoid CB1 receptor knockout mice. Proc. Natl. Acad. Sci. USA. 96: 5780-5785.

377- Zou S. and Kumar U. (2018): Cannabinoid receptors and the endocannabinoid system: signaling and function in the central nervous system. Int. J. Mol. Sci. 19: 833.

378- Zygmunt P. M., Petersson J., Andersson D. A., Chuang H., Sørgård M., Di Marzo V., et al. (1999): Vanilloid receptors on sensory nerves mediate the vasodilator action of anandamide. Nature. 400: 452-457.